

**Monitoring Fatigue Damage Behavior of Glass/Epoxy  
Composites Using Carbon Nanotubes as Sensors**

Hasna Hena Zamal

A Thesis  
in  
the Department  
of  
Mechanical and Industrial Engineering

Presented in Partial Fulfillment of the Requirements  
for the Degree of Master of Applied Science (Mechanical Engineering) at  
Concordia University  
Montreal, Quebec, Canada

April 2011

© Hasna Hena Zamal, 2011

**CONCORDIA UNIVERSITY**  
**SCHOOL OF GRADUATE STUDIES**

This is to certify that the Thesis prepared,

By: **Hasna Hena Zamal**

Entitled: **“Monitoring Fatigue Damage Behavior of Glass/Epoxy Composites using Carbon Nanotubes as Sensors”**

and submitted in partial fulfillment of the requirements for the Degree of  
**Master of Applied Science (Mechanical Engineering)**

complies with the regulations of this University and meets the accepted standards with respect to originality and quality.

Signed by the Final Examining Committee:

_____	Chair
_____	Examiner
Dr. M. Pugh	
_____	Examiner
Dr. A. Bagchi	External
Building, Civil and Environmental Engineering	
_____	Supervisor
Dr. S.V. Hoa	

Approved by:

\_\_\_\_\_  
Dr. A.K.W. Ahmed, MASc Program Director  
Department of Mechanical and Industrial Engineering

\_\_\_\_\_  
Dean Robin Drew  
Faculty of Engineering & Computer Science

Date: \_\_\_\_\_

# Abstract

## **Monitoring Fatigue Damage Behavior of Glass/Epoxy Composites Using Carbon Nanotubes as Sensors**

**Hasna Hena Zamal**

Carbon nanotubes have been used as sensors in glass fiber/epoxy laminates for monitoring damage under fatigue loading. Carbon nanotubes are embedded in epoxy resin. The modified resin is infused between glass fibers to make composites. Silver paste electrodes are deposited on the surface of the laminate. Changes in electrical resistance are measured along several in-plane and through-thickness positions of the laminate. The changes in resistance are compared with the strain changes measured by strain gages. It is found that the changes in electrical resistance are sensitive to the degradation in the composite laminate. The electrical resistance method is proved to be more reliable in detecting damage in CNT incorporated GFRP composites than strain measurements as it senses the initiation of damage earlier than strain measurement. Among the in-plane and through- thickness resistance response, the through-thickness response can represent the initiation of damages more sensitively and quickly. This technique may be used to provide effective in-situ monitoring of damages in composites.

# Acknowledgements

I like to express my sincere gratitude to my supervisor, Dr. S.V. Hoa, for his support and tireless effort in guiding me towards achieving my MSc degree in Concordia University. His cooperation and continuous inspiration made my stay here pleasant as well as fruitful.

I would like to thank Dr. Ming Xie, Mr. Heng Wang and also Dr. Rosca for their support and valuable suggestions which helped me a lot in understanding my work.

I thank all the members of the CONCOM research group of Dr. Hoa, for their help and support during my research.

I also like to thank my husband and all my family members who were always a source of inspiration for me in accomplishing this work.

Finally, the financial support from NSERC (Natural Sciences and Engineering Research Council of Canada) in carrying out this study is gratefully acknowledged.

# Table of Contents

<b>List of Figures</b> .....	vii
<b>List of Tables</b> .....	xii
<b>CHAPTER 1 Framework and Scope of the Current Work</b> .....	1
1.1. Introduction.....	1
1.2. Motivation.....	3
1.3. Thesis framework.....	4
<b>CHAPTER 2 Literature Review</b> .....	6
<b>2.1 Fatigue in composites materials</b> .....	6
<b>2.2 Damage monitoring in composite materials</b> .....	8
<b>2.3 Carbon nanotubes</b> .....	9
2.3.1 Synthesis of Carbon Nanotubes.....	12
2.3.2. Properties and application of carbon nanotubes.....	12
2.3.3. Conduction mechanism with CNTs in composite laminate.....	15
2.3.5 Dispersion techniques.....	21
<b>2.4 Fatigue damage monitoring in composite laminates</b> .....	24
2.4.1 Monitoring fatigue damage of composite laminate by electrical resistance measurement.....	24
2.4.1.1 Fatigue damage monitoring in conductive FRP composites.....	25
2.4.1.2 Fatigue damage monitoring in non-conductive FRP composites.....	28
<b>2.5 Objectives of the present work</b> .....	33
<b>CHAPTER 3 Materials and Experimental Procedure</b> .....	35
3.1 Materials used for the fabrication of laminate sample.....	36
3.2 Multiwall carbon nanotubes (MWCNTs).....	36
3.3 Epoxy and curing agent.....	37
3.4 Glass fibers.....	39
3.5 Dispersion of carbon nanotubes in the matrix.....	41
3.6 Fabrication of CNT incorporated glass fiber-epoxy composites.....	42
3.6.1 Fiber preform:.....	42
3.6.2 Tool preparation (mold):.....	42
3.6.3 Laying up on the tool:.....	43
3.6.4 Autoclave Curing and Consolidation of the part:.....	44

<b>3.7 Quality of the samples .....</b>	<b>45</b>
<b>3.8 Test schedule and arrangement of electrical connections .....</b>	<b>49</b>
<b>CHAPTER 4 Results and Discussions.....</b>	<b>55</b>
4.1 Tensile test .....	55
4.2 Fatigue test .....	58
4.2.1 Fatigue test for higher load levels (above the first-ply-failure load) .....	59
4.2.2 Fatigue test for lower load levels (below the first-ply-failure load) .....	71
<b>CHAPTER 5 Conclusion, Contributions and Recommendations.....</b>	<b>87</b>
5.1 Conclusion .....	87
5.2 Contribution .....	88
5.3 Recommendations.....	88
<b>References .....</b>	<b>89</b>

# List of Figures

Figure 2.1	Damage mechanisms in fibre-reinforced composites a) Fibre cracking b)Matrix cracking c) Interface debonding .....	7
Figure 2.2	Crack propagation in an isotropic material. The crack propagates in a direction perpendicular to the cyclic loading axis .....	7
Figure 2.3	a) Graphene sheet b) SWNT is formed by wrapping a grapheme sheet into a cylinder .....	10
Figure 2.4	a) Different types of SWCNT b) MWNT formed by several SWNTs.....	11
Figure 2.5	Three types of CNT .....	11
Figure 2.6	Three-dimensional model showing the penetration of nanotubes throughout a fiber array due to their relative scale.....	16
Figure 2.7	Electrical conductivity of the nanocomposites as function of filler content in weight percent.....	18
Figure 2.8	Percolation curve of the nanocomposites as a function of weight percent of MWCNTs.....	19
Figure 2.9	Percolation curve of the nanocomposites as a function of volume percentage of MWCNTs .....	20
Figure 2.10	Volume resistivity of the thermosetting Epoxy-2000 resin as a function of weight fraction of nanotube additives.....	20
Figure 2.11	a) Three-roll mill for dispersing nanotubes b) The flow conditions in the roller clearance.....	22
Figure 2.12	Key steps in realizing the objectives of this work.....	34

Figure 3.1	TEM for purified multiwall carbon nanotubes (MWCNTs) .....	36
Figure 3.2	a) Chemical structure b) Molecular model of Epon 862 resin .....	38
Figure 3.3	a) Chemical structure b) Molecular model of DETDA curing agent .....	38
Figure 3.4	Uni-web S-glass fiber .....	40
Figure 3.5	a) A complete vacuum bag b) Vacuum bag is attached with autoclave vacuum pump line .....	44
Figure 3.6	Cure cycle for S-glass/ Epon 862 epoxy composite laminate .....	45
Figure 3.7	DSC results of the composite sample after curing .....	47
Figure 3.8	TGA result of the composite sample after curing .....	47
Figure 3.9	SEM picture of the matrix showing the dispersion of nanotubes.....	48
Figure 3.10	Fiber distribution of the sample (Optical). .....	48
Figure 3.11	Dimensions of a typical sample for fatigue test .....	49
Figure 3.12	After installing the strain gauge on the sample .....	49
Figure 3.13	Mechanical testing on MTS machine .....	50
Figure 3.14	Arrangement of electrical connections for tests above the first ply failure	51
Figure 3.15	a) 1-2-3-4- points on one side of the sample b) 4'-point on other side of the sample .....	52
Figure 3.16	Arrangement of electrical connections for tests below the first ply failure	52
Figure 4.1	Tensile test sample with two electrodes and the direction of applied force	55
Figure 4.2	Tensile test result of a glass fiber $[0_2/90_2]_s$ laminate, showing the variation of strain and electrical resistance with applied load.....	56
Figure 4.3	SEM images of undamaged sample before testing.....	59

Figure 4.4 a) Variation of change (%) in electrical resistance with loading cycle for sample I, (maximum 6000 N) .....	60
Figure 4.4 b) Variation of change in strain with loading cycle for sample I, ..... (maximum 6000N).....	61
Figure 4.4 c-1, c-2) Optical images of sample I after 500 cycles, ..... (maximum 6000 N).....	62
Figure 4.5 a) Variation of change (%) in electrical resistance with loading cycle for sample II, (maximum 8000 N).....	64
Figure 4.5 b) Variation of change in strain with loading cycle for sample II,..... (maximum 8000N).....	64
Figure 4.5 c-1, c-2) Optical images of sample II after 200 cycles, ..... (maximum 8000N).....	65
Figure 4.6 a) Variation of change (%) in electrical resistance with loading cycles for sample III, (maximum 10000N) .....	66
Figure 4.6 b) Variation of change in strain with loading cycles for sample III, ..... (maximum 10000N).....	67
Figure 4.6 c-1) Optical image of sample III after 150 cycles, (maximum 10000N) .....	67
Figure 4.6 c-2) Optical image of sample III after 150 cycles, (maximum 10000N) .....	68
Figure 4.7 a) Variation of change (%) in electrical resistance with loading cycles for sample IV, (maximum 12000N) .....	68
Figure 4.7 b) Variation of change in strain with loading cycles for sample IV, ..... (maximum 12000N).....	69
Figure 4.7 c-1) Optical image of sample IV, (maximum 12000N) .....	69

Figure 4.7 c-2) Optical image of sample IV, (maximum 12000N) .....	70
Figure 4.8 Variation of percentage change in electrical resistance in a) in-plane, and b) through thickness positions with loading cycle for sample I, (maximum 3000N) .....	72
Figure 4.8 c) Variation of change in strain with loading cycles for sample I, (maximum 3000 N) .....	73
Figure 4.9 a) SEM images at different through thickness positions for sample I,..... (maximum 3000 N).....	73
Figure 4.9 b, c) SEM images at different through thickness positions for sample I, (maximum 3000 N).....	74
Figure 4.10 a) Variation of percentage change in electrical resistance in ..... in-plane positions with loading cycles for sample II, (maximum 3000 N) .....	75
Figure 4.10 b) Variation of percentage change in electrical resistance in ..... Through-thickness positions with loading cycles for sample II, (maximum 3000 N).....	76
Figure 4.10 c) Variation of change in strain with loading cycles for sample II, (maximum 3000 N).....	76
Figure 4.11 a, b) SEM images at different through thickness positions for sample II, . (maximum 3000 N).....	77
Figure 4.11 c) SEM images at different through thickness positions for sample II, (maximum 3000 N).....	78
Figure 4.12 Variation of percentage change in electrical resistance in a) in-plane and b) through-thickness positions with loading cycle for sample III, (maximum 3000 N) .....	79
Figure 4.12 c) Variation of change in strain with loading cycles for sample III, ..... (maximum 3000 N).....	80

Figure 4.13	a) SEM images at different through thickness positions for sample III, (maximum 3000 N).....	80
Figure 4.13	b, c) SEM images at different through-thickness positions for sample III, (maximum 3000 N).....	81
Figure 4.14	Variation of percentage change in electrical resistance in a) in-plane and b) through-thickness positions with loading cycle for sample IV, (maximum 3000 N).....	83
Figure 4.14	c) Variation of change in strain with loading cycles for sample IV, (maximum 3000 N).....	84
Figure 4.15	a) SEM images at different through thickness positions for sample IV, (maximum 3000 N).....	84
Figure 4.15	b, c) SEM images at different through thickness positions for sample IV, (maximum 3000 N).....	85

## List of Tables

Table 2.1	Dispersion sequences with different shearing intensity.....	23
Table 3.1	Typical properties of Multiwall carbon nanotubes (MWCNTs) .....	37
Table 3.2	Typical properties of Epon 862 .....	38
Table 3.3	Typical properties of Epicure W .....	39
Table 3.4	Typical properties of S-glass fiber.....	41
Table 3.5	Number of passes through calendering machine with different gap distance	42
Table 3.6	Test schedule of different samples above first-ply-failure load .....	54
Table 3.7	Test schedule of different samples below first-ply-failure load .....	54

# CHAPTER 1

## Framework and Scope of the Current Work

### 1.1. Introduction

Fiber reinforced polymer (FRP) composite materials are widely used in aerospace applications. Fatigue behavior of FRP composite materials is significantly different from its metal counterpart and often becomes a dominant factor in determining the competitive advantages over one another. Fibers such as carbon, glass, boron or kevlar exhibit excellent specific properties and exceptional fatigue strength which lead to their successful application in the aeronautic industry. However, the detection and monitoring of fatigue damage of composite materials have become a growing concerns in maintaining and controlling their engineering integrity while in operation. Measurement of the change in electrical resistance during loading of a composite material part is one of the most attractive methods among the various available damage detection and monitoring techniques because of its effectiveness, simplicity, less expense and easy handling characteristics. Further, this technique enables the detection of damage in situ without any weakening effect on the part being tested. However, the main limitation of this technique evolves due to the requirement of electrical conductivity of the part being tested. This limitation can be overcome by making the part conductive by using carbon nanotubes. Carbon nanotubes possess extraordinary properties with high stiffness and strength, exceptionally high thermal and electrical conductivity [1-3]. The integration of conductive carbon-nanotubes (CNTs) in conventional, fiber reinforced polymers (FRPs) initiates the possibility of making non-

conductive materials, combined with high mechanical efficiency. On the other hand, carbon nanotube fillers can impart a strain sensing functionality to a composite laminate. As mechanical deformation causes changes in electrical resistivity of a conductive composite part, carbon nanotube serves as an excellent candidate for potential sensing materials. This sensitivity of carbon nanotube fillers to strain can be effectively utilized to detect the extent and rate of defects that may arise from the strain inputs. A small percentage of multi-walled CNT is first dispersed into the host matrix before fabricating the composite part. When subjected to some static or dynamic strain inputs, the electrical resistance of the nanocomposite changes, which, in turn, affects the electrical conductivity of the laminate. It is possible for carbon nanotubes to form a conductive network in the fiber/polymer matrix and make a non-conductive composite like glass/epoxy conductive [4, 5]. For a conductive composite structure the mechanical deformation and the electric resistance are closely connected. Thus the conductive carbon nanotube network can act as an inherent sensor when the composite part is subjected to any damage. Thostenson et al. [4, 5] showed that when carbon nanotubes are dispersed properly in glass fiber composites, a continuous conductive network of sensors is produced. These carbon nanotube based composites have potential for detecting the formation of cracks because of their piezoresistive (deformation/resistance change) behavior. During cyclic loading, due to formation of cracks, the resistance/strain relations show substantial hysteresis. The co-relation of strain and direct current resistance measurements enables tracking of damage accumulation during cyclic loading. The objective of this work is to examine the sensitivity of CNT networks for detection and monitoring of fatigue damage and to compare the effectiveness of electrical resistance method

for the same, particularly between in-plane and through thickness positions of the GFRP composite laminate.

## **1.2. Motivation**

A reliable and easily applicable method for damage detection and health monitoring of composite materials offers better utilization of the great specific mechanical properties of composite materials. At the same time, it improves the durability and safety of the structure. During the last decades, a number of damage detection by non destructive evaluation technique was in use although most of them were not suitable for in situ damage detection. This is because; some of these methods require special laboratory set ups to analyze the damage conditions. The electrical resistance measurement technique is the best method in this regard as it allows in-situ measurement with simplicity and low cost without compromising the properties of host materials. Carbon nanotubes are incorporated into the host matrix of glass fiber reinforced polymer composite (where both the matrix and reinforcement are non-conductive) to make it conductive which facilitates the application of electrical resistance measurement as a damage sensing technique. The outstanding thermal and electrical properties combined with their high specific stiffness and strength, and very large aspect ratios ( $l/d$ ) and surface area have motivated many researchers for the development of nanotube incorporated composites for both structural and functional applications. In this thesis multi walled carbon nanotubes (MWCNT) are used as they offers the highest potential for enhancement of electrical conductivity in polymer composites. As a result, even at very low concentration, MWCNT can create a conductive network in interfacial surface area when well dispersed in polymer resin system. At the same

time, the incorporation of MWCNT improves the mechanical properties and increases the fatigue life of the composite structure.

Many researchers investigated the fatigue damage of fiber reinforced polymer composite which is a critical concern for most of its structural applications. In a few recent research works [6-13], it is established that electrical resistance measurement is more sensitive than any existing methods for damage detection. The electrical resistance is very sensitive to the formation of micro damage in a structure which changes in a regular pattern making it easy to detect and characterize the extent of damage in the composite structure. Thus, incorporation of carbon nanotube into GFRP composite is an attractive choice in monitoring fatigue damage via the measurement of change in electrical resistance. In conjunction with longitudinal and in-plane transverse resistance, the through-thickness electrical resistance can be utilized in developing simple and cost-effective means of health monitoring of GFRP laminated composites. From this motivation, a series of experiments have been designed and carried out to accomplish the objectives of this work.

### **1.3. Thesis framework**

In the first chapter of the thesis, the importance of studying the fatigue damage behavior of FRP composite structure is realized. The attributes of electrical resistance measurement technique in detecting damage in composite structure are identified. The application of carbon nanotube in the GFRP composite as a conductivity imparting material is recognized. The sensitivity and effectiveness of this damage detection technique in relation to the piezoresistive behavior of carbon nanotube incorporated GFRP composite is briefly discussed. Finally, the overall motivation behind the current work and objectives of the present work is described.

In the second chapter, a detailed literature survey has been carried out. The review premise includes different types of non destructive evaluation technique for monitoring damage in composite structure. Synthesis, properties and application of carbon nanotube, their conduction mechanism in non-conductive host matrix are addressed. Further, the percolation behavior of CNT, their methods of dispersion with relative advantages and limitations and their effect on electrical and thermal properties of the composite material are discussed in detail. Finally, the related works in this area carried out by various researchers are reviewed and analyzed in detail. A brief summary of the literature survey and objectives of the thesis are given at the end of this chapter.

The design of experiments, fabrication of samples and experimental set ups are described in chapter 3. The physical and chemical properties of the materials (i.e. carbon nanotube, epoxy resin, curing agent, long fiber) used in the current work are given at the beginning of the chapter. The arrangement of electrical connections, selection of various load levels and test schedules for different composite specimens are illustrated.

Tensile and fatigue test results are summarized in chapter 4. The changes in resistance with different maximum loading under different number of cycles are analyzed. The results from numerous experiments carried out in this work are correlated and discussed in details.

The significant outcomes of this work are presented in chapter 5. Finally, the contribution of this work to the knowledge and better understanding in this field of study along with the suggestions for future improvements are given.

# CHAPTER 2

## Literature Review

### 2.1 Fatigue in composites materials

The replacement of metals by composite materials is an achievement for aeronautical applications. However, fatigue of composite materials is an important problem from an engineering point of view as fatigue behavior of composite materials differs significantly from that of metals. For long time fatigue, the maximum stress can be reached in 60% to 80% of the ultimate stress in composites materials, while with metal only 30% of the ultimate strength can be reached [14]. Crack initiation and multiplication are the two main stages of fatigue process in composite materials whereas in metals a single dominant crack initiates and propagates to final fracture. While in metals, crack growth accelerates during fatigue, the crack multiplication in composites decelerates, resulting in the uncontrolled final fracture of composite [14]. In actual practice, composites are used in the form of laminates with different orientations of the plies. As a result, some plies are weaker in the loading direction and, consequently, crack initiation which causes the failure of the first weakest ply takes place very early in the fatigue life of composites. Physically, ply failure is defined by the presence of micro-cracks which initiates at the location of high stress concentration and low strength. When a crack is formed in homogeneous, isotropic materials, it grows rapidly until leading to final fracture. But in composite materials, visible cracks do not lead to immediate fracture. They grow in such a way that may reduce stress concentrations. Decrease of modulus may arise because they take place throughout the volume of weak plies in a laminate [15]. In particular, the fatigue behaviour of composite laminate depends on the various damage mechanisms such as transverse cracks, delamination, debonding,

edge effects, thickness and stacking sequence [16,17] . Different damage mechanisms and the crack propagation of composite materials are illustrated in figure 2.1 as compared to metal in figure 2.2.

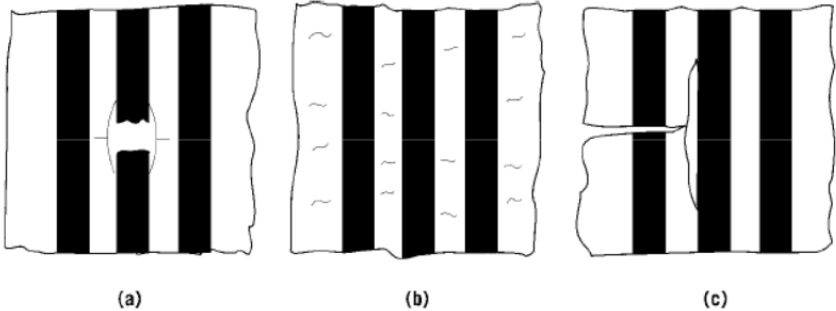


Figure 2.1 Damage mechanisms in fibre-reinforced composites a) Fibre cracking b)Matrix cracking c) Interface debonding [18]

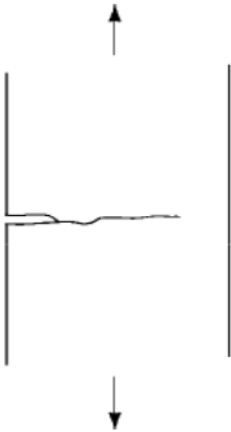


Figure 2.2 Crack propagation in an isotropic material. The crack propagates in a direction perpendicular to the cyclic loading axis [18]

Thus, the detection and monitoring of fatigue damage of composite materials is a vital issue in many engineering applications. The various available methods for this are described in the following sections.

## **2.2 Damage monitoring in composite materials**

Damage in composites, especially, fatigue damage can be detected simply by monitoring the variation of loads. Most of the literature involving the study of the fatigue behavior of composites focuses on the changes in macroscopic-scale mechanical properties. The degradation of the material is characterized in terms of reduction of stiffness and fatigue-life curves. The stiffness and strength degrade with increasing fatigue cycles due to the formation of microstructural damages [19-23]. Thus the development of damage during fatigue loading can be studied by continuously monitoring the reduction in stiffness using strain gauges [24-26]. Although the change in the elastic modulus of fiber reinforced composites with the accumulation of cracks is often utilized as a relative measure of damage, the accumulation of cracks in the matrix results in relatively small changes in elastic modulus since the elastic properties of the composite are dominated by the load-carrying fibers [6].

A number of nondestructive evaluation (NDE) techniques such as, ultrasonic, eddy current, radiography, dye penetrants, magnetic particles, fiber optical sensor, electrical resistance methods are available. Among them electrical resistance and fibre optical sensors are more popular in industry in recent times because of their greater reliability, accuracy, simplicity and applicability in situ.

Recently, researchers have focused on using the embedded sensor like optical fibers inside the composite structure for its health monitoring. Crane [27] demonstrated that optical fiber systems were capable of detecting damage in glass fiber-reinforced structures. He indicated that optical

fibers embedded in structure during lay-up could detect damage in the composite by fracturing itself. Light transmitted through an optical fiber has been shown to drop substantially whenever a fiber is fractured [28]. By monitoring the light transmitted through the fiber, the damage state of the structure can be determined [29]. However, embedding optical fibers inside composite structures can significantly degrade its mechanical properties.

On the other hand, the electrical resistance measurement technique or piezoelectric method which utilizes the piezoelectric characteristics of material is free from most of the practical limitations of embedded sensors like optical fibers. It can monitor continuously the damage of composite structures without producing any defects. It's only significant drawback is that this method can only be applied for electrically conductive materials such as carbon fiber reinforced polymer (CFRP) composite where carbon fibers itself are utilized as sensors. This technique cannot be directly applied in the case of non-conductive material such as glass fiber reinforced polymer (GFRP) composites where both glass fibers and polymer matrix are non-conductive. In such case [30], matrix filler such as carbon black (CB) or carbon nanotubes (CNT) which have excellent conductive properties are incorporated into the material in order to impart sufficient electrical conductivity. These filler materials can build a conductive network inside the non-conductive matrix region and thus CB and CNT adopt the responsibility of a resistance sensor. Since carbon nanotubes are used as sensors in the current work, their development, configurations, and working principles are discussed in detail in the following sections.

### **2.3 Carbon nanotubes**

A new field of novel materials is developed after discovering of the C<sub>60</sub> fullerene molecule by Kroto, Heath and Smalley in 1985 and the subsequent discovery of carbon nanotubes by Iijima in

1991 [31]. Based on carbon nanotubes chirality (i.e. atomic structural variation), they can be metallic or semi-conductive as chirality have strong impact on the electronic properties of nanotubes. Nanotubes can be single walled, double walled or multi-walled [32]. A nanotube with just one cylinder is referred to as a single-wall nanotube. A Single-Walled Carbon Nano Tube (SWCNT) is formed by wrapping a single sheet of graphite (graphene) into tubular forms (shown in figure 2.3). The conducting properties of a graphene tubule mainly depend on the nature of wrapping (chirality) and the diameter (typically, SWCNTs have diameters in the range 0.4nm-2nm) [33]. Other varieties of SWCNTs include ropes, bundles and arrays [1] and few of them are shown in figure 2.4 (a).

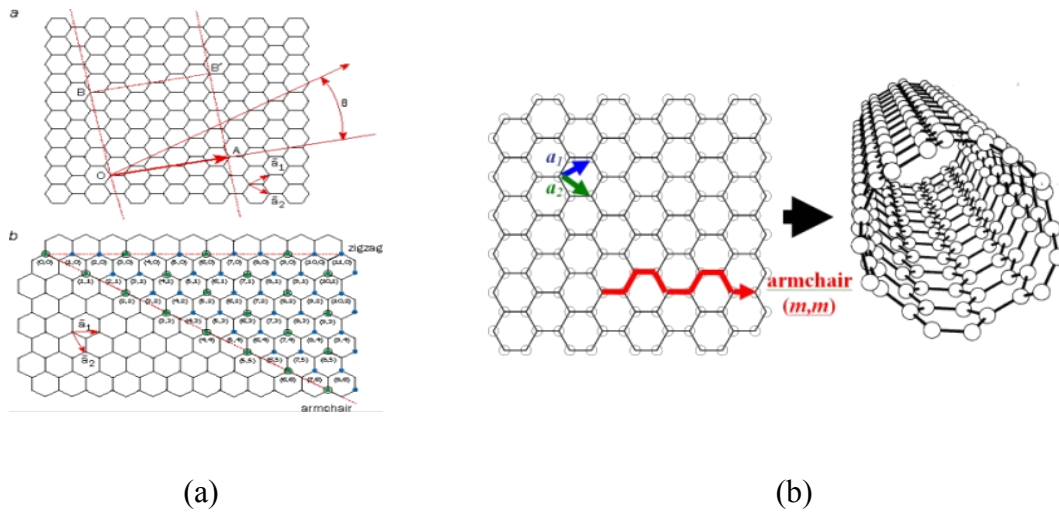


Figure 2.3 a) Graphene sheet b) SWCNT is formed by wrapping a grapheme sheet into a cylinder [34]

A nanotube can also contain multiple cylinders of different diameters nested inside one another. This type is called a multi-walled nanotube as shown in figure 2.4 (b). Multi-Walled Carbon Nanotubes (MWCNTs) are composed of a number of concentric single-walled carbon nanotubes (SWCNTs).

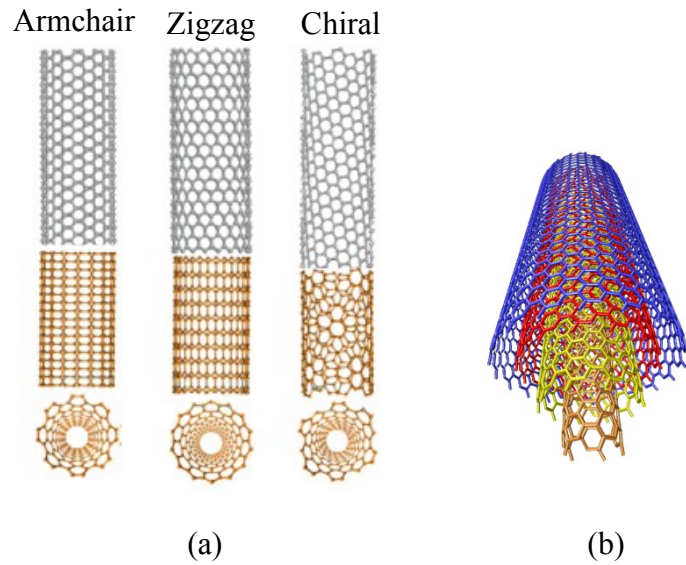


Figure 2.4 a) Different types of SWCNT [34] b) MWNT formed by several SWNTs [35]



Figure 2.5 Three types of CNT [36]

Figure 2.5 shows three different types of CNT based on the number of walls. Both SWCNTs and MWCNTs have been utilized for reinforcing thermoset polymers (epoxy, polyimide, and phenolic), as well as thermoplastic polymers (polypropylene, polystyrene, poly methyl methacrylate (PMMA), nylon 12, and poly ether ether ketone (PEEK)). However, in this work, MWCNTs are used for the purpose of imparting conductivity to the GFRP composite laminate.

### **2.3.1 Synthesis of Carbon Nanotubes**

There have been a variety of techniques for producing carbon nanotubes. Iijima [37] first observed multi-walled nanotubes, and Iijima et al. [38] and Bethune et al. [39] reported the synthesis of single-walled nanotubes. Most important synthesis methods for single and multi-walled carbon nanotubes include arc-discharge, laser ablation, gas-phase catalytic growth from carbon monoxide and chemical vapor deposition (CVD) methods from hydrocarbons. For application of carbon nanotubes in composites, large quantities of nanotubes are required, and the scale-up limitations of the arc discharge and laser ablation techniques would make the cost of nanotube-based composites prohibitive. During nanotube synthesis, impurities in the form of catalyst particles, amorphous carbon, and non-tubular fullerenes are also produced. Thus, consequent refinement steps are required to separate the tubes. The gas-phase processes tend to produce nanotubes with fewer impurities and are more willing to large-scale processing. Erik et al. [1] found that for nanotubes growth, the gas-phase techniques, such as CVD, has the greatest potential for increasing the nanotube production for the processing of composites.

### **2.3.2. Properties and application of carbon nanotubes**

The curling of a graphitic sheet to form carbon nanotubes produces a class of materials that have extraordinary electrical and mechanical properties. In particular, the high elastic modulus of the graphite sheets means that the nanotubes might be stiffer and stronger than any other known material, with beneficial consequences for their application in composite bulk materials and as individual elements of nanometre-scale devices and sensors. The multi-walled carbon nanotubes can be bent repeatedly through large angles using the tip of an atomic force microscope without

undergoing catastrophic failure. As a result of the high-strain deformation responses, nanotubes are remarkably flexible and resilient [40].

The properties of nanotubes depend on atomic arrangement, the diameter and length, and the morphology, or nano structure. Numerous investigators have reported remarkable physical and mechanical properties of carbon nanotubes. Theoretical and experimental results have shown extremely high elastic modulus, greater than 1 TPa (the elastic modulus of diamond is 1.2 TPa) and reported strengths 10–100 times higher than the strongest steel at a fraction of the weight [41]. Extremely large thermal conductivities have been theoretically predicted in terms of the strong carbon *sp*<sup>2</sup> bond network of the CNTs [42]. The three dimensional anisotropic structure of nanotubes leads to the anisotropic nature of their electrical and thermal transport properties. The electrical conductivity of the MWCNT films exhibit anisotropic characteristics with respect to the nanotube axis. Heer et al. [43] have investigated the electrical conductivity of aligned MWCNT films which is found to be around 1000  $\Omega$ /m along the nanotube axis and 150  $\Omega$ /m perpendicular to the nanotube axis, respectively, at room temperature. They [43] also demonstrated a strong anisotropic electrical transport characteristic of MWNTs.

These exclusive features of carbon nanotubes attract numerous researchers in many fields around the globe and thus the scope of their application is very broad. Carbon nanotubes (CNTs) are promising materials for nanoscale molecular devices due to their tiny structure, high chemical stability, high tensile strength, and unique electrical properties. Multi-walled carbon nanotubes (MWNTs) can be used as nanowires since they possess much higher current carrying capability than those of metallic wires of the similar dimension [44]. High current induced damage is expected to be avoided due to their high heat-transfer capability. MWCNT films have been

demonstrated to be excellent candidates for electron field emitters, integrated circuit heat sink and conducting materials because of their unique electrical and thermal properties [45-47]. Both the electrical and thermal properties of MWNTs are also critical for their practical applications in microelectronics devices. The anisotropic characteristics of nanotubes also determine the performance when they are employed in nanoelectronic devices.

On the other hand, the outstanding thermal and electric properties combined with their high specific stiffness and strength, and very large aspect ratios ( $l/d$ ) and surface area have motivated the development of nanotube incorporated composites for both structural and functional applications [1, 48, 49]. Dispersion of nanotubes in composites plays a crucial role in determining the effectiveness of its intended application. Li et al. [50] computed the elastic deformation of single-walled carbon nanotubes and found that the Young's moduli of carbon nanotubes vary with the tube diameter and are affected by their helicity. Larger diameter nanotubes show a lower effective modulus and occupy a greater volume fraction in the composite relative to smaller-diameter nanotubes. While there is a slight increase in elastic modulus at a given nanotube diameter and volume fraction with increasing nanotube length, the diameter of the nanotubes plays the most significant role in determining the composite elastic modulus. This strong diameter-dependence of the composite elastic modulus highlights the need to accurately model the dispersion of nanotube diameters in the composite [51]. The MWCNTs have a much larger diameter and consist of several concentric walls. These nanotubes provide a specific surface area (SSA) of only  $200 \text{ m}^2/\text{g}$  or less. Therefore, MWCNTs exhibit a much better dispersibility but smaller interface for stress transfer and a lower aspect ratio [52].

The electrical conductivity of individual carbon nanotubes is in the order of  $10^4$ – $10^7$  S/m [53]. In their recent study, Gojny et al. [54] concluded that multi-walled carbon nanotubes offer the highest potential for enhancement of electrical conductivity in polymer composites.

Incorporation of carbon nanotubes with nanometer-level diameters into fiber reinforced polymer composite, thus, provides unique opportunity for the development of multi-functional materials, e.g., conductive polymers with improved mechanical performance and with a perspective of damage sensing and “life”-monitoring [55]. The sensitivity of CNT incorporated composites to its deformation, i.e., its piezoresistive features, determines the effectiveness of the in situ damage monitoring ability.

### **2.3.3. Conduction mechanism with CNTs in composite laminate**

Polymeric matrix composites are usually considered as non-conductive materials because of their extremely low electrical conductivity (in the order of  $10^{-10}$ – $10^{-15}$  S/m) [56]. The presence of conductive particles in an insulating material can change the composite system's electrical conductivity. Dispersion of conductive materials into the non-conductive matrix can form conductive composites. For example, the addition of carbon nanotubes to the epoxy stimulates the initiation of electrical conductivity in the material. The conductivity depends critically on the volume content of the filler. For very low filler fractions, the mean distance between conducting particles is large and the conductance is limited by the polymer matrix. When a sufficient amount of conductive filler is loaded, the conductive filler particles get closer and form insulator-to-conductor transitions and make a continuous linkage which results in an initial conducting path through the whole material where current can flow. The phenomenon is known as percolation and can be well explained by classical percolation theory [57]. The corresponding filler content

is called the percolation threshold. In this concentration range, the conductivity can change drastically by several orders of magnitude for small variations of the filler content. Finally, at high loading of the filler, the increasing number of conducting paths forms a three-dimensional network. In this range the conductivity is high and less sensitive to small changes in volume fraction. In order to create a well conducting polymer composite, the filler's conductivity has to be much higher than the matrix and four different conduction aspects have to be taken into account. These include the conduction in the polymer matrix, in the filler material, between adjacent filler particles and from the filler into the matrix and vice versa. [56].

Carbon nanotubes can penetrate the matrix-rich areas between fibers in individual bundles as well as between adjacent plies. As a result, it is possible to achieve a percolating nerve-like network of sensors throughout the arrays of fibers in a composite, as illustrated in figure 2.6. By first dispersing carbon nanotubes in an epoxy polymer matrix and infusing throughout a fiber perform, a conductive percolating network is formed [58].

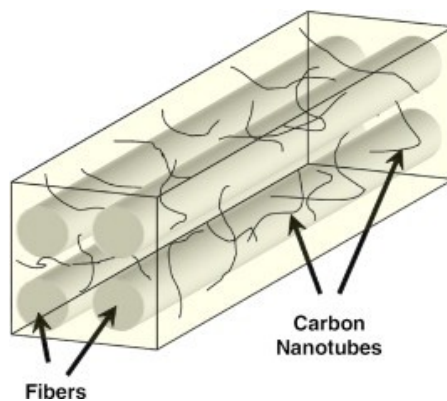


Figure 2.6 Three-dimensional model showing the penetration of nanotubes throughout a fiber array due to their relative scale [58]

### **2.3.4 Percolation behavior and electrical conductivity**

The percolation behavior, as discussed earlier, plays an important role in the damage sensing process. The electrical percolation threshold of conductive fillers embedded in an insulating matrix is sensitive to the geometrical shape of the conductive phase. The small size and large aspect ratio are helpful to lower the percolation threshold [59, 60]. As carbon nanotubes have tremendously large aspect ratios (100–10,000), many researchers have observed exceptionally low electrical percolation thresholds for CNT incorporated polymer composites. Sandler et al. [61] and Moisala et al. [62] have reported ultra-low percolation thresholds for MWCNT composites. Sandler et al. [61] showed that electrical percolation threshold in epoxy composites can be achieved at an average CNT loading of approximately 0.005 wt.%. Moisala et al. [62] identified the electrical percolation threshold of 0.005 wt. % for MWCNT/epoxy composites, and 0.05–0.23 wt.% for SWCNT composites. Bryning et al. [56] reported very low percolation thresholds in single-walled nanotube composites. Thostenson and Chou [63] examined the influence of the nanoscale structure on the composite electrical properties. In their work, composites were processed using the calendering technique of dispersion in order to obtain a highly dispersed structure and a dispersed and partially agglomerated structure. For both structures, the composites exhibited percolation thresholds below 0.1 wt%. Depending on the matrix, the processing technique, and the nanotube types used, percolation thresholds ranging from 0.001 wt% to more than 10 wt% have been reported [57, 64, 65].

Gojny et al. [58] performed an extensive experimental study on the electrical conductivity of CNT/epoxy composites. The results were presented with the influences of types of nanotubes (SWCNT, DWCNT and MWCNT), the significance of surface aminofunctionalization, as well as the content, dispersibility, aspect ratio and specific surface area. They [58] adopted the

criterion of percolation threshold as the filler content to achieve a conductivity of  $10^{-6}$  S/m. Their [58] results of specific conductivity vs. filler content (figure 2.7) indicate some significant trends. The lowest percolation thresholds were observed for non-functionalized CNTs, while 0.75 wt. % carbon black (CB) were required to achieve a comparable conductivity.

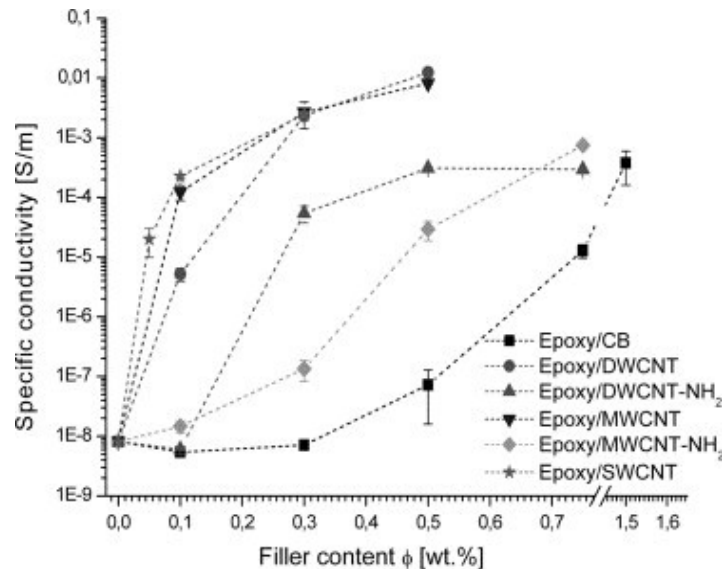


Figure 2.7 Electrical conductivity of the nanocomposites as function of filler content in weight percent [58]

The percolation threshold, defined as the filler content to achieve a conductivity of  $\sigma \geq 10^{-6}$  S/m, occurred at lower concentration for fiber-shaped fillers (high aspect ratio) than for spherical particles. The lowest percolation thresholds were observed for the non-functionalised CNTs, being in all cases below 0.1 wt% CNTs, while 0.75 wt% CB were required to achieve a similar conductivity. The overall conductivity of these composites turned out to be insignificantly influenced by the structural quality (graphitization) of the CNTs [63].

Schulte et al. [66] examined the variation of electrical conductivity as a function of filler content for different types of MWCNT which is shown in figure 2.8. They found that aligned CVD-grown MWCNTs possess a higher potential for producing highly conductive epoxies due to their

very high aspect ratio and thus less number of tunnelling contacts. The inclusion of aligned-CVD-MWCNTs also leads to epoxy nanocomposites with a very low percolation threshold. CVD-MWCNTs thus seem to be favorable for an electrical modification of epoxies [66].

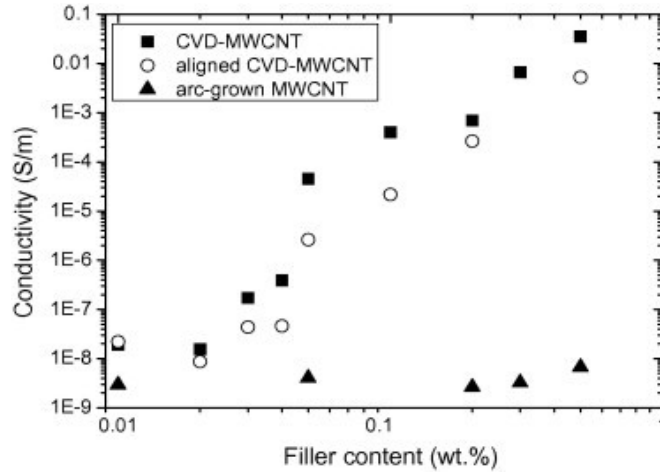


Figure 2.8 Percolation curve of the nanocomposites as a function of weight percent of MWCNTs [66]

They [66] also explained the electrical conductivity of the two CVD-MWCNT systems as a function of volume filler content normalized by the calculated densities and observed similar results. From their result shown in figure 2.9, the volume percolation thresholds seem to be comparable. Furthermore, the conductivities at high filler content for both CVD-MWCNT modifications range lie within the same order of magnitude as observed in [67]. Since the electrical conductivity of particle filled polymers is strongly dependent on the number of tunnelling contacts, it seems likely that both CVD-MWCNT and aligned-CVD-MWCNT systems exhibit similar nanotube–nanotube contact distances [67]. Contrarily, it was found in [66] that the intrinsic CNT conductivity is not an important parameter for the electrical properties of CNT nanocomposites. Other parameters such as state of dispersion/reagglomeration, CNT

length or CNT diameter are found to be more important since the controlling tunnelling mechanism of charge carriers is strongly dependent on these parameters [66].

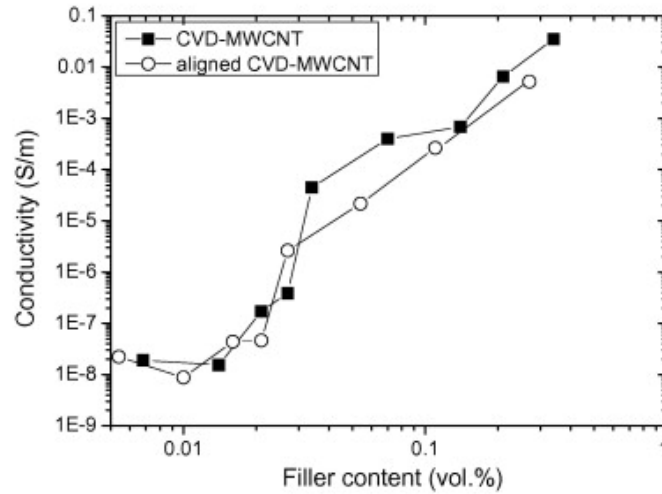


Figure 2.9 Percolation curve of the nanocomposites as a function of volume percentage of MWCNTs [66]

Figure 2.10 shows the volume resistivity of epoxy/carbon nanotube composites as a function of carbon nanotube loading as found in [6]. The volume resistance of the composite decreases with increasing weight fraction of nanotubes.

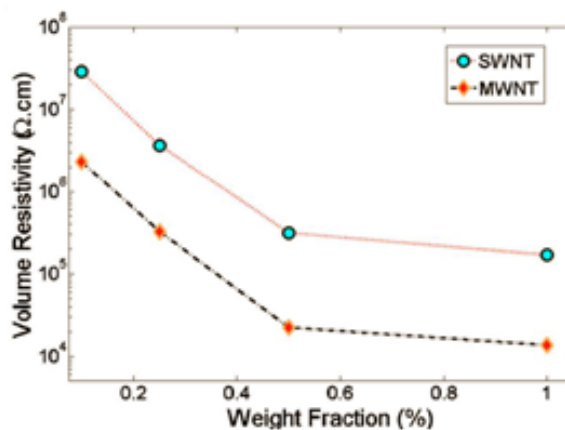


Figure 2.10 Volume resistivity of the thermosetting Epoxy-2000 resin as a function of weight fraction of nanotube additives [6]

Interestingly, MWNT gave an order of magnitude reduction in resistivity compared to SWNT over the full range of weight fractions that were tested in [6]. Over two orders of magnitude reduction in the volume electrical resistivity of the composite material was observed as the weight fraction of nanotube fillers was increased from 0.1% to 1% as shown in figure 2.10.

### **2.3.5 Dispersion techniques**

The better utilization of the CNT properties in polymers is related to their uniform dispersion in the matrix or an exfoliation of the agglomerates and a good wetting/adhesion with the polymer [1]. However, MWCNTs are difficult to be dispersed in polymers due to the strong intermolecular van der Waals interactions among the nanotubes, which can lead to the formation of aggregates [68, 69]. Functionalization of the surface of MWCNTs is a solution to improve the compatibility between MWCNTs and polymers [70-72].

Among the various dispersion techniques, stirring, extrusion, kneading etc. are either limited in capacity or not powerful enough to separate the agglomerates into individual nanotubes. One common technique to distribute CNTs in epoxies is the sonication technique. A pulsed ultrasound separates the CNTs within agglomerates and disperses them in the matrix effectively. However, this method is only convenient for small batches due to the extreme reduction of the vibrational energy with increasing distance from the sonic tip [55]. For thermoset polymer composites, calendering (three-roll mill) is one of the new nanotube dispersion methods for the development of high volume, high rate and cost-effective manufacturing of nanocomposites.

Some researchers [54, 73] obtained very effective exfoliation and dispersion of nano-scaled particles in epoxy resin by the use of a three-roll calander. A three-roll mill as shown in figure

2.11 is usually used to disperse/exfoliate the nanoparticles in an epoxy matrix. The condition of flow of the nanotubes when processed in this type of machine is also shown in the figure.

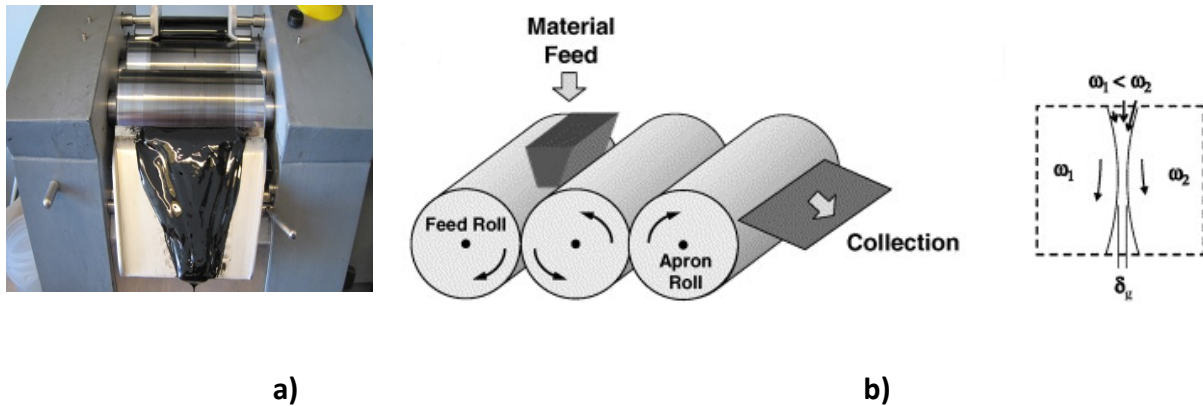


Figure 2.11 a) Three-roll mill for dispersing nanotubes b) The flow conditions in the roller clearance [63]

The advantage of calanders over other common dispersion methods is the possibility of scaling-up the capacity without losing the efficiency of the distribution. Another important advantage of this method over the sonication method is the homogeneous introduction of shear forces over the whole volume of the composite on the rolls while the sonication process introduces the energy locally. Thus, a significant shortening of the nanotubes is not caused by this processing [65].

Gojny et al. [73] compared the efficiency of the achieved dispersion of nanotubes by calandering and sonication techniques. They found the common shear-mixing technique (calandering technique) provides the best dispersion of the nanotubes in an epoxy resin. This method is highly efficient and environmentally friendly for achieving high levels of exfoliation and dispersion within a short period of time. A further improvement of the functional properties of nanotube/epoxy-composites can be achieved by the variation of the processing parameters.

Thostenson et al. [63] investigated the use of a laboratory scale calendering method for dispersion of CVD grown multi-walled carbon nanotubes in an epoxy matrix. It was revealed in their work that the shear mixing induced by the calendering method results in high degree of nanotube dispersion and forms a conductive percolating network at concentrations below 0.1% by weight. The thermal conductivity also increased linearly with nanotube concentration to a maximum increase of 60% at 5 wt. % carbon nanotubes.

Rosca and Hoa [74] explained the influence of the processing parameters for dispersion of carbon nanotubes in polymer matrix. According to their work, mainly two parameters, namely, shear intensity and number of passes of material between the rolls, control the degree of dispersion of CNTs into polymer matrix. The shear intensity was controlled by adjusting the gap between the rolls and the revolving speed. They combined several parameters into groups on the basis of shear intensity as Low (L), Medium-low (ML), Medium-high (MH) and High (H) as shown in Table 2.1. They concluded that, the medium-low milling sequence gives the best conductivity at 1 wt% loading for most of the nanotubes.

Table 2.1 Dispersion sequences with different shearing intensity [74]

<b>Shear intensity</b>	<b>Parameter combination [gap (μm)-speed (rpm)-passes]</b>	<b>Acronym</b>
Low	[50-100-2]-[20-100-1]	L
Medium-low	[50-100-2]-[20-100-1]-[10-100-3]	ML
Medium-high	[50-100-2]-[20-100-1]-[5-100-3]	MH
High	[50-100-2]-[20-100-1]-[5-500-3]	H

In this work, 1 wt% MWCNT has been incorporated into the GFRP composites using the three-roll mill following the Medium-low (ML) mixing scheme followed by Rosca and Hoa [74].

## **2.4 Fatigue damage monitoring in composite laminates**

The damage behavior of composites, such as, the initiation and evolution of damage under fatigue loading is usually different than those of other loading conditions. Fatigue performance is generally governed by the matrix and fiber/matrix interface properties. Flaws or minute cracks initiated in the matrix can propagate during cyclic loading and ultimately lead to final failure of the composite [41, 75]. In most advanced composites, the early damage process comprises an increase in the crack density rather than the crack growth. Following initial transverse ply cracking, delamination may eventually develop which can also be preceded by the transverse ply cracks. Actually, transverse cracking may exist in the initial state which might be caused during the processing due to the mismatch in thermo mechanical properties between adjacent plies [76]. As the current work deals with the damage sensing capability of electrical resistance method of CNT incorporated non-conductive composites under fatigue loading, the subsequent sections are devoted to the review of the related earlier works, with focus on the glass/epoxy composite system.

### **2.4.1 Monitoring fatigue damage of composite laminate by electrical resistance measurement**

Electrical resistance measurement, as discussed earlier, is one of the attractive methods allowing in-situ observation of possible degradation of composite parts thus predicting serious damage or failure under static or fatigue loading. Special attention to the load-carrying fibres is needed as the failure in FRP composite is always coupled with fibre failure [77]. The piezoresistive

(deformation/resistance coupling) behavior in nanotube incorporated composites has expanded the use of CNTs as sensing materials. Strain sensing is possible by tracking the deformation/resistance behavior and nanotubes can detect the formation of microscale cracks in polymer matrix. Due to the extremely small size of carbon nanotubes relative to the microscale crack, the formation of a crack in the matrix breaks conducting pathways in the percolating nanotube network. This capability is unique to nanostructured composites as a nanoscale conductor is required to sense a micron-sized crack. [78, 79]

For multi-walled nanotubes grown by the CVD process, there is a high degree of nanoscale entanglement and interlacing of the nanotubes which prevent dispersion. The elastic properties of the composite are dominated by the plies with fibers oriented in the direction of load. Therefore, the accumulation of cracks in the transverse plies results in only a slight degradation in elastic modulus but the development of microcracks affects the long-term durability and performance of fiber composites. While laminate stiffness is relatively insensitive to the accumulation of damage, the resistance response shows a much higher sensitivity to the accumulation of cracks [80]. Thus this method can more reliably predict the degradation of parts as compared to the stiffness monitoring method.

#### **2.4.1.1 Fatigue damage monitoring in conductive FRP composites**

In carbon fibre reinforced polymer, the electrically conductive carbon fibres are used as electrical resistors. When there is an applied strain, the overall cross section of the carbon fibres decreases as a result of the Poisson effect and this is used for the correlation between strain and measured resistance [7]. When electrically conductive carbon fibers are broken, large changes in composite electrical properties occur. Thus, carbon fibers hold the potential for self-sensing of damages and

no embedded CNT networks are essential for this purpose. Wang and Chung [8], Irving and Thiagarajan [9], Kupke et al. [10] and Seo and Lee [11] utilized this self sensing capabilities of CFRP composites to evaluate the effectiveness of electrical resistance method in monitoring damage evolution under fatigue loading. Naturally, they did not use additional CNT networks inside the composites.

Wang and Chung [8] demonstrated the sensing of delamination in cross-ply carbon-fiber-reinforced polymer composites, made from carbon fiber prepreg tape, under fatigue loading by tracking through-thickness electrical property changes.

Irving and Thiagarajan [9] studied fatigue damage in unidirectional and cross-ply carbon fiber composites made from prepregs using electrical resistance measurement in the longitudinal direction. He found that the resistance change contained both reversible and permanent components. They concluded that the initial resistance changes which occurred during the first few thousand cycles could be correlated with the ultimate fatigue life. They concluded that the fatigue life of CFRP composite laminates might be predicted from monitoring of resistance changes in the longitudinal direction. Although the inherent conductivity of the carbon fiber shows promise in the detection of damage in composites, the electrical properties are primarily sensitive to fiber breakage. Thus, the onset and accumulation of fatigue damage which initiates in the polymer matrix is less sensitive to the changes in bulk resistance [9]. However, Kupke et al. [10] found that it is possible to observe delamination processes and even to separate these from other damage mechanisms using the technique.

The change in strain, stiffness and longitudinal electrical resistance of unidirectional and cross ply CFRP specimens, made from prepregs, under fatigue loading was studied by Seo and Lee [11]. Their fatigue tests showed a very similar trend in stiffness and electrical resistance. They

recommended the longitudinal electrical resistance change as a damage parameter representing the fatigue damage.

Zhang et al. [6] on the other hand, studied the fatigue damage in the vicinity of artificially induced stress concentrations in CFRP composite specimens embedded with additional CNT additives. They made laminate specimens from MWCNT incorporated epoxy-2000 resin and twill-weaved graphite fibers and introduced artificial delamination in the central plies during the lay-up. They tested the specimens under fatigue loading while measuring its through-thickness resistance change. They demonstrated that the crack growth near the stress concentrations can be detected via through-thickness resistance measurement.

Vavouliotis et al. [12] and Kostopoulos et al. [13] studied the damage growth and propagation via monitoring the electrical conductivity during fatigue loading of unidirectional and quasi-isotropic  $[0/\pm 45/90]_{2S}$  CFRP laminates incorporated with MWCNTs. Specimens with different CNT contents were subjected to monotonous and cyclic tension tests and the resistance along the longitudinal direction was measured. They [12, 13] observed that fiber breakage and matrix cracking caused resistance to increase irreversibly. However, due to the conductive nature of both doped matrix and continuous fibers the two mechanisms of damage could not be easily distinguished.

Although the electrical resistance method has been established as an effective means for monitoring damage in CFRP composites, this technique is not suitable to composites where the fibers are non-conductive, such as glass or advanced polymer fibers. In addition, the technique is most sensitive to the fracture of the load carrying fibers and provides less information on the development of cracks in the polymer matrix, where the microscale damage is initiated [81]. Hence, the current work is dedicated to identify explicitly the moment of damage initiation and

subsequent monitoring of damage during fatigue loading of non conductive composites embedded with CNT network, specifically, the CNT incorporated glass/epoxy composites using the electrical resistance method.

#### **2.4.1.2 Fatigue damage monitoring in non-conductive FRP composites**

For composites where the load-carrying fibers are nonconductive, such as with glass or advanced polymer fibers, it is not directly possible to monitor the evolution of damage using electrical resistance method. This is because both matrix and fiber phases are nonconductive. In advanced composites, carbon nanotubes are frequently used to impart conductivity to the part enabling the effective monitoring of fatigue damage in situ.

Thostenson and Chou [5, 58, 82] established that the formation of electrically conductive carbon nanotube networks in glass fiber reinforced polymer composites combined with measurements of electrical resistance during static and cyclic loading, is a powerful technique for the monitoring of damage in the polymer matrix. They fabricated the fiber/epoxy composites using unidirectional non-woven glass fiber mats with Epon 862 epoxy and Epi-Kure W curing agent using vacuum assisted resin transfer molding (VARTM). Different composite specimens were tested under tensile and flexural loading but no cyclic loading in [58], under tensile and cyclic loading in [5] and only under cyclic loading in [82]. They placed electrodes by applying silver paints at the end of the specimens and measured electrical resistance between these two points in the longitudinal direction using a voltage/current meter and a customized computer interface which allowed recording the transient changes in resistance during the tests. [5] Loaded their specimens cyclically with increasing peak loads and observed the change in stress, strain and resistance for different concentration of CNTs. Both the stress and strain gage data were

observed to be followed by the instantaneous response of the in-plane resistance change per unit length (resistivity) confirming the sensitivity of this method to the applied deformation. [82] Studied the electrical resistance and strain response for first few loading cycles. They claimed to be able to detect the damage initiation during the third cycle of their test by observing very slight shift in resistivity-strain curve. However, their specimen failed only after 6 loading cycles apparently indicating much high peak loads which might cause substantial damage already during the beginning of the tests. They found striking similarity between the strain and resistance response up to a substantial progression of their tests and recommended an integration of these two in order to enable tracking of damage accumulation during cyclic loading. Comparing stiffness degradation with electrical resistance response they found electrical resistance to be much more sensitive and effective indicator of damage. They also introduced 'damaged resistance change' parameter to quantitatively evaluate the damage state. Contrary to current work, they did not study the through thickness resistance response under fatigue loading.

Gao et al. [81, 83-85] performed several works devoted to studying the damage sensing mechanism of CNT incorporated E-glass/epoxy composites using the electrical resistance method under incremental cyclic loading [81], quasi-static and incremental cyclic loading [83], fatigue loading [84], and quasi-static, incremental cyclic and fatigue loading [85] conditions in the same laboratory as in [5, 58, 82]. They also measured the electrical resistance between two points only in the longitudinal direction on their specimens similarly as in [5, 58, 82]. They used edge replication and optical microscopy to study the crack mode and growth in the specimen after certain cycles of loading. In [84, 85], the resin system used was vinyl ester monomer cured with styrene, cobalt naphthenate accelerator and cumene hydroperoxide initiator instead of Epon 862/Epi-Kure W resin system used in [81, 85] and the current work. They [83, 85] found that the

electrical response of the composite observed due to the crack re-opening and closing during cyclic loading can shed light on the microstructural mechanism of damage evolution. [81, 84, 85] examined the resistance response of the 0.5 wt% CNT incorporated cross-ply GFRP composite with varying thickness manufactured by VARTM technique. For all laminate configurations,  $[0/90_n/0]$   $n = 1, 2, 4, 5$ , they divided the general damage accumulation represented by stress-strain-resistivity (change in resistance per unit length) curves under incremental cyclic loading [81, 85] and resistivity-loading cycle-normalized modulus curve under fatigue loading [84, 85] into the three distinct stages according to the changes in slopes of the curves and validated it by the observation of edge replica. In their fatigue tests, [84, 85] used the peak load equal to 30% of the ultimate strength of the laminate and found a linear increase in specimen resistance up to 20% of the fatigue life. In these works, they have established the effectiveness of 'damaged resistance parameter' introduced by Thostenson and Chou [5] in evaluating the damage states quantitatively by means of curve fitting. They also demonstrated that 'damaged resistance' change is more effective indicator of the damage state than stiffness degradation.

Using the in-plane resistance measurements between two longitudinal points on the specimen in these above works of Gao et al. [81, 83-85], they attributed the initial linear increase of the in-plane resistance to the initiation of damage and could not find, in fact, any sharp signal identifying the initiation of damage. Beyond the initiation of matrix cracks, they [84, 85] correlated the non-linear behavior of in-plane resistances with the subsequent damages and major defects under fatigue loading. In the current work, on the other hand, electrical resistances are measured between several in-plane and through thickness points of the S-glass/epoxy laminate in order to compare their effectiveness in identifying explicitly the initiation and monitoring of damage under constant stress tension-tension fatigue loads.

Boger et al. [86] investigated the damage behavior of 0.3 wt% CNT and carbon black incorporated GFRP composite laminates produced by VARTM using the electrical resistance method under static (interlaminar shear strength test, incremental tensile test) and dynamic (fatigue test) loading. The resin system used in this work was Araldite LY 556 with anhydride hardener Aradur 917 and imidazole accelerator DY070. As fiber reinforcement, they used two layers of E-glass non-crimp fabrics to finally achieve a laminate with unsymmetrical lay-up sequence  $[0^\circ, +45^\circ, 90^\circ, -45^\circ, +45^\circ, 90^\circ, -45^\circ, 0^\circ]$  and the composite part produced had a fiber volume content of 35%. They measured electrical resistance between two points both in longitudinal direction and through thickness direction of their specimens. They painted the two opposite front and back sides of the specimen with conductive silver paint for resistance measurement in  $0^\circ$  direction and 15 mm wide electrode was applied to both sides in the middle of the specimen for resistance measurement in through-thickness direction. The electrical resistance of the specimens under mechanical loading was measured in-situ using a source meter instrument. With the incremental tensile tests they found that the change in through-thickness electrical resistance follows the applied tensile loading data as in in-plane resistivity data in [5]. They found a linear resistance-strain relation where a value of 2.5% mechanical strain corresponded to a resistance change of 6.3% for the MWCNT modified  $[0^\circ, +45^\circ, 90^\circ, -45^\circ, +45^\circ, 90^\circ, -45^\circ, 0^\circ]$  laminates with fiber volume content 35% under the incremental tensile test. They also found that under this loading condition, the sensitivity of the carbon black (CB) modified system has better sensitivity to damage compared to the CNT modified system. Further, for the fatigue tests, they demonstrated that for this glass/epoxy system, the major defects, such as large delamination, could be detected more easily by resistance measurements in thickness direction where the resistance increases abruptly. The current work differs from [86] in a number of

several aspects. Firstly, material and architectural variables which controls the damage mechanism, and hence, the sensing capability, of composite laminate under fatigue loading is different. In this work, 1 wt% MWCNT incorporated EPON 862 resin cured with epicure W was used with unidirectional S-glass fibres to fabricate symmetric cross ply laminate using autoclave molding which produced a fiber volume content of about 68%. Secondly, the electrodes, in this work, are placed in different in-plane and through-thickness positions of the laminate in order to detect the location of damage initiation and monitoring of damage between different conducting paths. Finally, it is established in this work that not only the major defects like delamination; the very initiation of damage, such as microcracks in matrix can be detected precisely with sharp response of through thickness resistance in specific location other than the middle of the specimen.

Nofar et al. [87] investigated the electrical resistance response of 1 wt% MWCNT incorporated woven GFRP composites under static and dynamic loading. They detected the elastic limit of the samples by the change in slope in their electrical resistance versus strain curves. They introduced delamination artificially in some of their samples and tested under cyclic loading for different maximum loads. They concluded that carbon nanotube networks in monitoring damage have better sensitivity than strain measurements.

From the review of the earlier works, it is established that electrical resistance method is a promising technique for monitoring damages in composites. Moreover, for non conductive GFRP composites, incorporation of carbon nanotubes in the matrix phase enables the effective in situ monitoring of damages by electrical resistance method. However, only a few studies [5, 58, 81-87] were found dedicated to the monitoring of fatigue damage behavior of GFRP composites using the electrical resistance method exploiting the embedded CNTs networks. The current

work further explores the effectiveness of electrical resistance method in detecting the initiation and propagation of fatigue damage of CNT incorporated GFRP composite by placing the electrodes at different selected positions allowing the electrical resistance measurements at various in-plane and through thickness regions of the laminate.

## **2.5 Objectives of the present work**

For the cross-ply GFRP composites embedded with 1 wt% MWCNTs subjected to cyclic loading, the general objectives of this work can be listed as follows:

- i) To verify whether the electrical resistance can effectively monitor the accumulation of damage at relatively higher load levels,
- ii) To observe whether this method can detect the initiation of damage at relatively lower load levels,
- iii) To examine and compare the electrical resistance response at various in-plane and through thickness regions in the composite laminate,
- iv) To compare the effectiveness of electrical resistance method with strain measurements, and
- v) To correlate the electrical resistance response under various combinations of loads and number of cycles with the state of damages through visual observations.

The key steps for realizing the objectives of this work are given in figure 2.12.

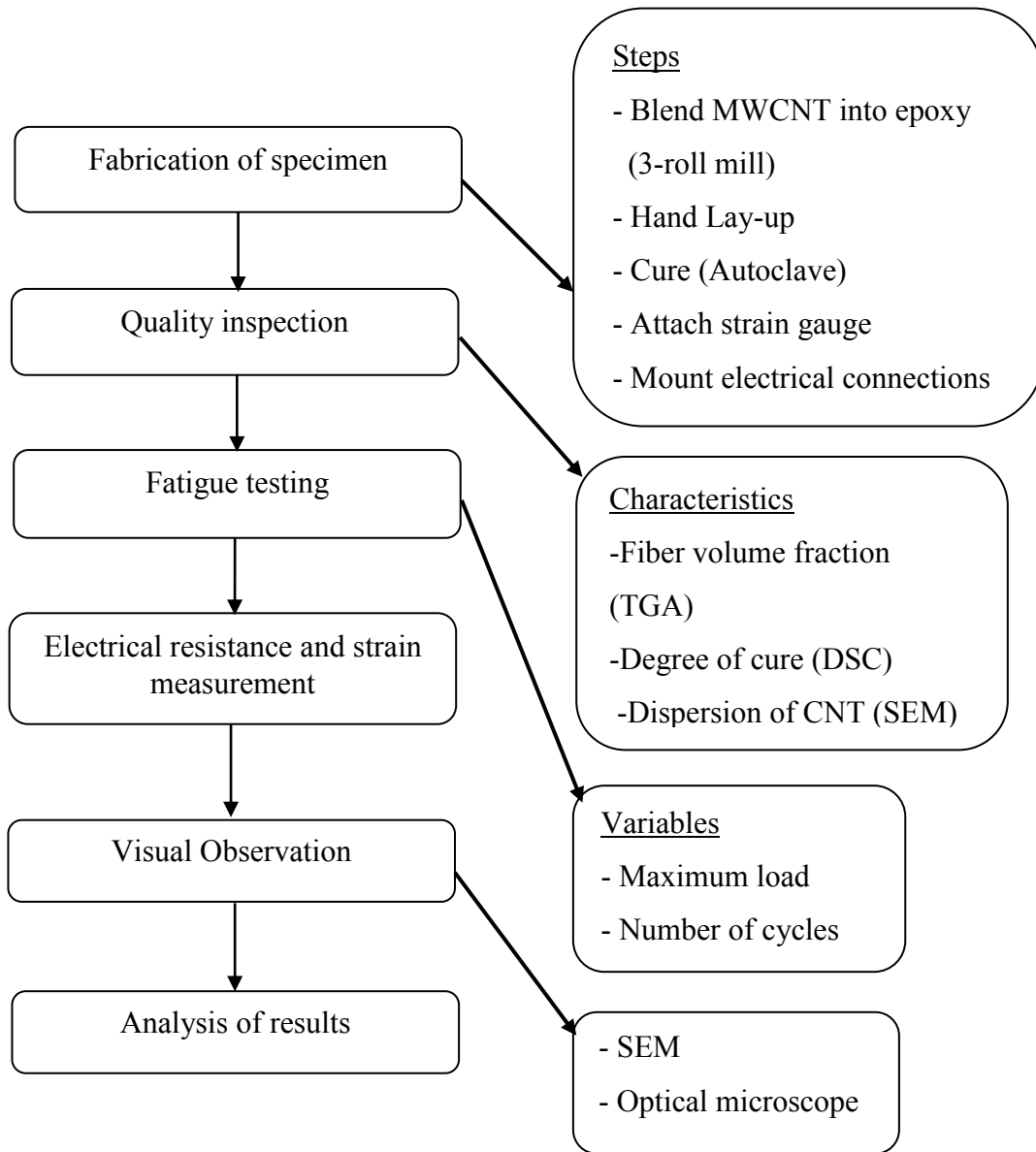


Figure 2.12 Key steps in realizing the objectives of this work

# CHAPTER 3

## Materials and Experimental Procedure

Advanced composite materials are used in the design of aerospace structures. Recently, these materials are also being used in the design of many primary structures. A large number of factors constitute the complexity of the design of composite materials. These design considerations involve many issues including compatible combinations of matrix and fibers, dispersion of multi walled carbon nanotube in resin, number of layers, ply orientation, fabrication procedure and various processing parameters.

Autoclave processing is the most widely used fabrication method for high performance composite structures. While this procedure provides a good quality product, it is expensive (high raw materials and autoclave costs) and time consuming. In this work, CNT incorporated GFRP composite laminate samples are manufactured using autoclave processing with hand layup method. Quality and performance of any composite structure incorporating dispersed phase like CNT depend on its various attributes such as bonding strength of the interface; shape (particles, flakes, fibers) and orientation (random or preferred) and uniformity of dispersion of the dispersed phase and obviously the processing parameters and curing conditions. In this chapter, properties of materials used, their chemical structure, dispersion method of multiwall carbon-nanotube, fabrication of sample, curing conditions and experimental procedure are described in detail.

### 3.1 Materials used for the fabrication of laminate sample

Carbon nanotube incorporated GFRP composite laminate samples were prepared by using Uniweb S-glass fiber (4.2 Oz.), cheap tube multiwall carbon nanotube, the epoxy polymer (bisphenol-F epoxy, Epon Resin 862), and the curing agent Epikure W (an aromatic amine curing agent), respectively.

### 3.2 Multiwall carbon nanotubes (MWCNTs)

Multiwall carbon nanotubes grown by the chemical vapor deposition technique have been used in this work. Figure 3.1 [87] shows the transmission electron micrograph of these nanotubes.



Figure 3.1 TEM for purified multiwall carbon nanotubes (MWCNTs) [87]

Multi-walled carbon nanotubes offer significant potential as a possible multifunctional reinforcement. High purity multi-walled nanotubes are readily available from a wide-variety of sources at a fraction of the cost of single-walled carbon nanotubes. Their high aspect ratios and large interfacial surface area makes multi-walled carbon nanotubes an attractive candidate for potentially enhancing electrical and thermal conductivities as well as mechanical properties such

as toughness, impact resistance and vibration damping. In Table 3.1, the typical properties of MWCNT are given.

Table 3.1 Typical properties of Multiwall carbon nanotubes (MWCNTs) [88]

Inside Diameter ( nm)	3-5
Outside Diameter ( nm)	13-16
Ash (wt %)	<1.5
Purity (wt %)	>95
Length ( $\mu\text{m}$ )	10-30
Specific Surface Area ( $\text{m}^2/\text{g}$ )	233
Electrical Conductivity ( S/cm)	$>10^{-2}$
Number of walls	3-15
Bulk density ( $\text{kg}/\text{m}^3$ )	140-160

### 3.3 Epoxy and curing agent

Epon Resin 862 is one of the most commonly used resins among epoxy family. It is a low viscosity and low molecular weight epoxy resin produced from bisphenol F and epichlorohydrin which can offer comprehensive mechanical properties of composite laminate. It contains no diluents. Epon 862 provides good pigment wetting, improved fiber and filler wetting and good resistance to filler settling. Epon 862 is considered to be prone to crystallisation on storage, particularly at low temperatures. When Epon 862 is cross-linked with appropriate curing agents, superior mechanical, adhesive, electrical and chemical resistance properties can be obtained [89].

The chemical structure and molecular model of Epon 862 resin and typical properties of Epon 862 is shown in Figure 3.2 (a, b) and Table 3.2 respectively.

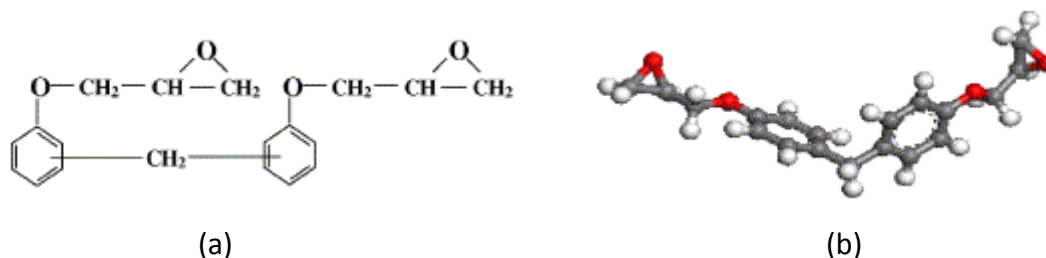


Figure 3.2 a) Chemical structure b) Molecular model of Epon 862 resin [90]

Table 3.2 Typical properties of Epon 862 [89]

Epoxy equivalent weight (g/eq)	165 - 173
Viscosity @ 25 °C (cP)	2500 to 4500
Density @ 25 °C (g/cm <sup>3</sup> )	1.17
Flash point (°C)	>150

The major ingredient of Epicure W curing agent is diethyltoluenediamine (DETDA), which is an aromatic amine curing agent. The chemical structure and molecular model of DETDA is given in figure 3.3 (a, b) [90]. The physical and chemical properties are given in Table 3.3.

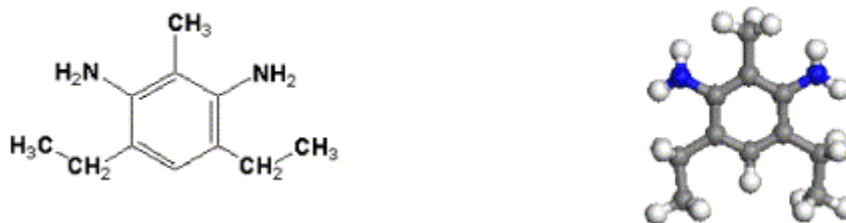


Figure 3.3 a) Chemical structure b) Molecular model of DETDA curing agent [90]

Table 3.3 Typical properties of Epicure W [89]

Amine hydrogen equivalent weight (AHEW) (g/eq)	200
Viscosity (cP)	500-2000
Density at 25°C (g/cm <sup>3</sup> )	1.02
Relative vapour density	6.2
Flash point (°C)	135
Boiling point (°C)	308
Odour	Pungent
Solubility in water	Slightly soluble.
phr (parts per hundred)	26.4

### 3.4 Glass fibers

Uni-web S-glass fiber manufactured by AGY World Headquarters and supplied by Aerospace Composites Products Inc. are used in this work.

#### S-Glass

S-Glass is used in military applications and in aerospace. These are stronger than E-Glass fibers. It consists of silica (SiO<sub>2</sub>), magnesia (MgO) and alumina (Al<sub>2</sub>O<sub>3</sub>). S-glass provides in the order of 85% more strength and 25% more linear elastic stiffness than conventional glass fiber.

Fiberglass (Glass fibers reinforced polymer matrix composites) is characterized by the following properties:

- High strength-to-weight ratio;
- High modulus of elasticity-to-weight ratio;
- Good corrosion resistance;
- Good insulating properties;
- Low thermal resistance (as compared to metals and ceramics).

### **Uni-web S-glass fiber (4.2 Oz.)**

Uni-Web S-Glass is an all-unidirectional S-Glass fabric held together with a unique "tissue" on the fibers. The tissue allows for easy handling of the fiber and almost dissolves into the laminate when curing. S-Glass fiber is superior in strength to standard E-Glass, making it perfect for high-strength, weight-critical applications where exact placement of the fiber is needed [91]. The Uni-Web S-Glass fiber preform is shown in Figure 3.4.

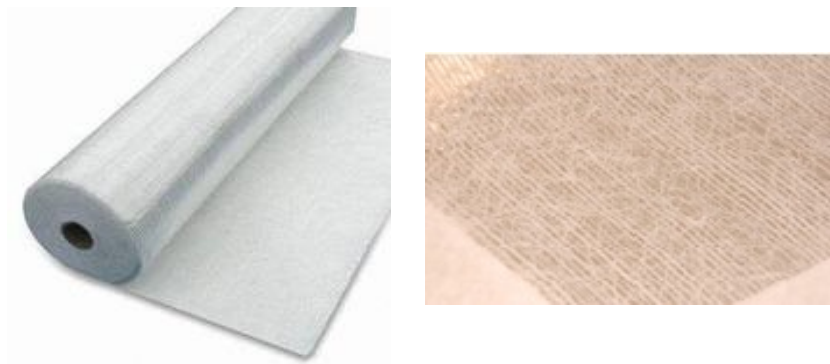


Figure 3.4 Uni-web S-glass fiber [91]

Typical physical and mechanical properties of S-glass are given in Table 3.4.

Table 3.4 Typical properties of S-glass fiber [91]

Density (g/cc)	2.46
Water absorption (%)	0
Loss On Ignition (LOI %)	0.100 – 1.40
Filament diameter ( $\mu\text{m}$ )	5 – 25
Tensile strength (MPa)	4890 @ room temperature
Modulus of elasticity (GPa)	86.9
Elongation at break (%)	5.70
Poisson's ratio	0.22

### 3.5 Dispersion of carbon nanotubes in the matrix

In this work, Medium-low milling sequence according to the work of Rosca and Hoa [74] was used for dispersing 1 wt% multiwall carbon nanotubes using the three-roll mill. The MWCNTs were mixed with the epoxy first by hand stirring and then by three-roll mill EXACT calendaring machine. Initial multi-walled nanotube agglomerates were quite large because mixture was first processed at a large gap setting of 50  $\mu\text{m}$ . The mixture was then subsequently passed through the mill at progressively smaller gap settings. The agglomeration was reduced after progressively dropping the gap setting from 50 $\mu\text{m}$  to 10 $\mu\text{m}$  where the speed of the apron roll was maintained at 100 rpm for all passes. The mixing scheme followed in this work is summarized in Table 3.5.

Table 3.5 Number of passes through calendering machine with different gap distance

Roll gap distance ( $\mu\text{m}$ )	Number of passes
50	2
20	1
10	3

### **3.6 Fabrication of CNT incorporated glass fiber-epoxy composites**

The process of fabrication of composite parts is very important for the good quality of the final product. The type of manufacturing process is selected based on the requirement of performance and geometry of parts. Autoclave processing is commonly used for manufacturing high performance long fiber reinforced polymer-based composite materials, such as, those used in aerospace and industrial applications. The main steps followed in this work for autoclave molding of composite samples are described in the following sections.

#### **3.6.1 Fiber preform:**

Fiber preform is cut from the fiber roll according to the desired dimension and lay-up sequence.

#### **3.6.2 Tool preparation (mold):**

Manufacturing using autoclave is a molding process. A steel plate of dimension 18"X18" is used as a mold to make a flat plate-like laminate. First the tool (mold/steel plate) surface is cleaned with acetone and then release agent "Safe Release 30" is applied on the top of the tool surface for easy removal of the part from the mold surface.

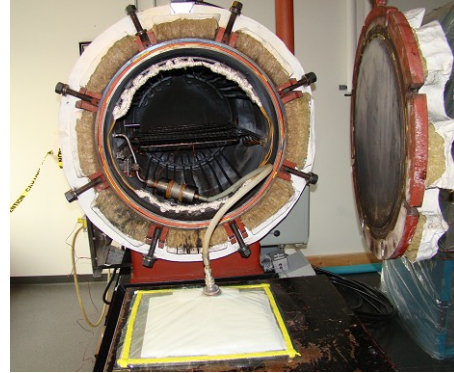
### **3.6.3 Laying up on the tool:**

After the release agent was applied on the surface of the mold, the desired number of layers of the fiber perform were placed on the tool. Then sufficient amount of resin (incorporated with required amount of hardener and dispersed carbon nanotubes) was applied to each of these layers. Eight layers of fibers were accordingly placed in the desired sequence  $[0_2/90_2]_s$ . Enough pressure was applied on each of the layers using a roller to compress the fiber plies and to facilitate removing entrapped air which may form voids in the final part. To ensure the good quality of the laminate, the stack of fibers were well placed maintaining the exact fiber orientations.

After the laminate was laid up, peel ply (perforated Teflon sheet) was put on the top of the laminate to facilitate squeezing out the excess resin during curing in autoclave and for easy removal of the part. Bleeder materials were then used to absorb excess resins that drip out during curing and molding process. After that breather materials are applied on the top of bleeders. Breather materials are perforated films of polymer with high temperature resistance. The holes allow volatiles such as water vapor or gases that are formed during the curing process to escape out of the laminate. The final layer that was put on the top of the whole assembly is the vacuum bag where a vacuum valve was attached. The vacuum bag was then sealed with the sealant tape. Finally, the vacuum valve was connected with the vacuum pump line and the whole lay-up assembly was placed inside the autoclave for curing. A complete vacuum bag and attachment of this with vacuum pump line inside autoclave is shown in figure 3.5 (a, b).



(a)



(b)

Figure 3.5 a) A complete vacuum bag b) Vacuum bag is attached with autoclave vacuum pump line

#### **3.6.4 Autoclave Curing and Consolidation of the part:**

An autoclave is a large pressure vessel with an integral heat, pressure and vacuum capacity. Inside the autoclave, the cross linking reaction starts with increasing temperature. The temperature was gradually increased from room temperature to 130°C in 60 minutes and held there for 360 minutes to allow the matrix to flow, removing entrapped air and attaining the desired curing of the final sample. 50 psi pressure was maintained inside the autoclave for the whole duration for maintaining the fiber orientation and squeezing out the excess resin. The applied pressure also facilitates to remove the volatiles such as water vapor and other gases that may be generated as the resin transforms from liquid to solid during curing. The curing cycle is shown in figure 3.6.

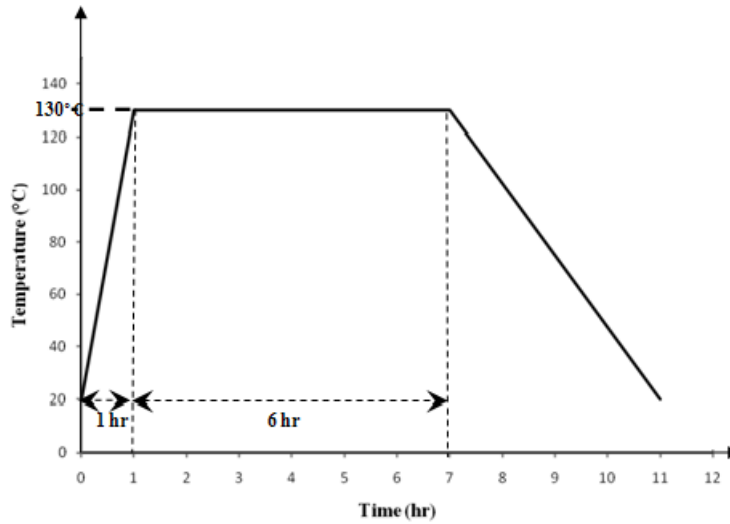


Figure 3.6 Cure cycle for S-glass/ Epon 862 epoxy composite laminate

### 3.7 Quality of the samples

For reliable test results good quality samples are required. The quality of the CNT incorporated composite samples are characterized by proper curing, fiber volume fraction, uniform distribution of fibers and dispersion of CNTs. The degree of cure and the glass fiber volume fraction for the sample was determined by DSC (Differential Scanning Calorimeter, TA instruments Q10) and TGA (Thermo Gravimetric Analysis, TA instruments Q50) tests respectively. From the typical DSC results, as shown in figure 3.7, it was found that the samples were cured properly. From the typical TGA results, as shown in figure 3.8, the fiber volume fraction of the samples was found to be around 68%.

## Calculation of fiber volume fraction

8-layer cross-ply laminate sample's weight before put inside TGA , 33.719 mg

∴ Weight of sample (fiber + epoxy),  $W_s = 33.719 \text{ mg}$

$$\therefore W_s = 0.033719 \text{ g}$$

After TGA, 82.91 % fiber remains from 0.033719 g laminate sample from figure 3.8

$$\text{Weight of fiber, } W_f = \frac{(0.033719 * 82.91)}{100}$$

$$\therefore W_f = 0.02795 \text{ g}$$

$$\text{Weight of Epoxy, } W_e = (0.033719 - 0.02795) \text{ g}$$

$$= 0.006 \text{ g}$$

$$\text{Volume of fiber, } v_f = \frac{W_f}{\rho_f} = \frac{0.02795}{2.49} = 0.01123 \text{ g/cm}^3$$

$$\text{Volume of epoxy, } v_e = \frac{W_e}{\rho_e} = \frac{0.006}{1.174} = 0.0051 \text{ g/cm}^3$$

Where,  $\rho_f$  and  $\rho_e$  represent the density of fiber and epoxy respectively.

$$\begin{aligned} \text{Fiber volume fraction, } V_f &= \frac{v_f}{v_f + v_e} \times 100 \% \\ &= \frac{0.01123}{0.01123 + 0.0051} \\ &= 68\% \end{aligned}$$

$$\therefore V_f = 68\%$$

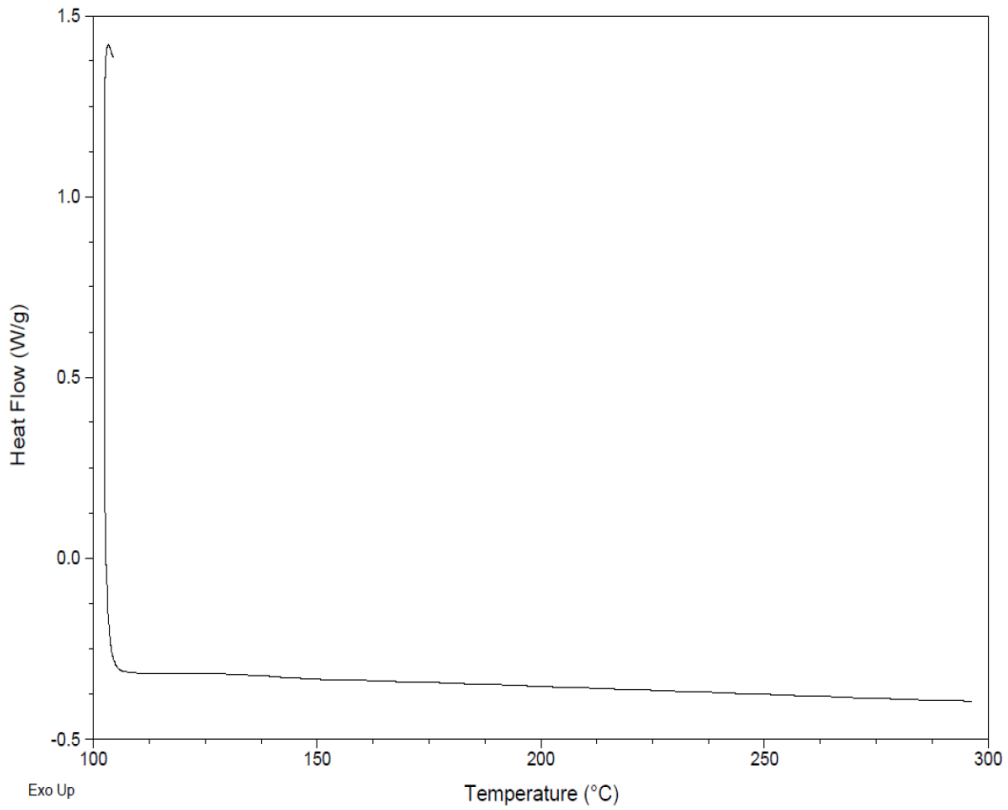


Figure 3.7 DSC results of the composite sample after curing

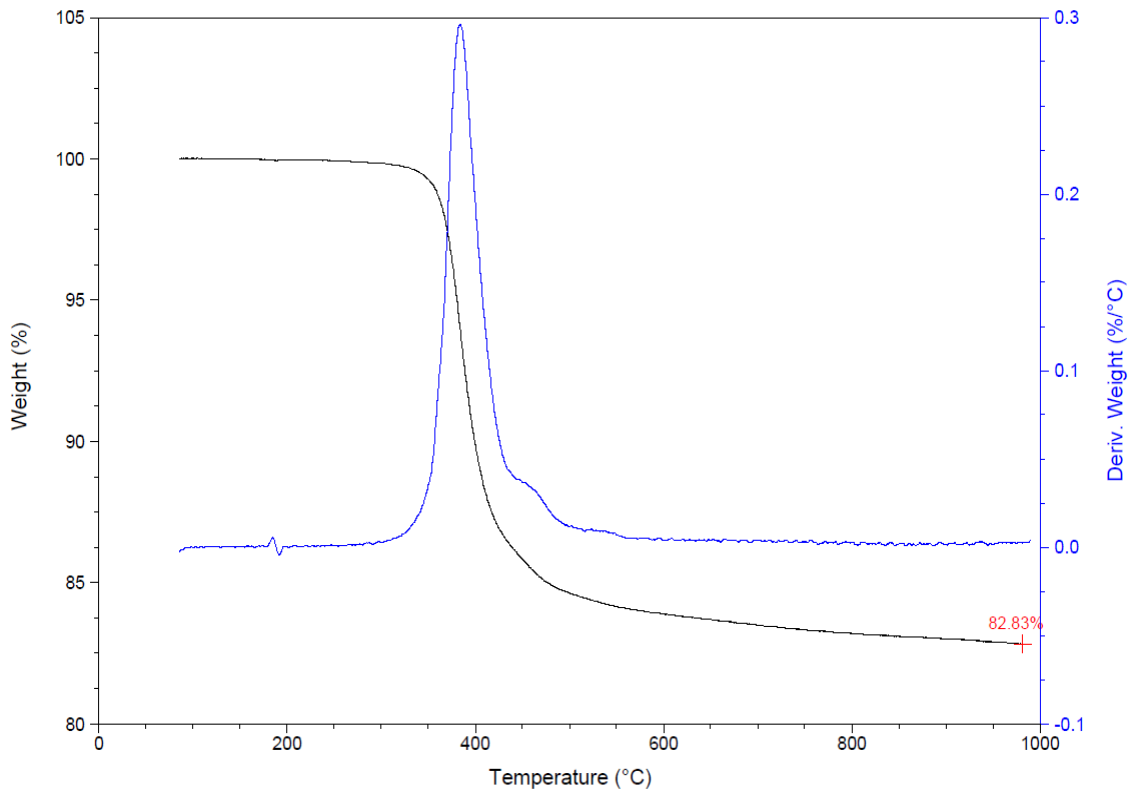


Figure 3.8 TGA result of the composite sample after curing

The scanning electron microscope (SEM) image of the sample showing the dispersion of CNTs within epoxy is given in figure 3.9. From this figure it can be observed that a good interface between epoxy and carbon nanotubes is established. Figure 3.10 (a, b) shows the optical microscopic image of a cross-ply laminate. It can be seen from these figures that fibers are uniformly distributed throughout the matrix. Almost all fibers are found coated with matrix and there is no resin-rich region.

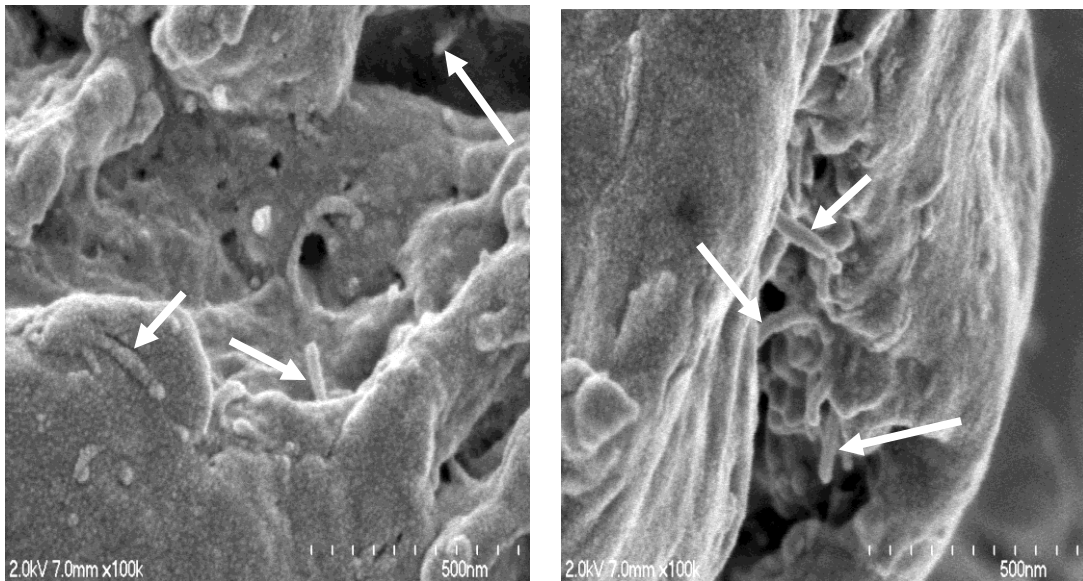


Figure 3.9 SEM picture of the matrix showing the dispersion of nanotubes (100000 x)

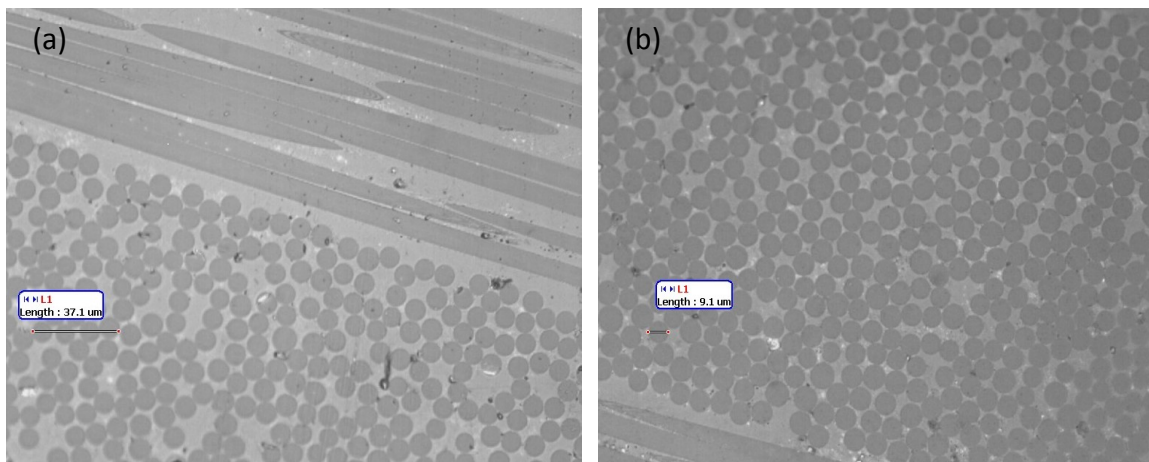


Figure 3.10 Fiber distribution of the sample (Optical) (200x)

### 3.8 Test schedule and arrangement of electrical connections

The specimens were prepared according to ASTM 3039-76 standard. The dimensions of the specimen are given in figure 3.11. The edges of the specimens were sanded with sandpaper. Screen sandpaper was bonded to both ends on both sides of the specimens. Silver epoxy-based glue was used as the conductive contact probes for electrical resistance measurement. The electrical resistance was measured using a high resistance Agilent meter. For measuring the mechanical deformation, a strain gauge was installed on the middle of the surface of the sample as in figure 3.12.

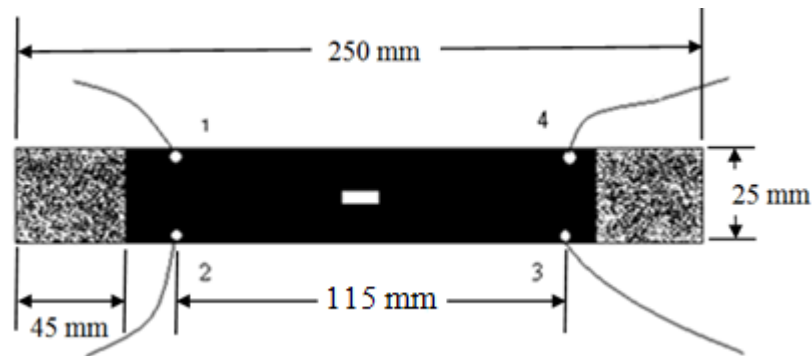


Figure 3.11 Dimensions of a typical sample for fatigue test

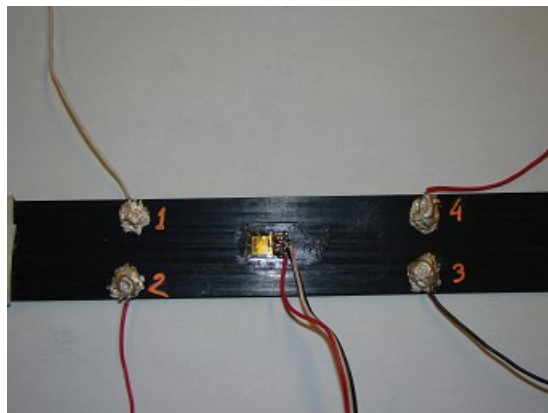


Figure 3.12 After installing the strain gauge on the sample

Tensile and fatigue tests were carried out on an MTS 100 KN universal testing machine as shown in figure 3.13. In order to obtain the tensile strength, three specimens were loaded until failure. Tensile tests were performed at a crosshead speed of 1.27 mm/min. The electrical resistance and strains were measured during the test.

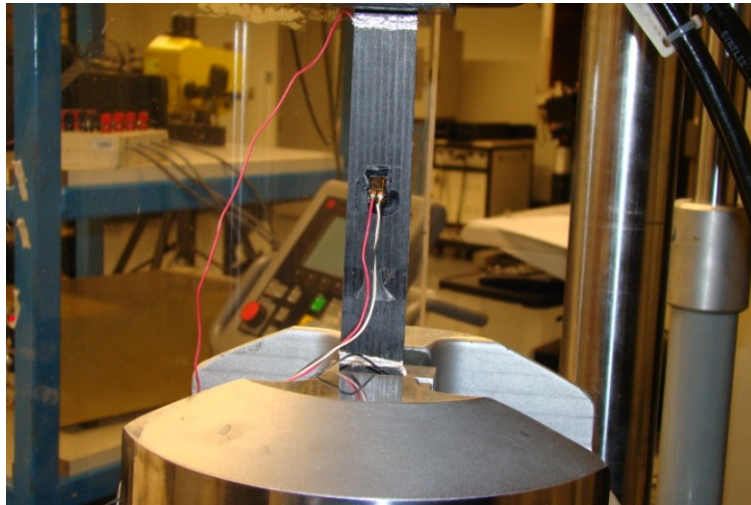


Figure 3.13 Mechanical testing on MTS machine

In fatigue tests, electrical resistance was measured in different in-plane and through thickness positions. With the stress analysis of glass/epoxy composite samples using laminate theory, it was found that the first ply failure occurred at around 3500N load. Thus these tests are carried out for two different levels of loads. The first sets of tests were done for maximum loads above the first ply failure load. The other sets of tests were carried out for maximum loads below the first ply failure load. The minimum load for the fatigue tests was maintained at 250N for all tests.

### 3.8.1 Arrangement of electrical connections for higher loads (above first ply failure load)

The arrangement of the electrical connections and strain gauge for fatigue tests above the first ply failure load are shown in figure 3.14. Four contact points (1, 2, 3, 4) in-plane and one contact point (4') in through-thickness plane were attached to the sample as can be seen from the figure.

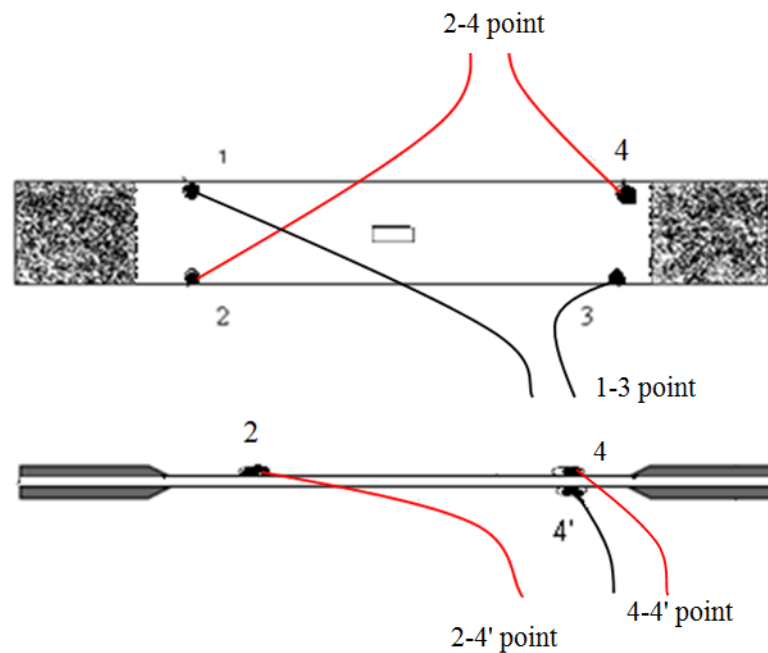


Figure 3.14 Arrangement of electrical connections for tests above the first ply failure

The electrical resistances were measured between the following points:

- 1-3 points
- 2-4 points
- 2-4' points
- 4-4' points

This arrangement is shown in figure 3.15 (a, b)



Figure 3.15 a) 1-2-3-4- points on one side of the sample b) 4'-point on other side of the sample

### 3.8.2 Arrangement of electrical connections for lower loads (below first ply failure load):

The arrangement of the electrical connections and strain gauge are shown in figure 3.16 for fatigue tests below the first ply failure load. In this case, five contact points (1, 2, 3, 4, C) in-plane and three contact points (1', 4', 3') in through thickness plane were attached to the sample as shown in the figure.

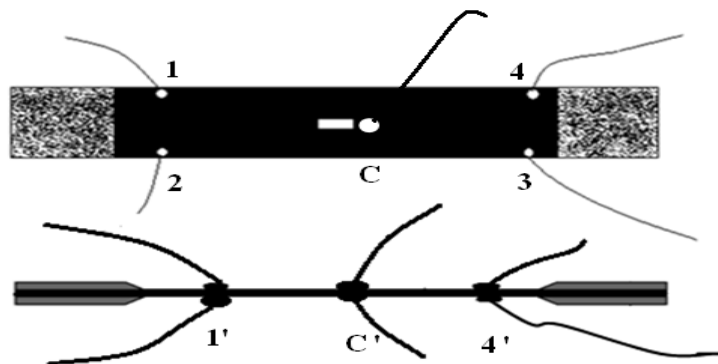


Figure 3.16 Arrangement of electrical connections for tests below the first ply failure

The electrical resistances below the first ply failure load are measured between the following points.

- 1-3 points
- 2-4 points
- 1-4 points
- 2-3 points
- 1-1' points
- 4-4' points
- C-C' points
- 2-4' points

The Cross-ply  $[0_2/90_2]_s$  GFRP composite laminate samples were tested under different maximum loads up to different number of cycles. During the tests, electrical resistances as well as strains were recorded as a function of loading cycles.

The percent change in electrical resistance was calculated as

$$\% \Delta R = \frac{(R_i - R_0)}{R_0} \times 100 \quad (1)$$

Where, in Eqn (1),  $R_0$  refers to the electrical resistance while the minimum load 250N was maintained on the sample at the beginning of the cyclic loading and  $R_i$  refers to the resistance after a specified number of cycles ended (the minimum load 250N was still maintained on the sample).

Similarly, the change in strains are calculated as

$$\Delta S = S_i - S_0 \quad (2)$$

Where, in Eqn (2),  $S_0$  refers to the reference strain value and  $S_i$  refers to the strain value recorded after a fixed number of cycles. All reference values were taken while the minimum load 250N was maintained on the sample.

The test schedules for various specimens are shown in Table 3.6 and 3.7. Each test was carried out using two replicates.

Table 3.6 Test schedule of different samples above first-ply-failure load

Sample No.	Maximum load (N)	Minimum load (N)	No. of cycles
I	6000	250	500
II	8000		200
III	10000		150
IV	12000		100

Table 3.7 Test schedule of different samples below first-ply-failure load

Sample No.	Maximum load (N)	Minimum load (N)	No. of cycles
I	3000	250	100
II	3000		500
III	3000		1000
IV	3000		1500
V	3000		2000

# CHAPTER 4

## Results and Discussions

Two types of tests were performed for 1 wt% MWCNT incorporated  $[0_2/90_2]_s$  glass/epoxy composite samples with different arrangements of the electrical probes. Initially, tensile test of the cross-ply laminate was carried out in order to investigate its elastic limit, failure load, the sensitivity of the electrical resistance method with strain in monitoring damage as well as the location of final failure on the specimen. The results of these tests were used to determine the load of the fatigue test experiments. The fatigue tests, which is the main concern of this work, were performed at different maximum load levels ranging from 20% to 80% of the tensile failure load. The results are discussed in the subsequent sections.

### 4.1 Tensile test

The dimension of the tensile specimen, the arrangement of electrodes, the location of the strain gauge and the loading direction are shown in figure 4.1.

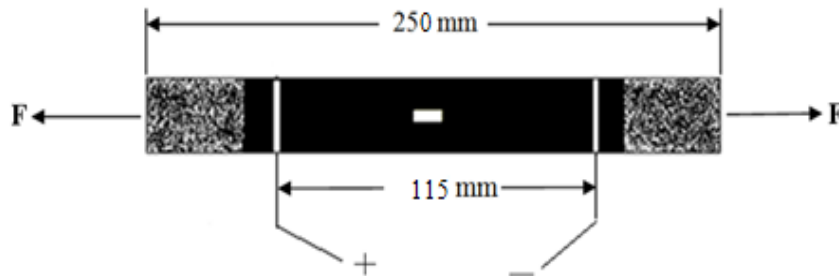


Figure 4.1 Tensile test sample with two electrodes and the direction of applied force

During the tensile test, it was not possible to see the fiber fracture with naked eye until the fiber splits off the specimen surface although fracture could be initiated by breaking of a single fiber. In order to obtain the tensile strength,  $\sigma_{ut}$ , three specimens were loaded until failure and at the same time electrical resistance as well as strain were measured with Agilent meter and strain gauge, respectively. A representative result of the tensile test is shown in figure 4.2

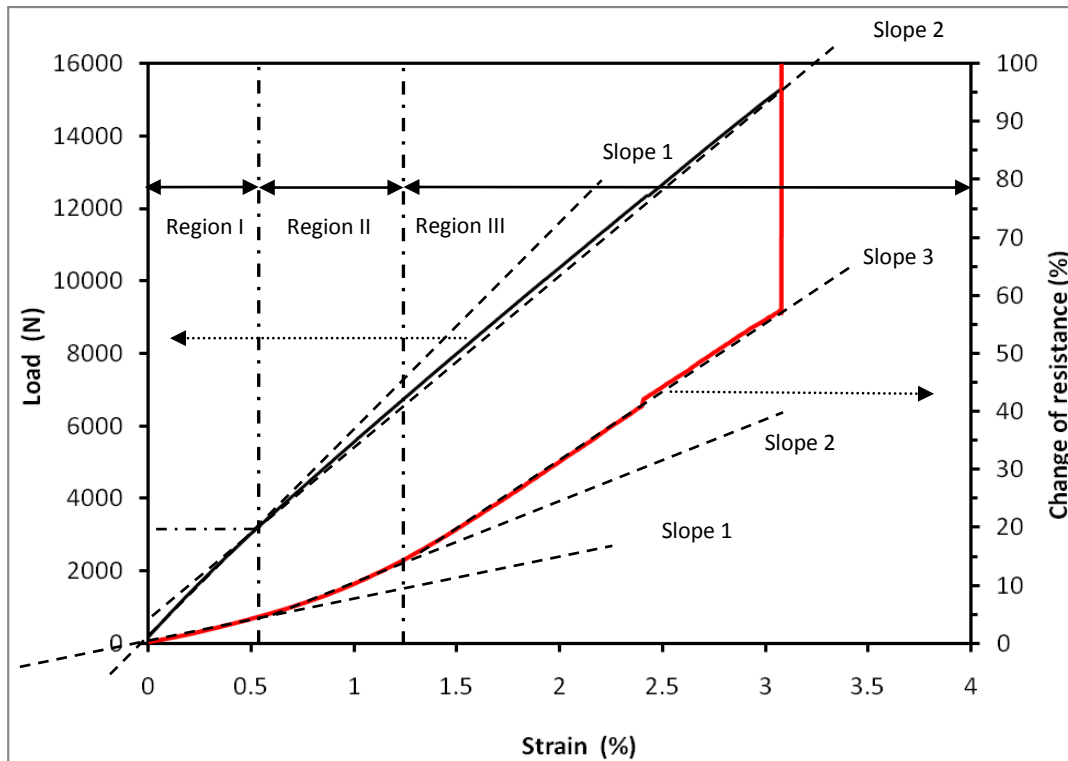


Figure 4.2 Tensile test result of a glass fiber  $[0_2/90_2]_s$  laminate, showing the variation of strain and electrical resistance with applied load

The change of resistance and strain (%) curves in figure 4.2 can be divided into three regions based on the changes in slopes. The first change in slope occurs at  $\epsilon = 0.51\%$  for 6 % change of resistance for a load of about 3500N which might correspond to the first ply failure load calculated from the stress analysis of the specimen. This region within the first slope change

which is evident in the load- strain curve in the same figure is termed as the elastic region of the specimen as in [87]. The second slope change occurs at  $\varepsilon = 1.25\%$  for 15% change in resistance corresponding to the load of about 7000N. This region of the second slope change is not clearly observed in the load-strain curve. Finally, failure of the specimen occurs at  $\varepsilon = 3.1\%$  for 57% change of resistance corresponding to the failure load of about 15000N where abrupt increase of resistance associated with the drop in load is seen. This load-strain-electrical resistance change behaviour is found to be the characteristic tensile load behavior for the 1 wt% MWCNT incorporated  $[0_2/90_2]_s$  glass/epoxy composite laminate samples tested under this test condition as discussed earlier.

It is evident from the above results that the electrical resistance response is very sensitive with the progression of damage associated with the increase of load during the tensile tests. When a  $[0_2/90_2]_s$  cross-ply laminate is loaded in tension,  $0^\circ$  plies are oriented along the loading direction and  $90^\circ$  plies which lie at the center of the laminate are oriented transverse to the loading direction. The linear increase in resistance at the very beginning (region I) is mainly due to the elongation of the sample which points toward the elastic limit. The linear increase in resistance at region II might be related to the formation of minor damages/cracks in the sample. In cross-ply laminates it is widely established [41] that microcracking initiates in the  $90^\circ$  plies where the fibres are oriented orthogonal to the direction of applied load, during tensile deformation. With increasing tensile load the ply becomes saturated with more microcracks causing further increase in resistance pointing towards the end of region II (location of second slope change). As the load continues to increase (region III) the microcracks accumulate to form macrocracks causing fiber fracture with splitting of fibers resulting in the final fracture of the laminate.

Thus, from the above results it is verified that, damage in glass fiber laminates can be monitored effectively by observing the variation of electrical resistance during the static loading. Also, the tensile test specimens were found to fail at the mid-span of the specimens.

The first ply failure load and the ultimate failure load for this cross ply  $[0_2/90_2]_S$  glass/epoxy laminate were found to be around 3500N and 15000N respectively as stated earlier. A certain fraction of this failure loads were used as the maximum loads during the fatigue tests. In fact, the maximum loads of 3000N, 6000N, 8000N, 10000N and 12000N which are 20%, 40%, 53.3%, 66.6% and 80% of the ultimate tensile failure loads, respectively, were used during the various fatigue tests. The results of these fatigue tests are discussed in the subsequent sections.

## **4.2 Fatigue test**

In these tests, the specimens were cycled between minimum and maximum stresses at a frequency of 3Hz at different peak loads. The tests were periodically paused at selected intervals to enable the measurement of electrical resistances. Two types of arrangements were used for all the specimens to measure the electrical resistances. In one arrangement, electrodes were placed on the same surface of the specimen (in-plane positions) while in the other type, electrodes were placed on the opposite sides (through-thickness positions) enabling the observation of through thickness resistance change behaviour.

**4.2.1 Fatigue test for higher load levels (above the first-ply-failure load)**

The samples as observed under SEM in the undamaged state before carrying out the tests are shown in figure 4.3.

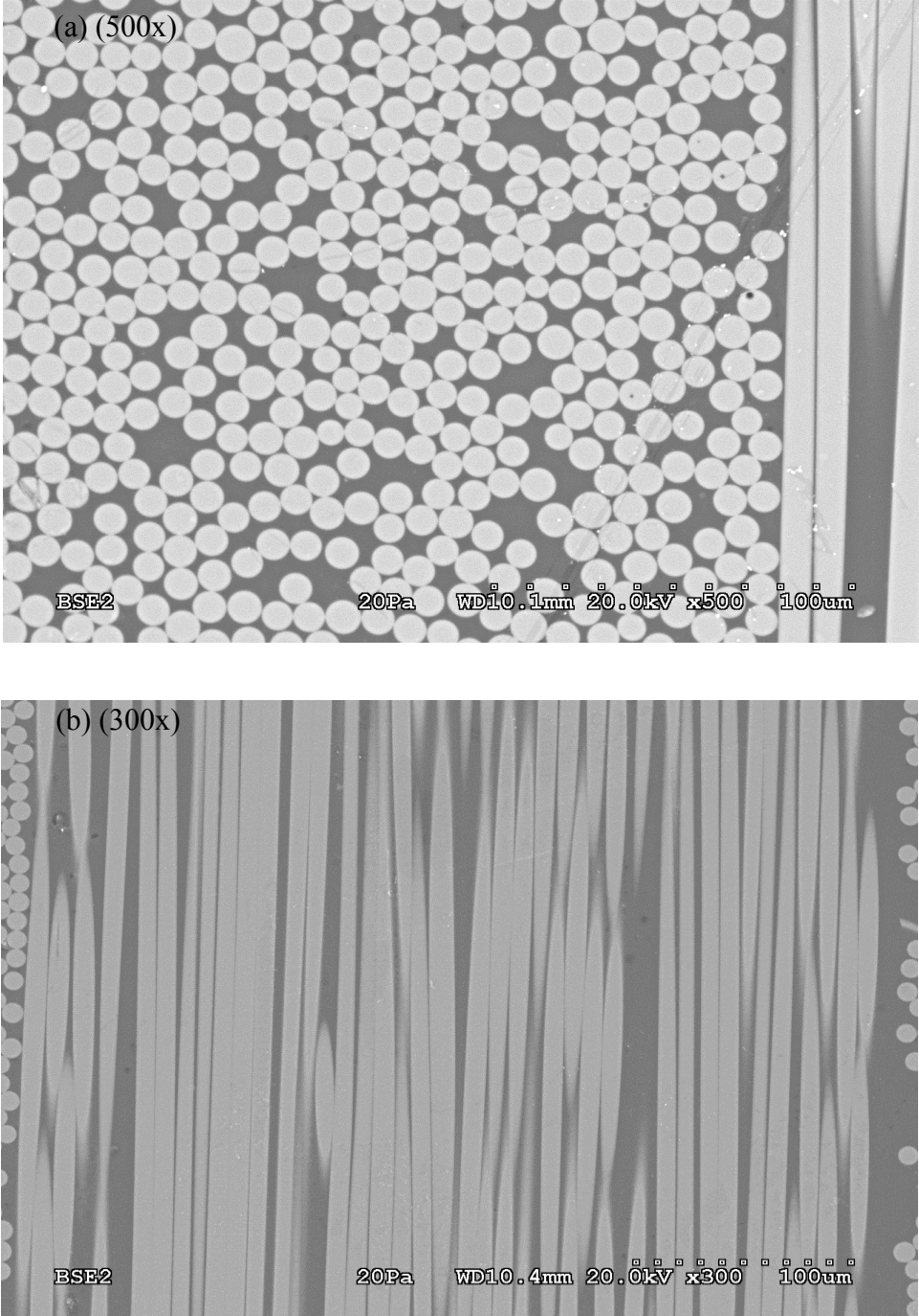


Figure 4.3 SEM images of undamaged sample before testing

For higher load above first-ply-failure, the tests were periodically paused at after every 4 cycles. During the fatigue tests, the percentage change of electrical resistance in both the in-plane and through thickness positions with loading cycles are shown in figure 4.4 (a) for sample I (see test schedule in Table 3.6). The corresponding variations of strains with loading cycles are shown in figure 4.4 (b). In figure 4.4 (c-1, c-2) the damaged conditions after 500 cycles as observed under optical microscope are shown for the same sample.

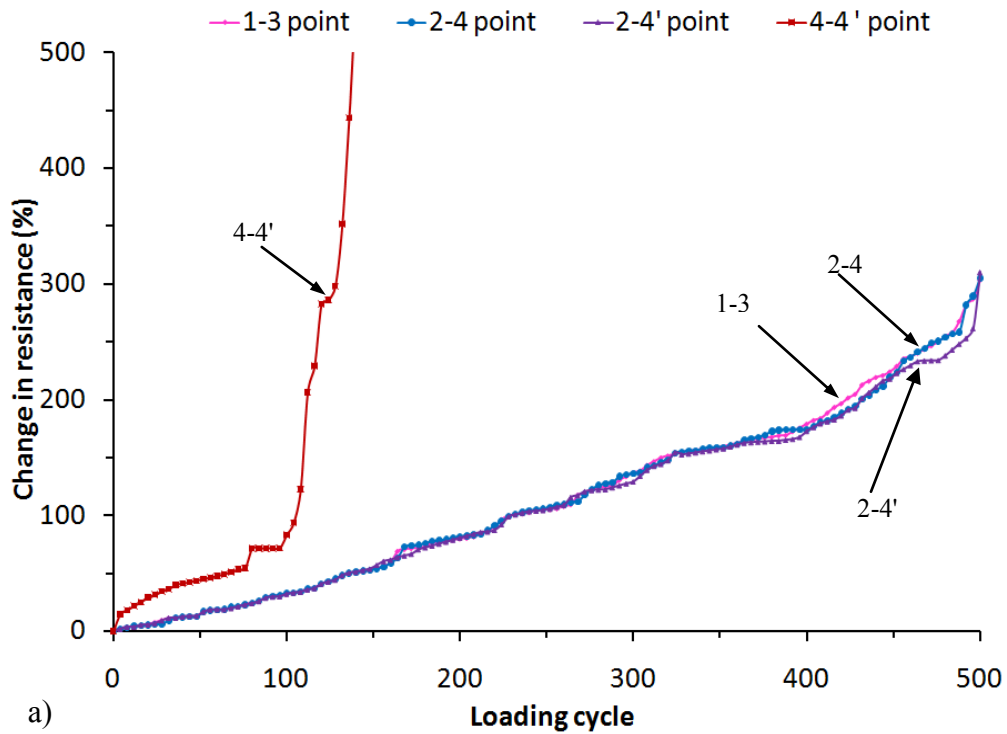


Figure 4.4 a) Variation of change (%) in electrical resistance with loading cycle for sample I, (maximum 6000 N)

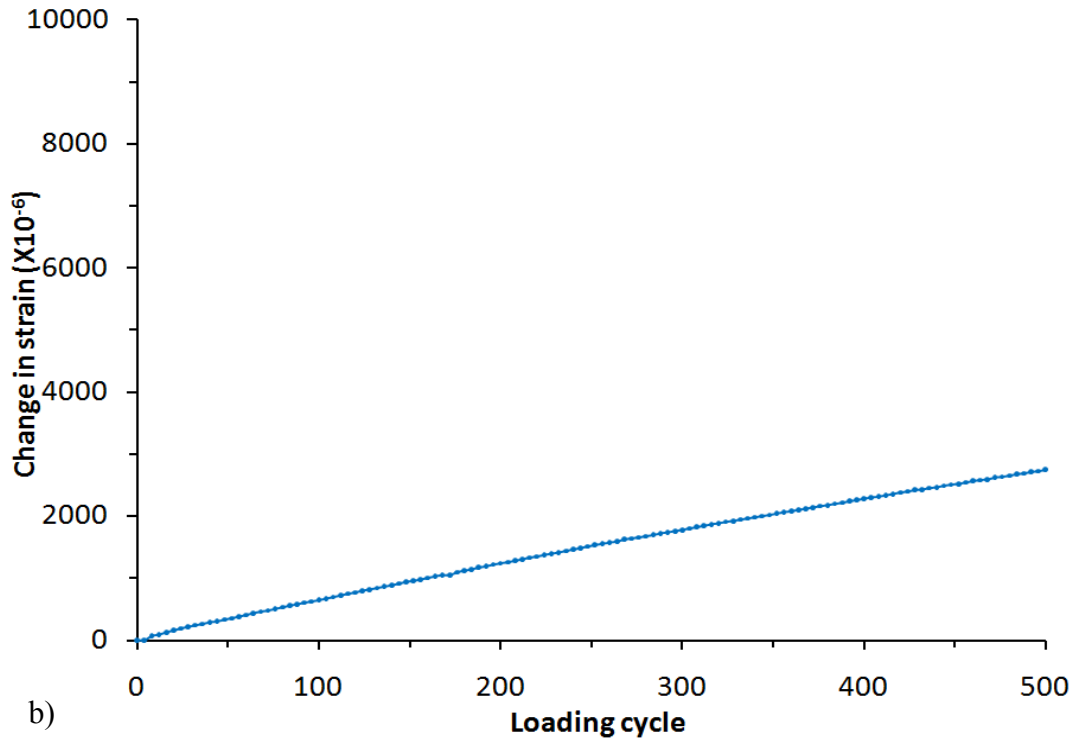


Figure 4.4 b) Variation of change in strain with loading cycle for sample I, (maximum 6000N)

From figures 4.4 (a) and 4.4 (b), it can be observed that the changes in resistances (%) in in-plane positions and changes in strain increase almost linearly up to 500 cycles while in through thickness positions the resistance increases linearly up to 100 cycles and then jumps suddenly. With the tensile test and stress analysis of glass/epoxy composite samples, it was found that the first ply failure occurred at around 3500N load. As the tests for sample I, II, III and IV (Table 3.6) were done with the maximum loads always above the first ply failure load, the changes in strain from the beginning of loading cycles were found to be high for all these samples.

The corresponding optical images of the samples in figure 4.4 (c-1, c-2) show propagation of matrix crack around the fibers which leads to the initiation of delamination.

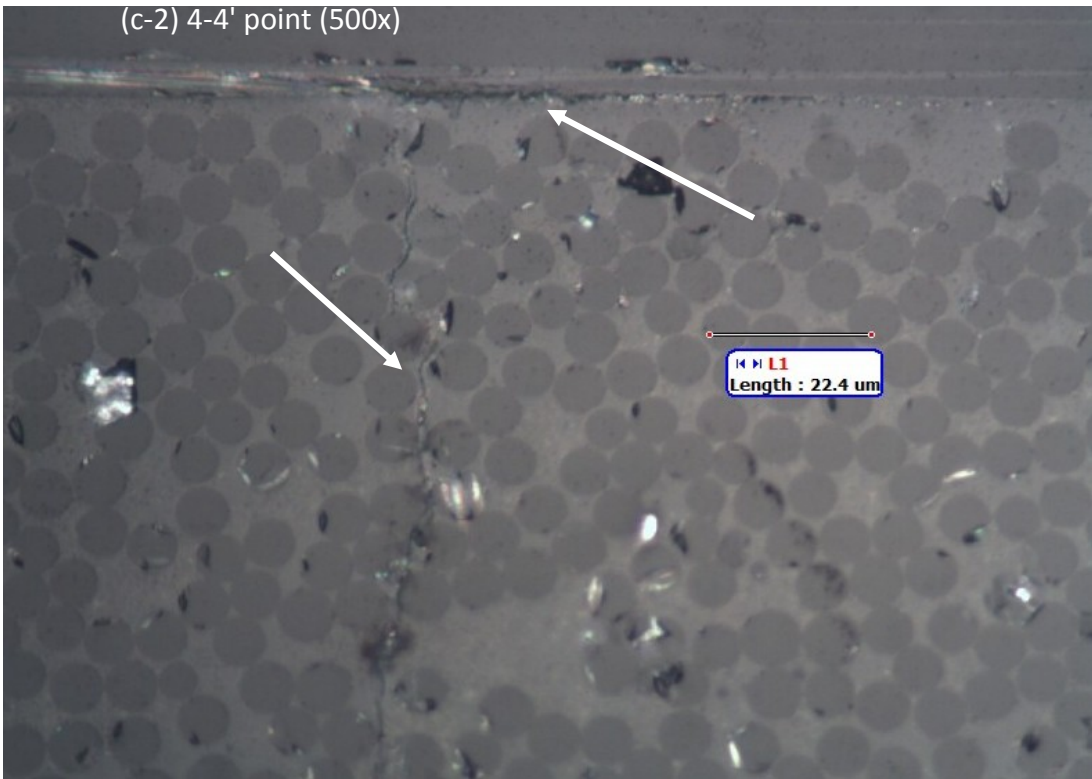
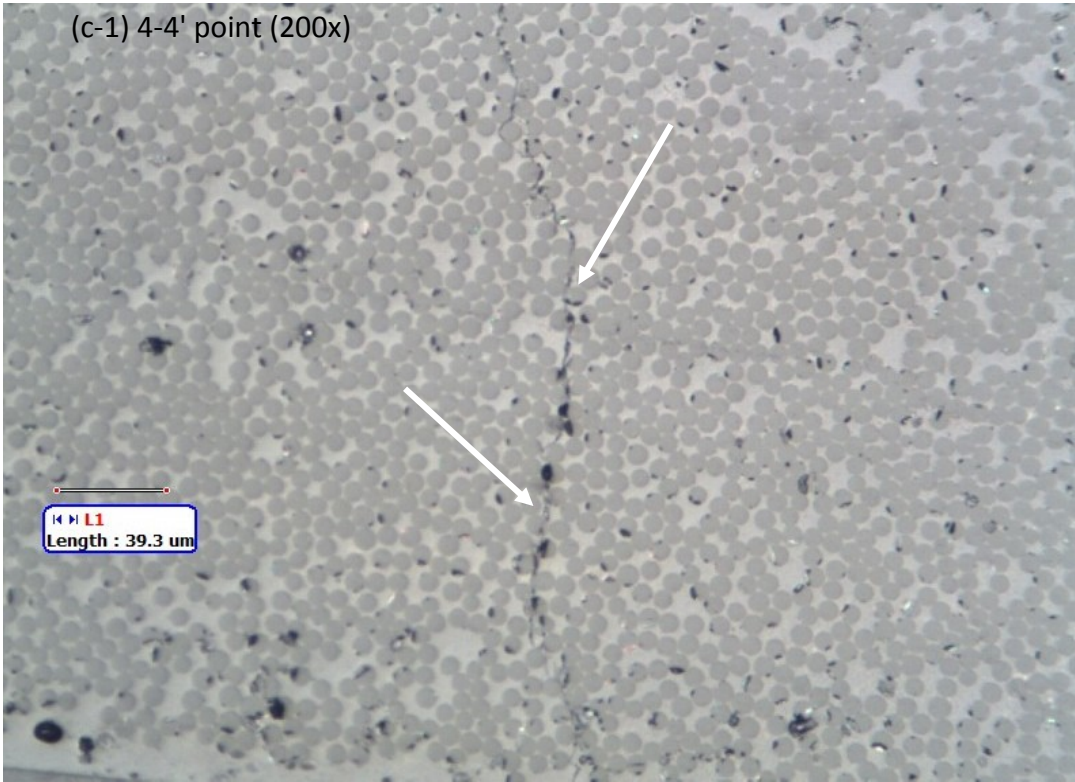


Figure 4.4 c-1, c-2) Optical images of sample I after 500 cycles, (maximum 6000 N)

The conductive percolated networks of CNTs are disturbed due to the occurrence of these damages leading to the variation of resistances and strains. In terms of sensitivity, the changes in in-plane resistances and strains follow the similar trend while the changes in through-thickness resistances jump much earlier in the loading cycles. This jump in electrical resistance at certain cycles corresponds to the accumulation of micro damages into macro damage events like initiation of delamination in the specimen.

Almost similar trend was found for sample II tested for 8000N maximum load for 200 cycles as shown in figure 4.5 (a, b, c). This is because the extent and mode of the damages are similar under this condition to the condition (6000N maximum load for 500 cycles) of the previous test as can be observed from figures 4.4 (c) and 4.5(c). For sample II, as the load was higher than sample I, fewer number of cycles causes similar extent of damages. This implies that, when the damage states (modes, severity, crack propagation etc.) are similar, the response of the electrical resistances resembles in terms of magnitude and trend of the changes as seen in figures 4.4 (a, b) and 4.5 (a, b).

It is worth noting that among the in-plane and through-thickness resistances, the latter is found more sensitive to the extent of damage. However, the through thickness resistance response between 2-4' points is similar to the in-plane resistance response. The reason is because along the path of 2-4', most contacts were still good and only a small portion closes to the point 4' was affected.

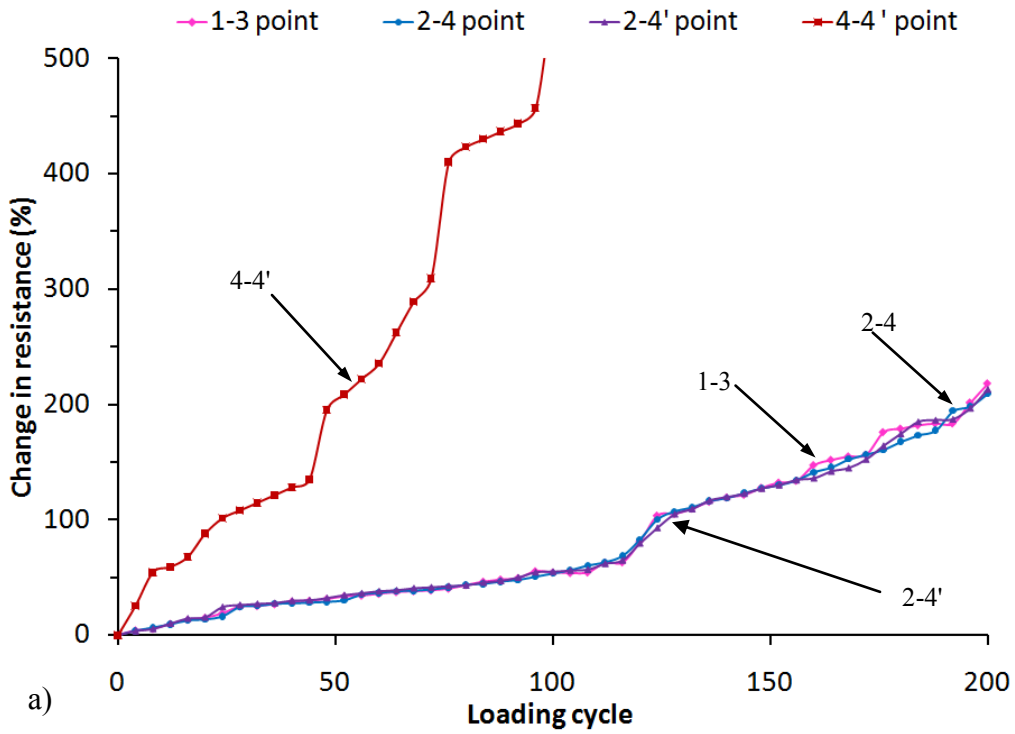


Figure 4.5 a) Variation of change (%) in electrical resistance with loading cycle for sample II, (maximum 8000 N)

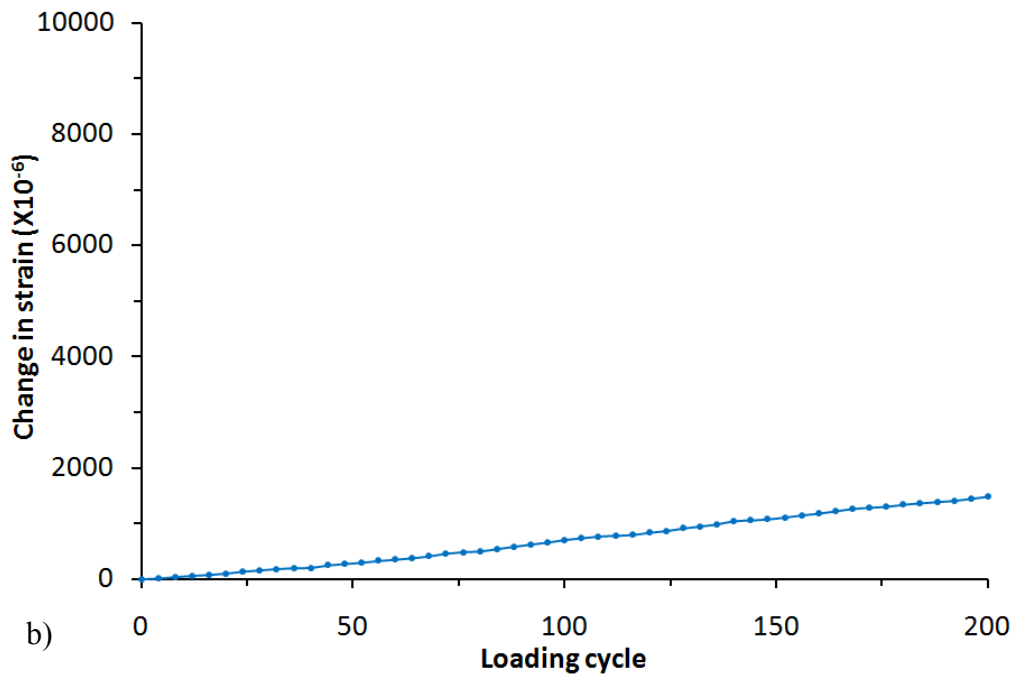


Figure 4.5 b) Variation of change in strain with loading cycle for sample II, (maximum 8000N)

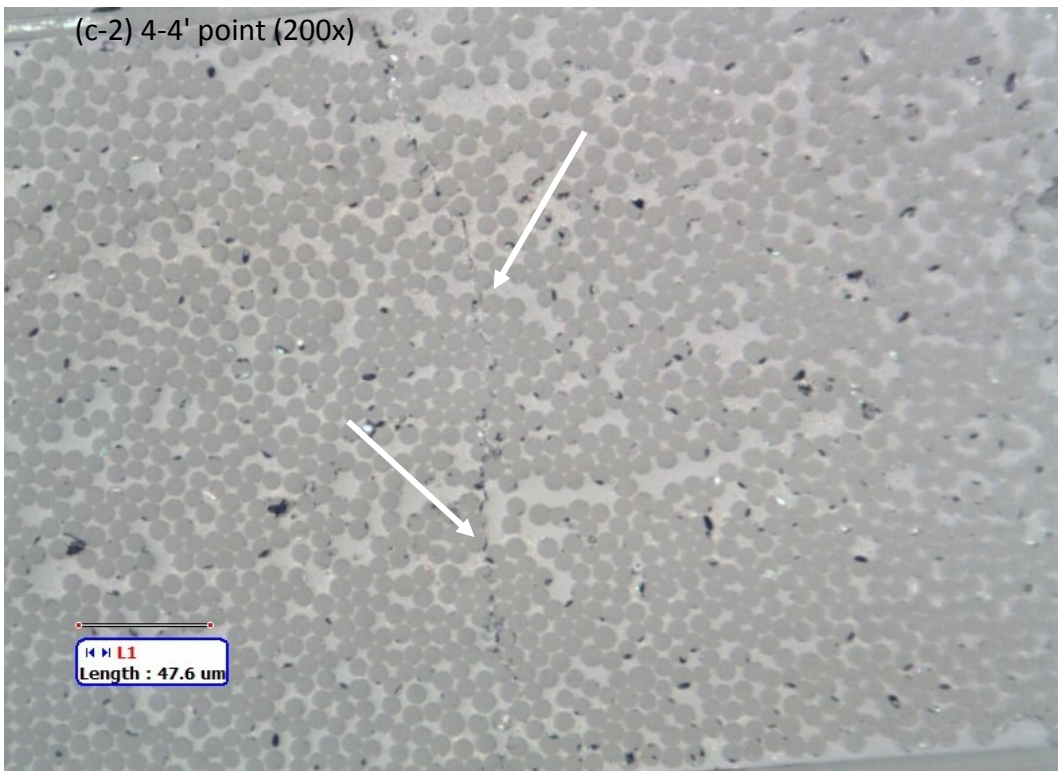
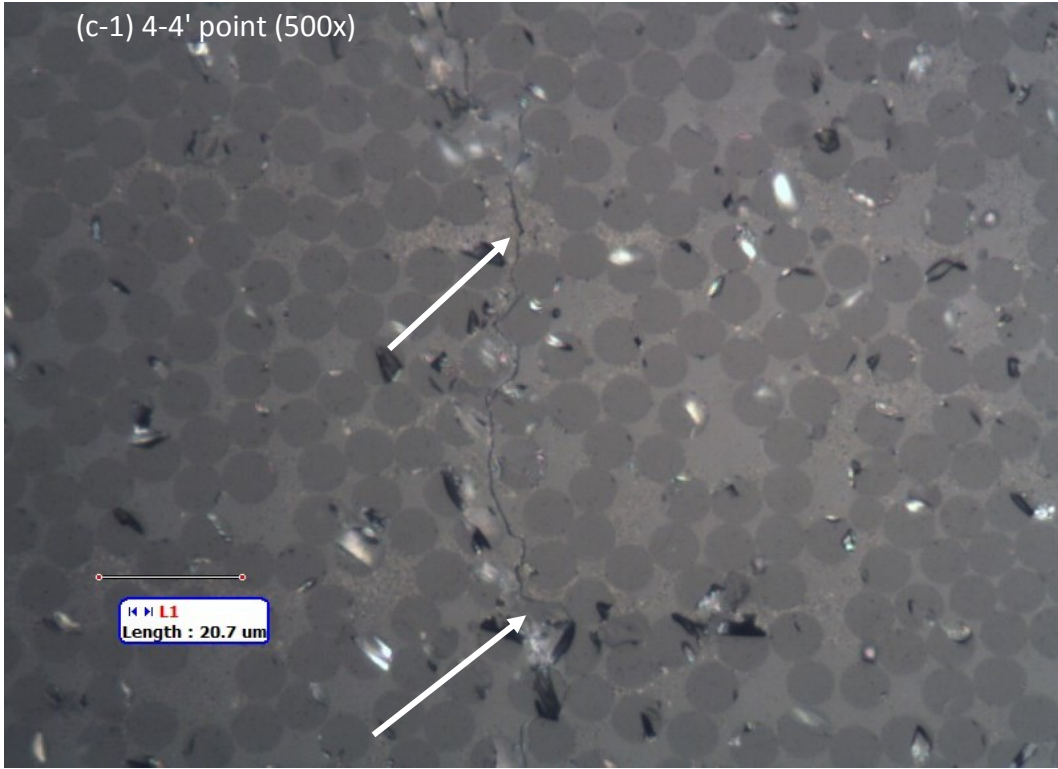


Figure 4.5 c-1, c-2) Optical images of sample II after 200 cycles, (maximum 8000N)

In the case of samples III and IV, severe damages (propagation of matrix cracks at multiple locations, delaminations etc.) occurred at the beginning of the loading cycles as shown in figures 4.6 (c1, c2) and 4.7 (c1, c2). The rate of change of strains, as shown in figures 4.6 (b) and 4.7 (b), was very high (very steep slope of strain curve) in these very high loads. Although the electrical resistances, at these instances, show similar behavior (linear increase initially with sudden jumps after a certain number of cycles) as in the previous cases, the sensitivity of this seems to be reduced when comparing the magnitude, slopes and jump events in figures 4.4 (a), 4.5 (a), 4.6 (a) and 4.7 (a). At these load levels, severe damages occur at multiple modes at multiple locations at the beginning of loading cycles leading to very high rate of changes of strains as shown in figures 4.6 (c1, c2) and 4.7 (c1, c2).

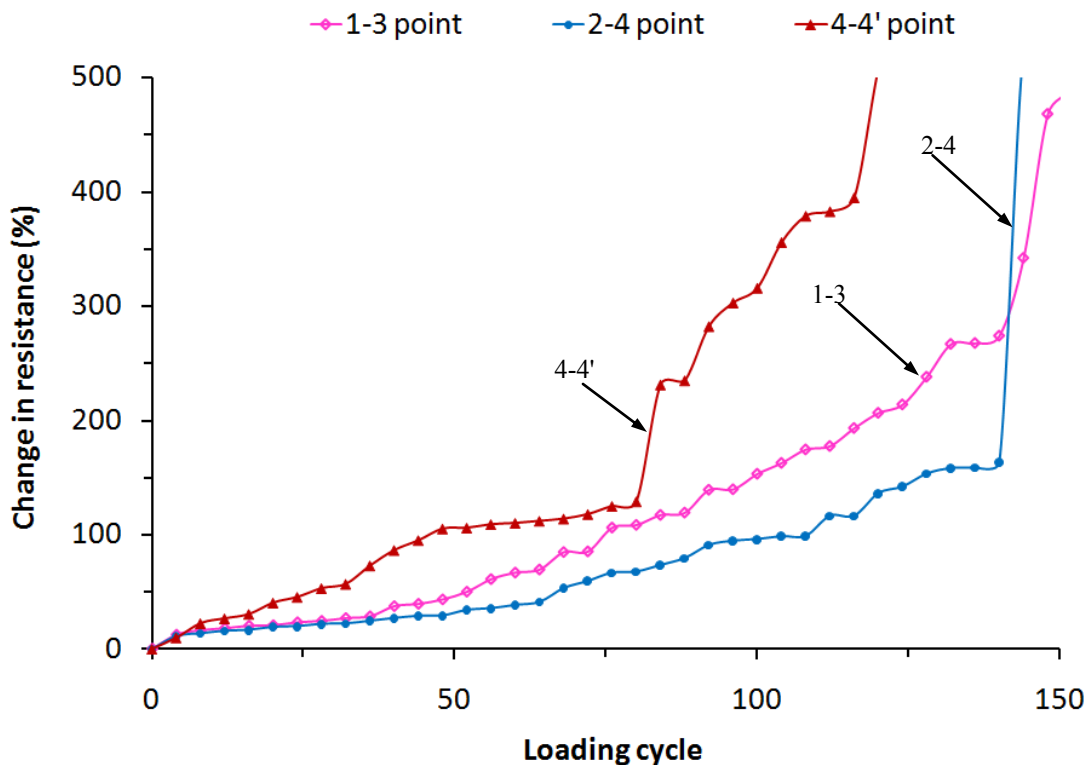


Figure 4.6 a) Variation of change (%) in electrical resistance with loading cycles for sample III, (maximum 10000N)

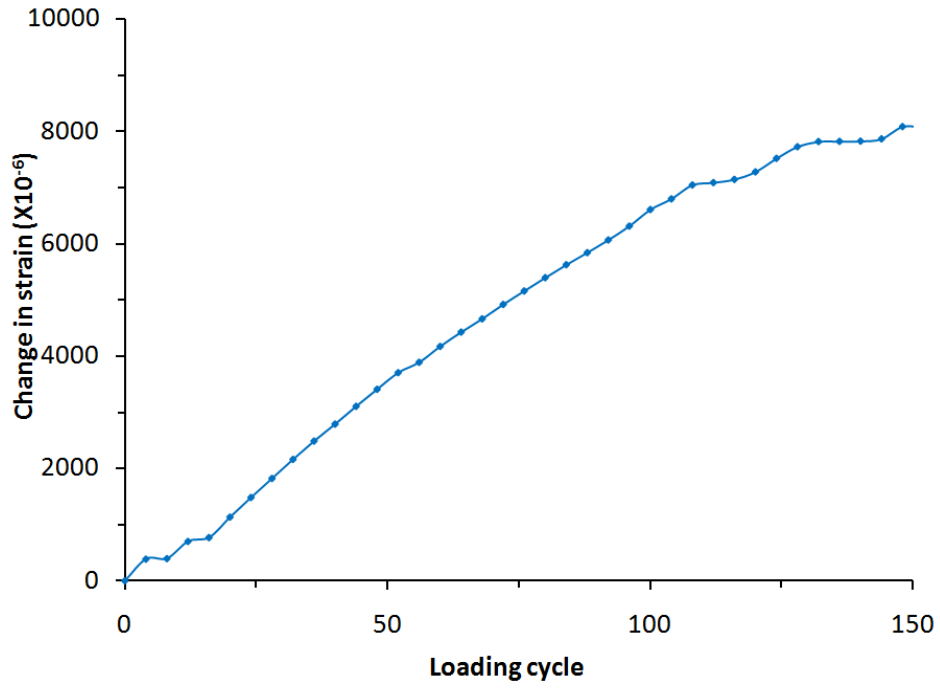


Figure 4.6 b) Variation of change in strain with loading cycles for sample III, (maximum 10000N)

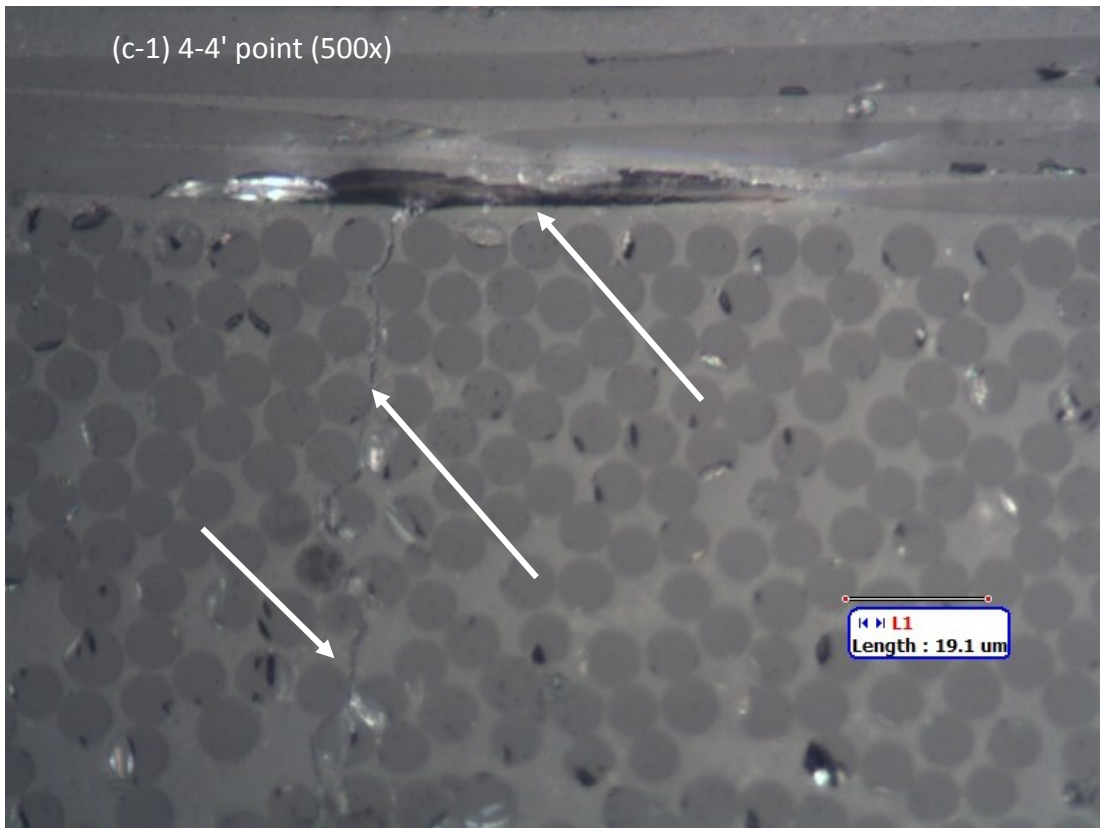


Figure 4.6 c-1) Optical image of sample III after 150 cycles, (maximum 10000N)

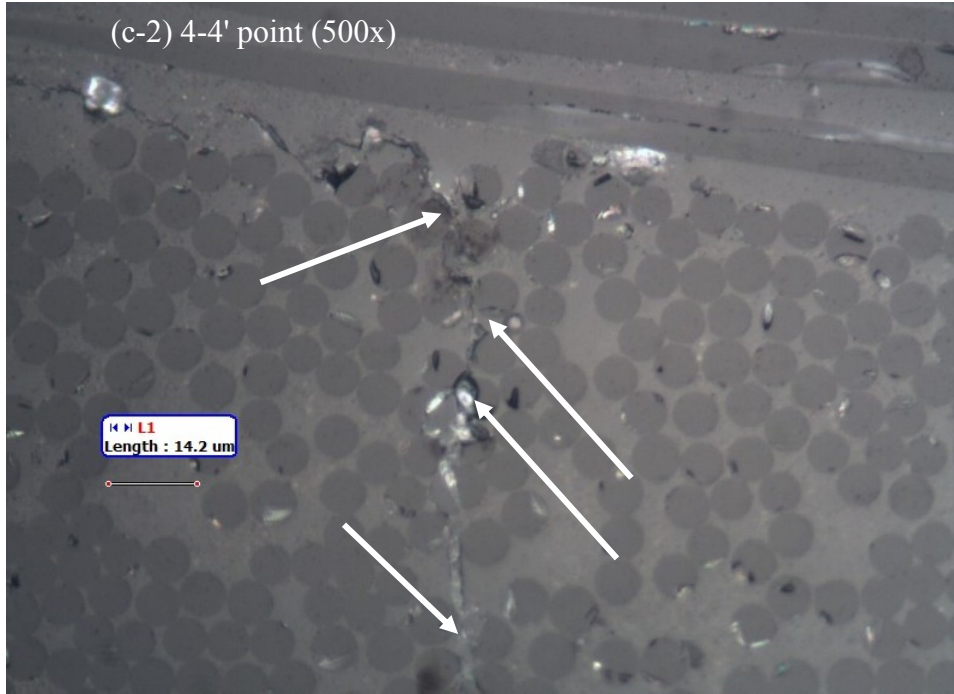


Figure 4.6 c-2) Optical image of sample III after 150 cycles, (maximum 10000N)

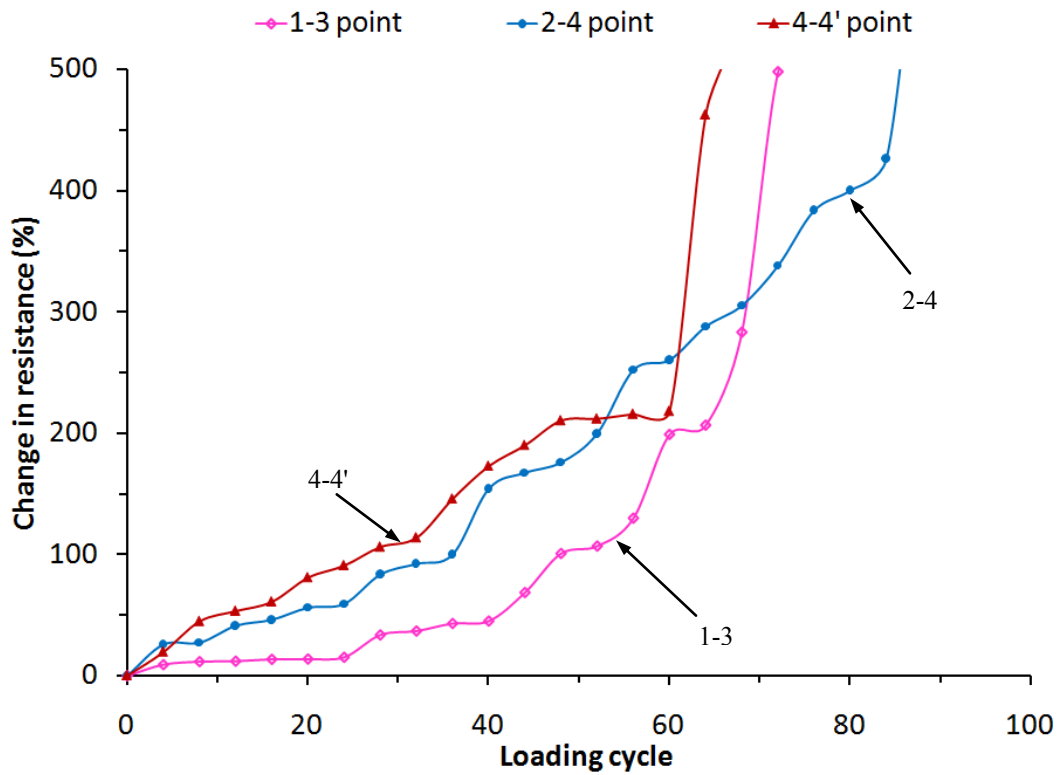


Figure 4.7 a) Variation of change (%) in electrical resistance with loading cycles for sample IV, (maximum 12000N)

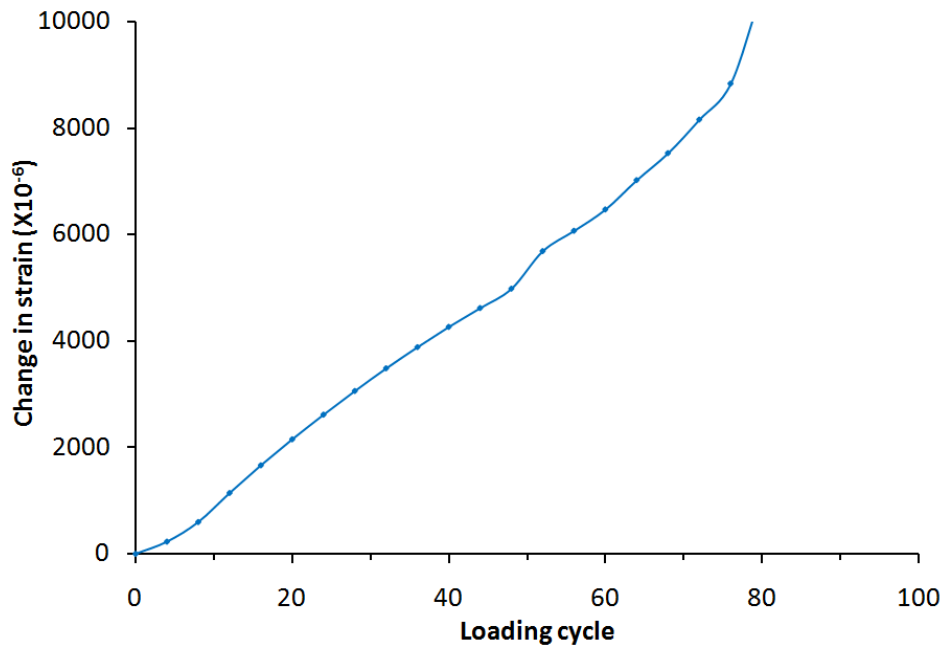


Figure 4.7 b) Variation of change in strain with loading cycles for sample IV, (maximum 12000N)

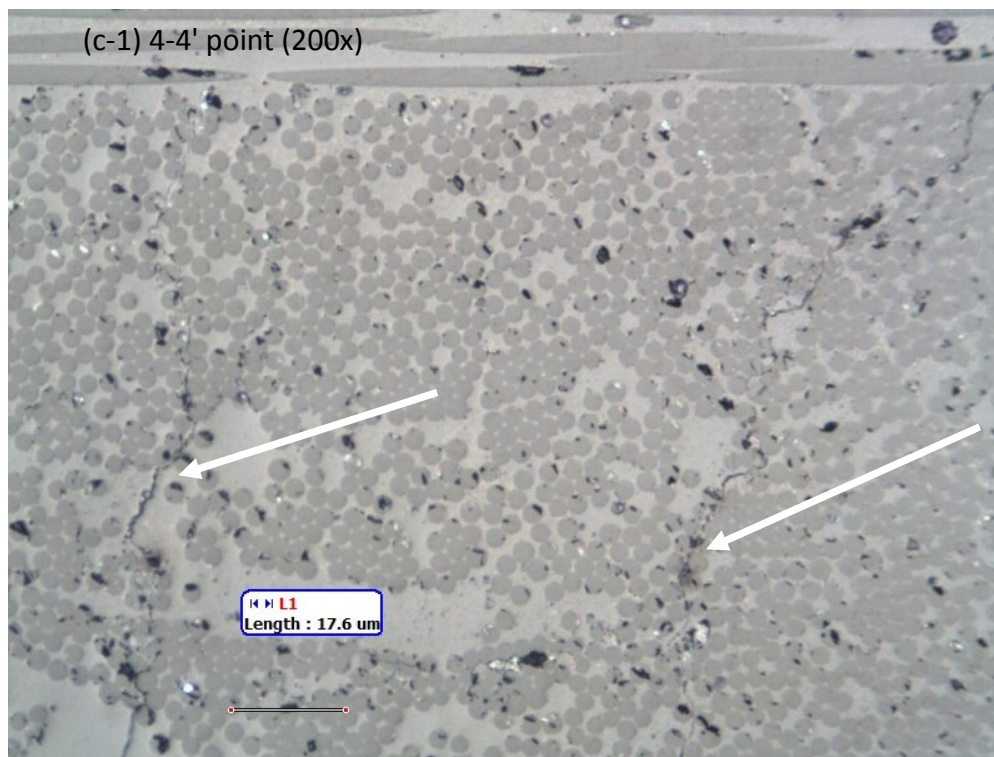


Figure 4.7 c-1) Optical image of sample IV, (maximum 12000N)

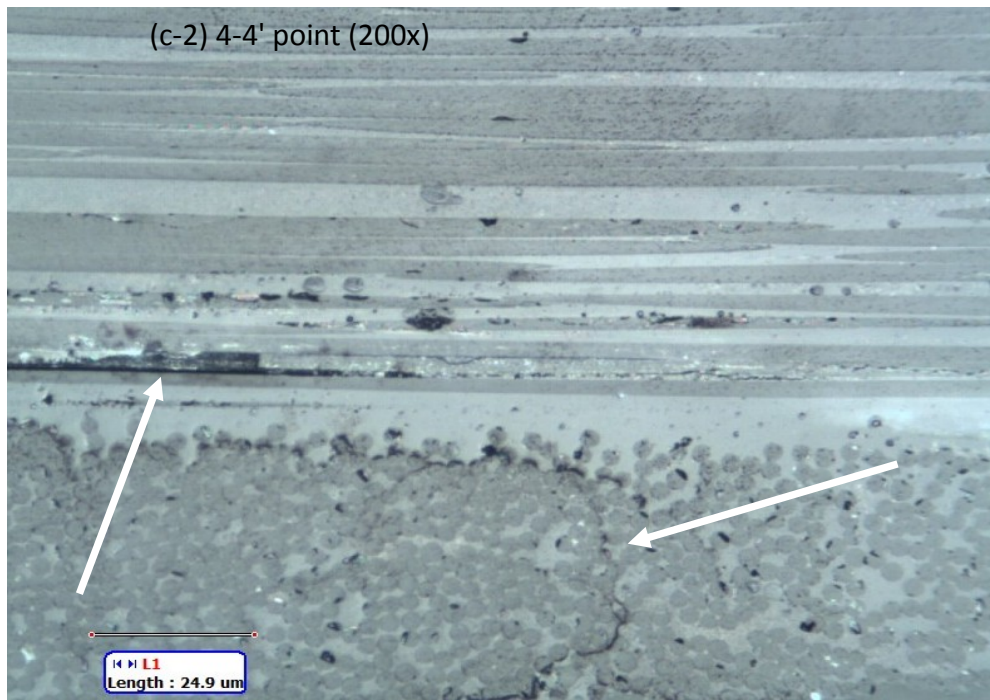


Figure 4.7 c-2) Optical image of sample IV, (maximum 12000N)

For higher loads it was found that at a given load, both the electrical resistance and strain increase with increasing loading cycles. For maximum loads of 6000N and 8000N, the through-thickness resistance show the jumps earlier than strains and in-plane resistances. This implies that the through thickness resistance can correspond well to the occurrence of damages like delamination. However, on the other hand, the in-plane resistance and strains could not detect this damage as effectively as through thickness resistance under these loads. Thus, it might not be safe to use strain gauges and in-plane resistance measurement for health monitoring of composite structures at these loads. For very high loads, e.g. at 10000N and 12000N maximum loads, all resistances and gauge reading increase.

#### **4.2.2 Fatigue test for lower load levels (below the first-ply-failure load)**

The first-ply-failure load was calculated from the stress analysis of the cross-ply  $[0_2/90_2]_S$  GFRP composite laminates and found to be around 3500N. The maximum load 3000N which is below the first ply failure load was thus chosen for these tests in order to detect the initiation of fatigue damages. Each test was carried out for two replicates. For lower load below first-ply-failure, the tests were periodically paused at after every 20 cycles. The first tests were done for sample I up to 500 cycles, the second tests were done for sample II up to 1000 cycles, the third tests were done for sample III up to 1500 cycles, and finally, the fourth tests were done for sample IV up to 2000 cycles. Table 3.7 summarizes this test schedule. All the results shown in this section are for maximum load 3000N and minimum load 250N.

In figure 4.8, the percentage change of electrical resistance in both a) in-plane and b) through-thickness positions with loading cycles are shown for sample I at 500 cycles. The corresponding variation of change in strains with loading cycles is shown in figure 4.8 (c). In figure 4.9 (a), (b) and (c), the SEM images as observed in different through thickness planes where the through thickness resistances were measured, are shown. It is observed from figure 4.8 (a-c) that up to 500 cycles, the changes in resistances (%) in in-plane positions and change in strains are almost constant while in through thickness positions the resistance (%) increases slightly. These facts can be correlated to the images shown in figure 4.9 (a, b, c) where no observable damage or cracks can be identified even in the through-thickness planes.

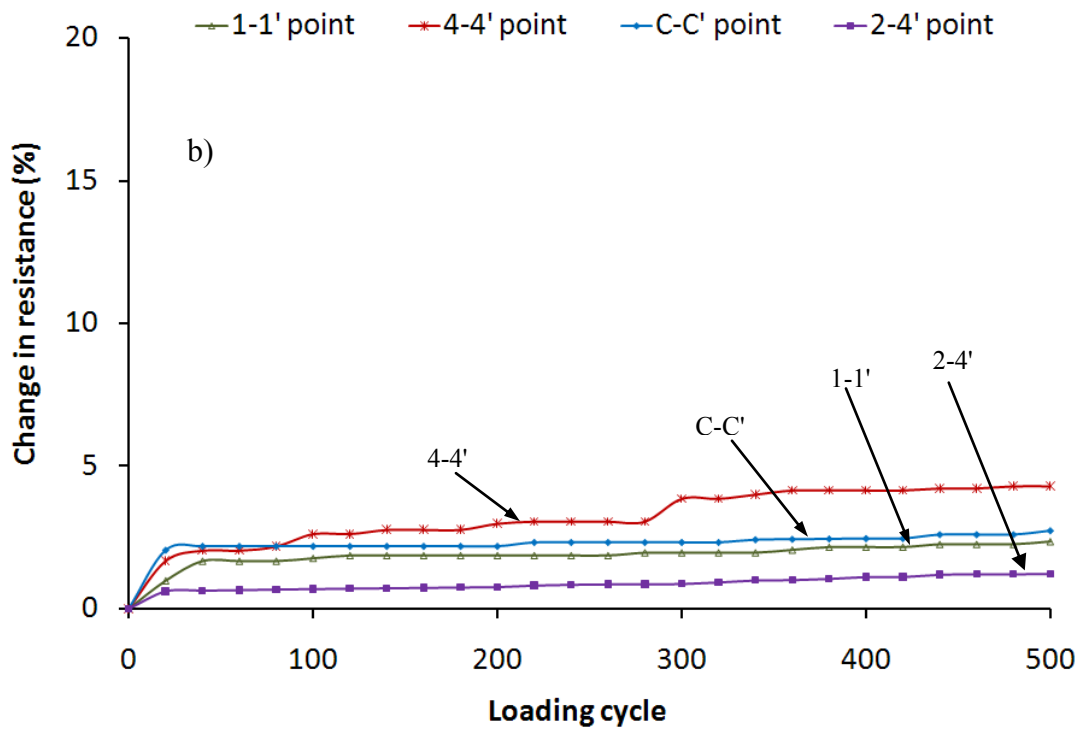
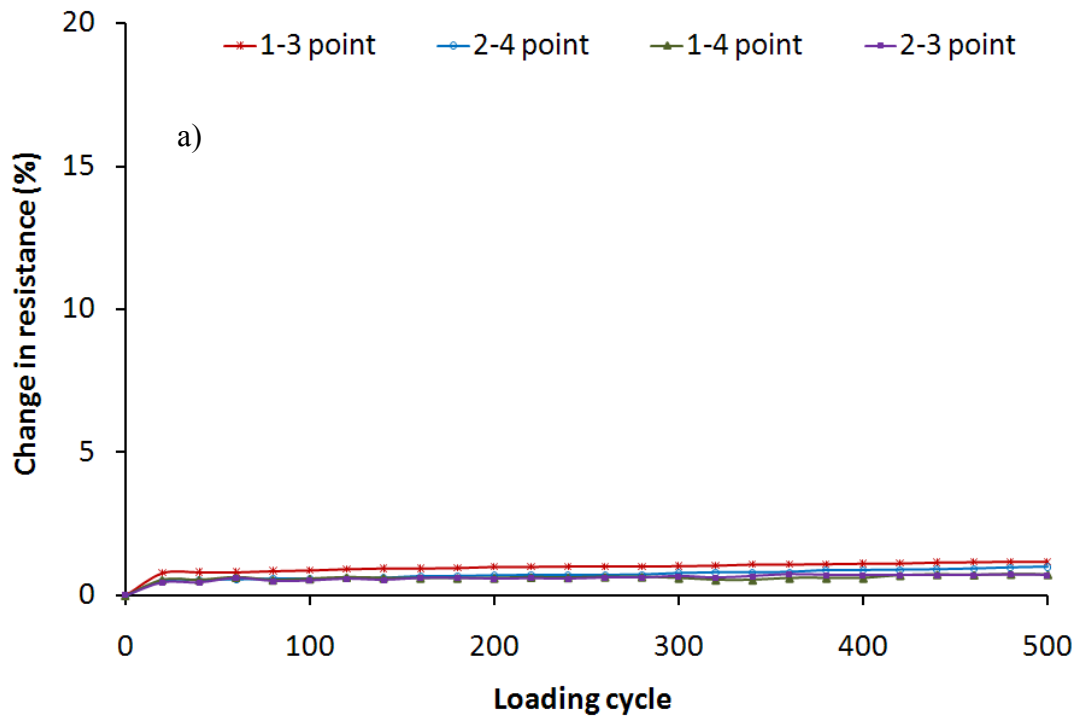


Figure 4.8 Variation of percentage change in electrical resistance in a) in-plane, and b) through thickness positions with loading cycle for sample I, (maximum 3000N)

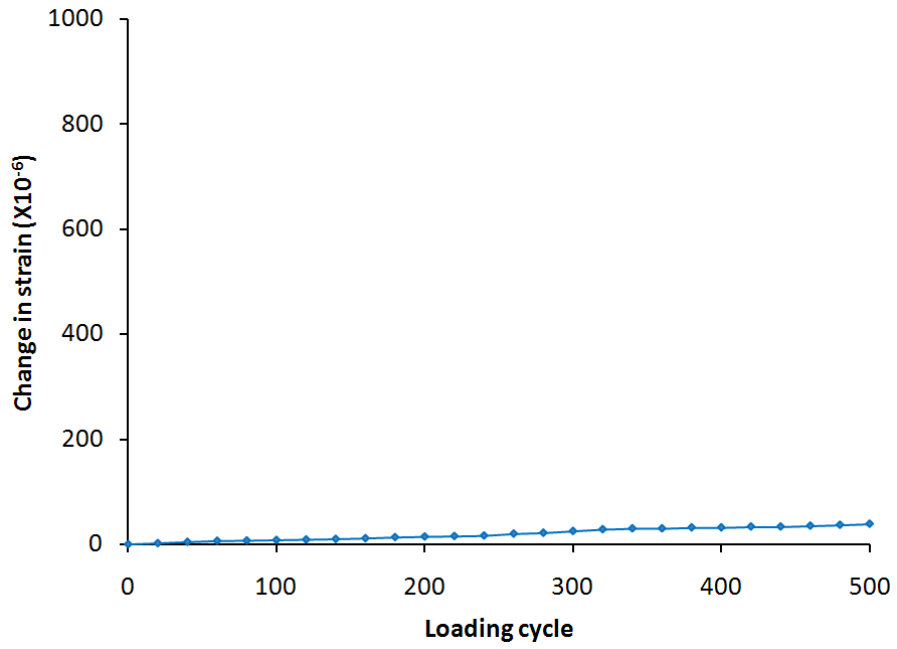


Figure 4.8 c) Variation of change in strain with loading cycles for sample I, (maximum 3000 N)

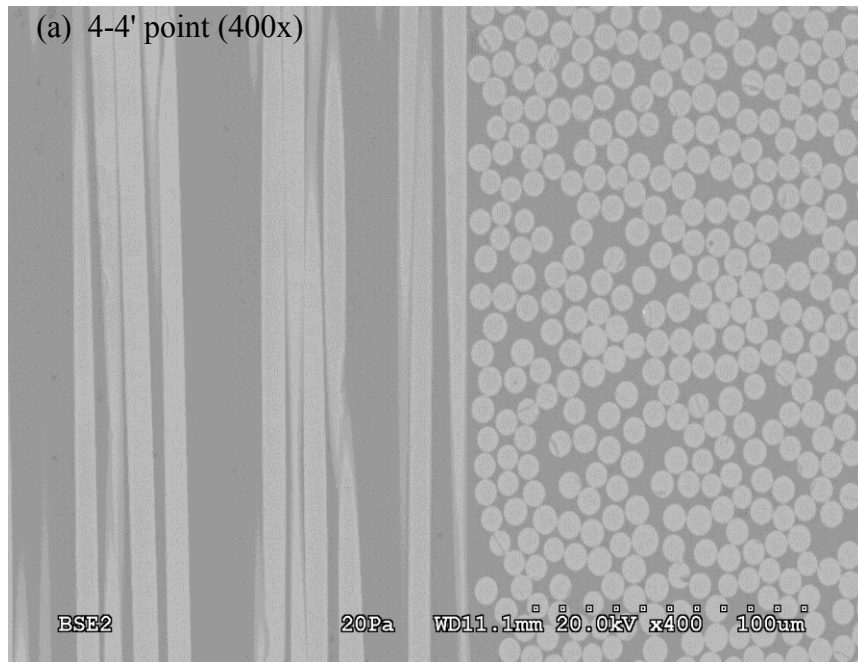


Figure 4.9 a) SEM images at different through thickness positions for sample I, (maximum 3000 N)

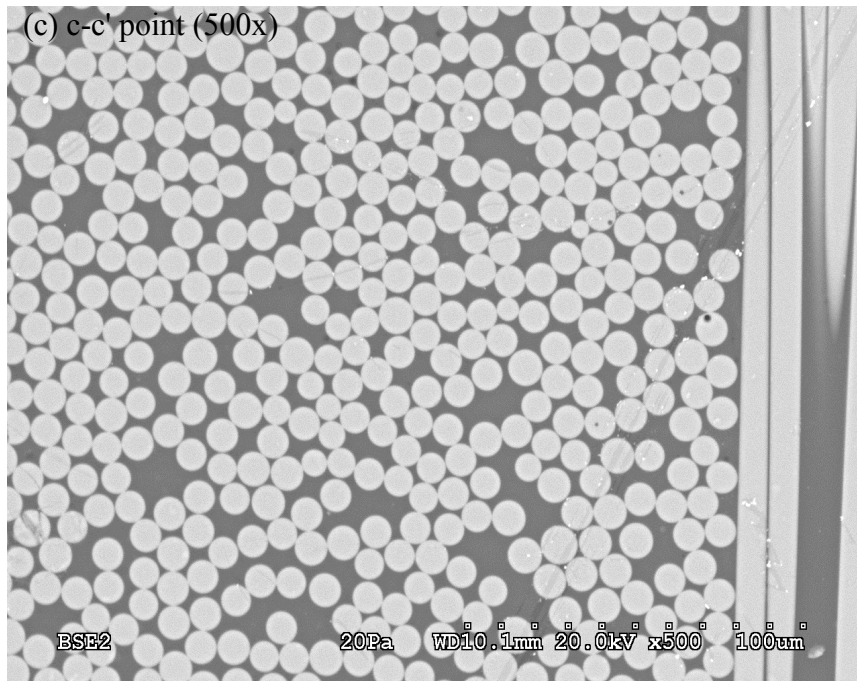
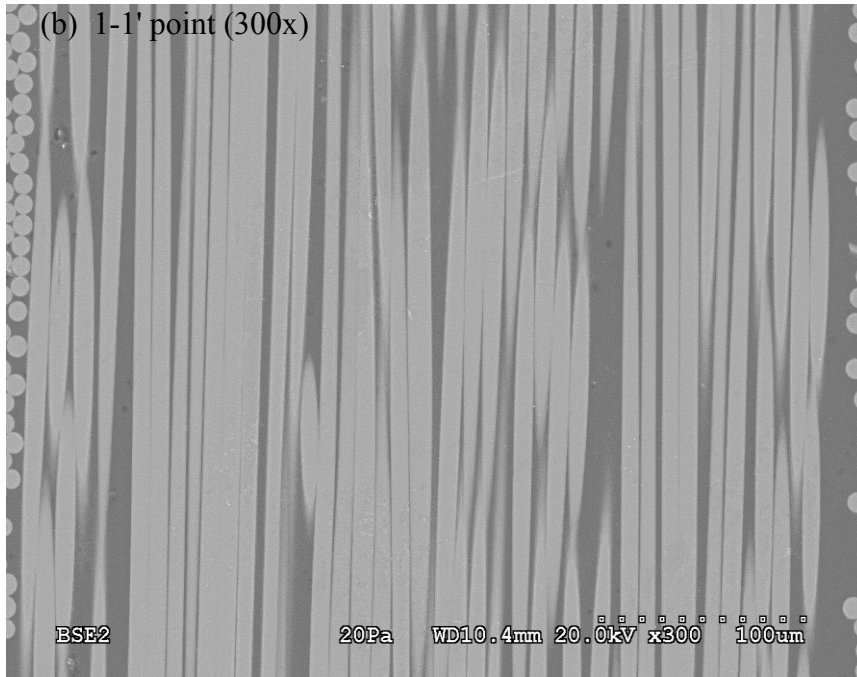


Figure 4.9 b, c) SEM images at different through thickness positions for sample I, (maximum 3000 N)

A similar trend was found for sample II tested up to 1000 cycles as shown in figure 4.10 (a, b, c) and 4.11 (a, b, c). It can thus be resolved that below the first ply failure load, up to 1000 cycles, no significant damages initiate in the samples. This is reflected in the result which shows no significant changes in electrical resistances.

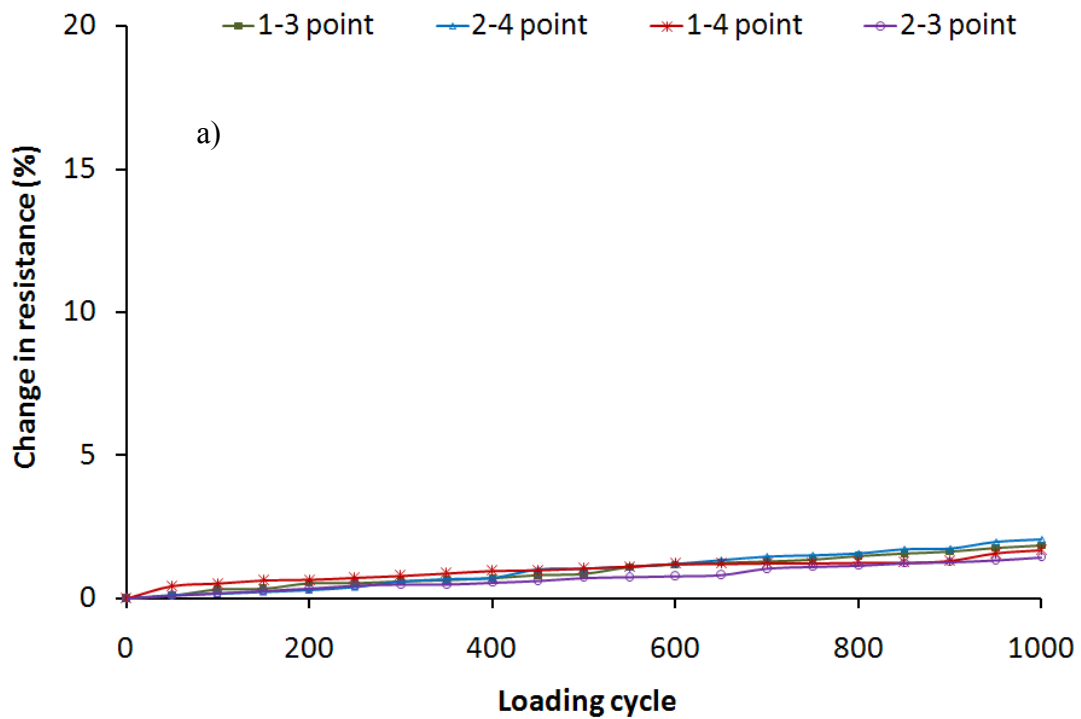


Figure 4.10 a) Variation of percentage change in electrical resistance in in-plane positions with loading cycles for sample II, (maximum 3000 N)

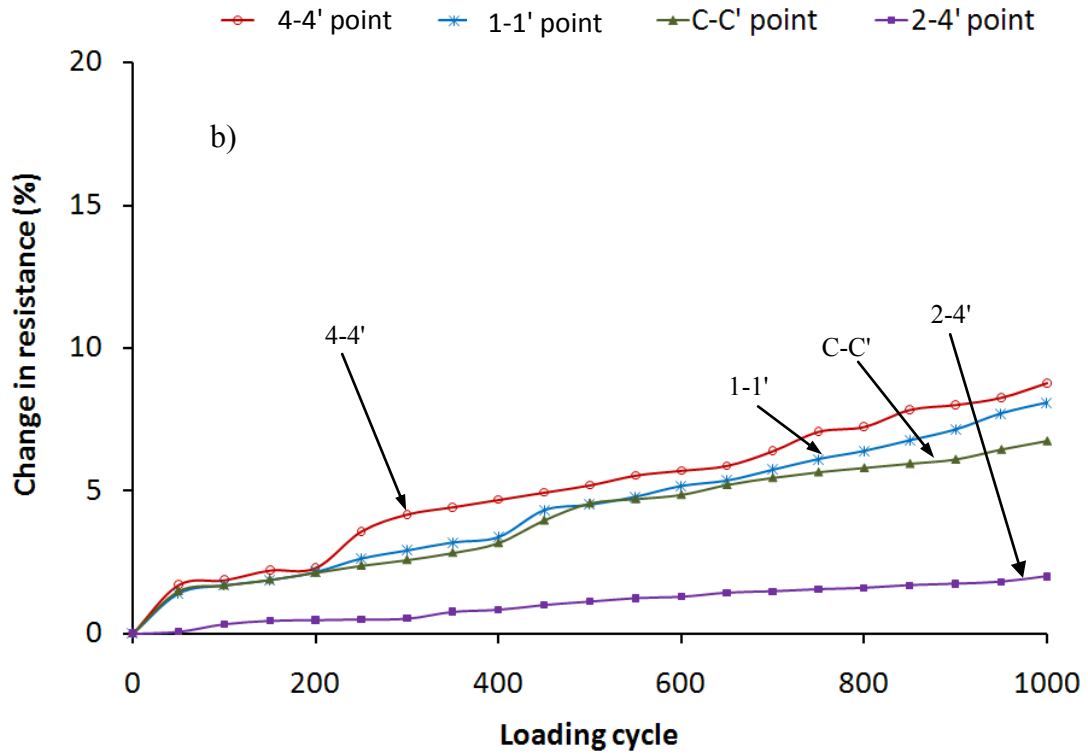


Figure 4.10 b) Variation of percentage change in electrical resistance in Through-thickness positions with loading cycles for sample II, (maximum 3000 N)

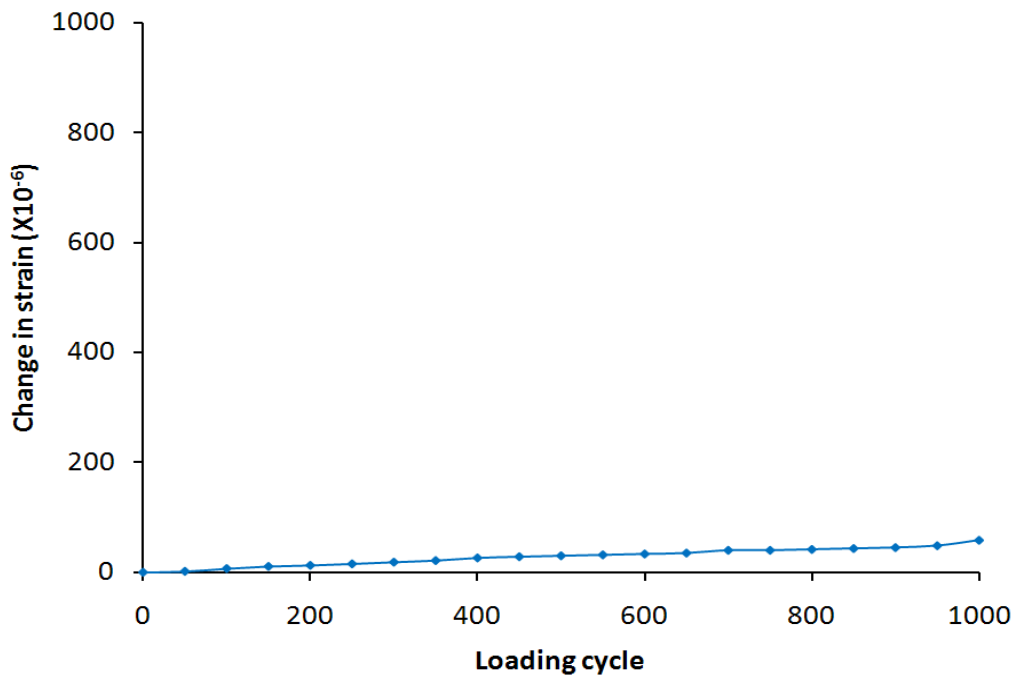


Figure 4.10 c) Variation of change in strain with loading cycles for sample II, (maximum 3000 N)

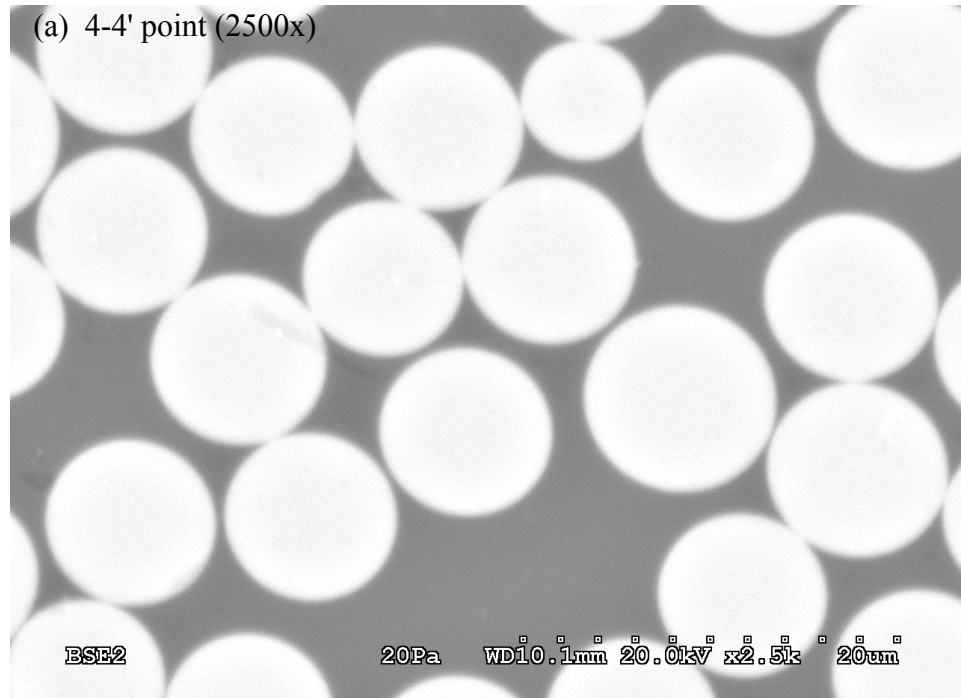


Figure 4.11 a, b) SEM images at different through thickness positions for sample II, (maximum 3000 N)

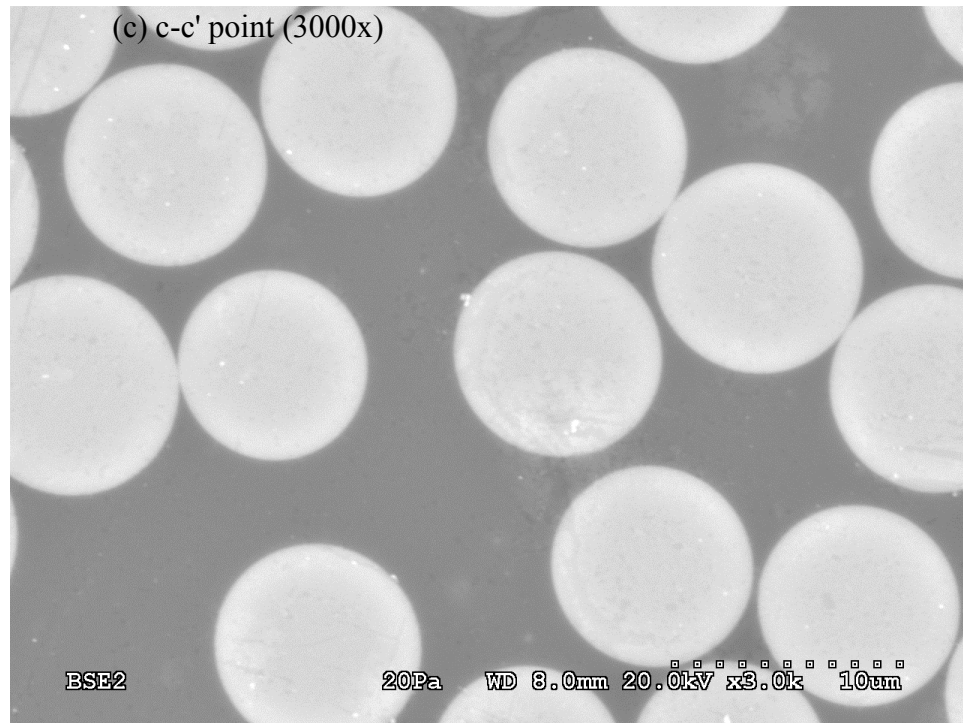


Figure 4.11 c) SEM images at different through thickness positions for sample II, (maximum 3000 N)

When the number of cycles increased to 1500, it is observed from figure 4.12, as shown below, that the in-plane change in resistances (%) (figure 4.12 a) and change in strains (figure 4.12 c) varies in slightly linear manner while the change in resistance (%) in through-thickness positions (figure 4.12 b) increases significantly, again, with sudden jumps after a number of certain cycles. Figure 4.13 (a, b, c) shows the corresponding SEM images of sample III at different through thickness planes where a few micro cracks are clearly observed.

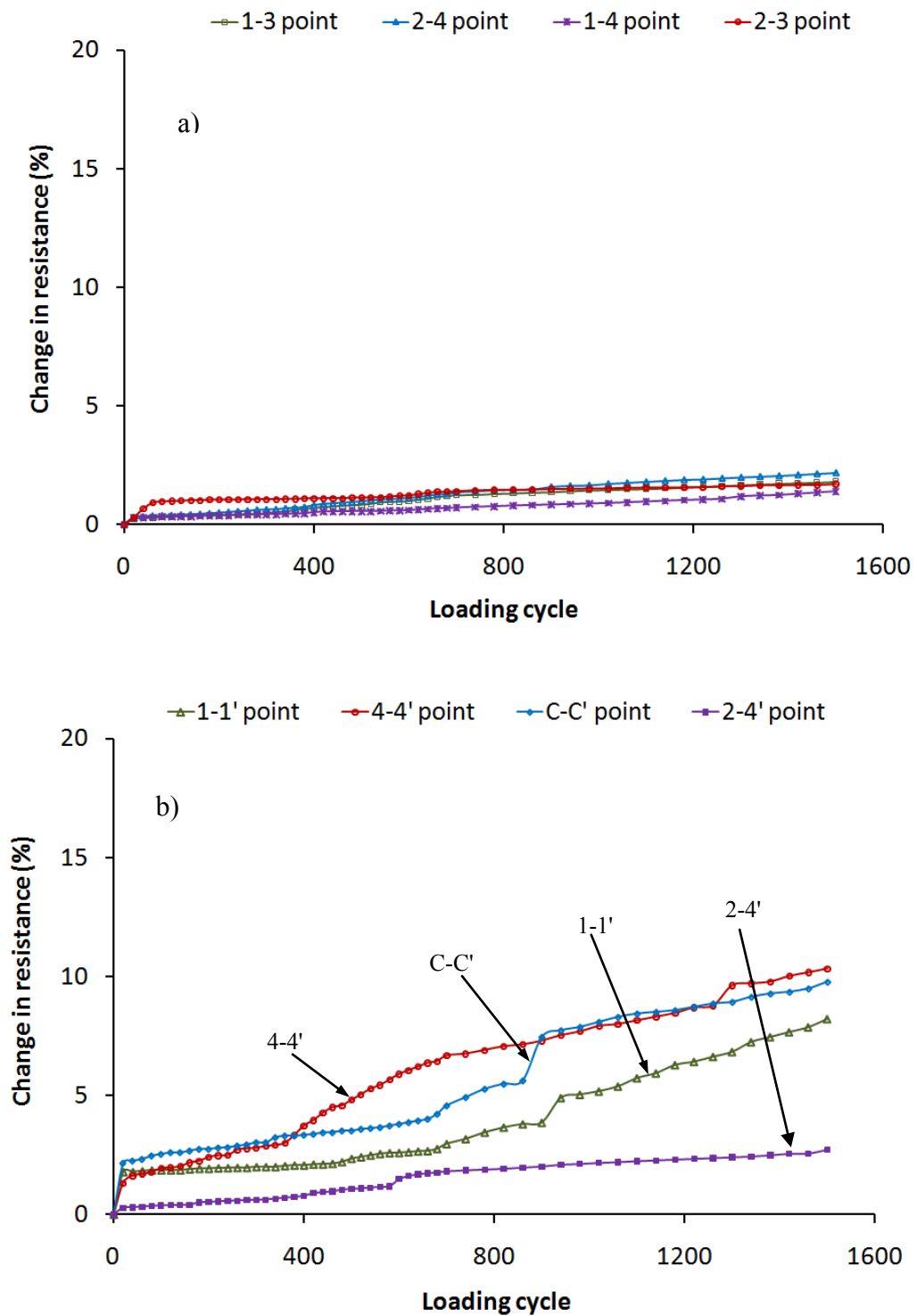


Figure 4.12 Variation of percentage change in electrical resistance in a) in-plane and b) through-thickness positions with loading cycle for sample III, (maximum 3000 N)

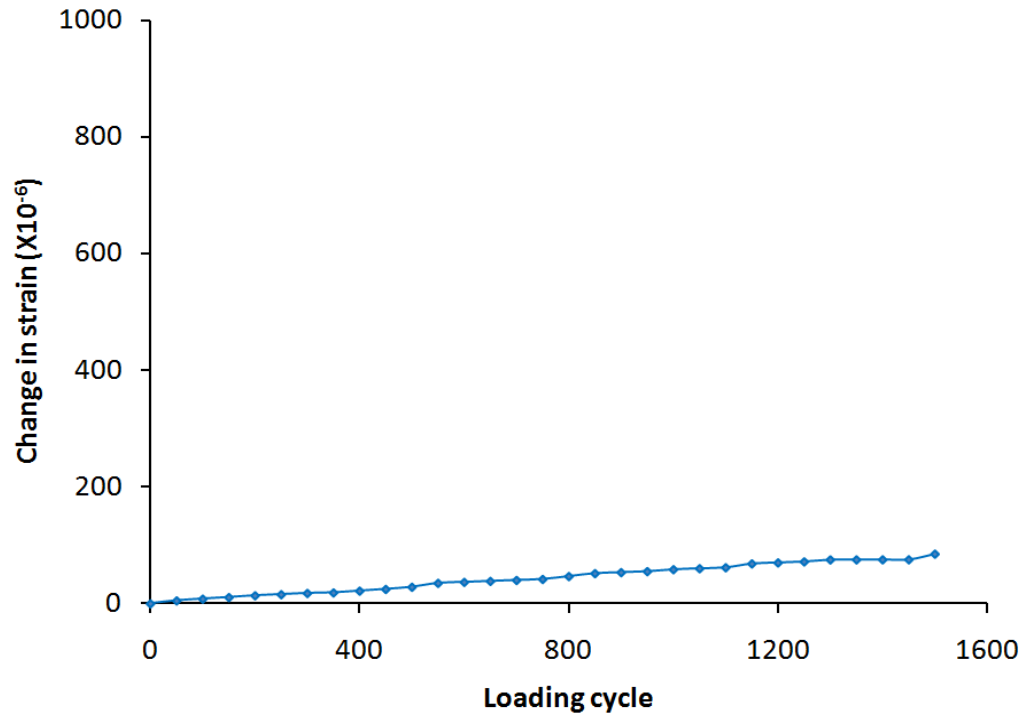


Figure 4.12 c) Variation of change in strain with loading cycles for sample III, (maximum 3000 N)

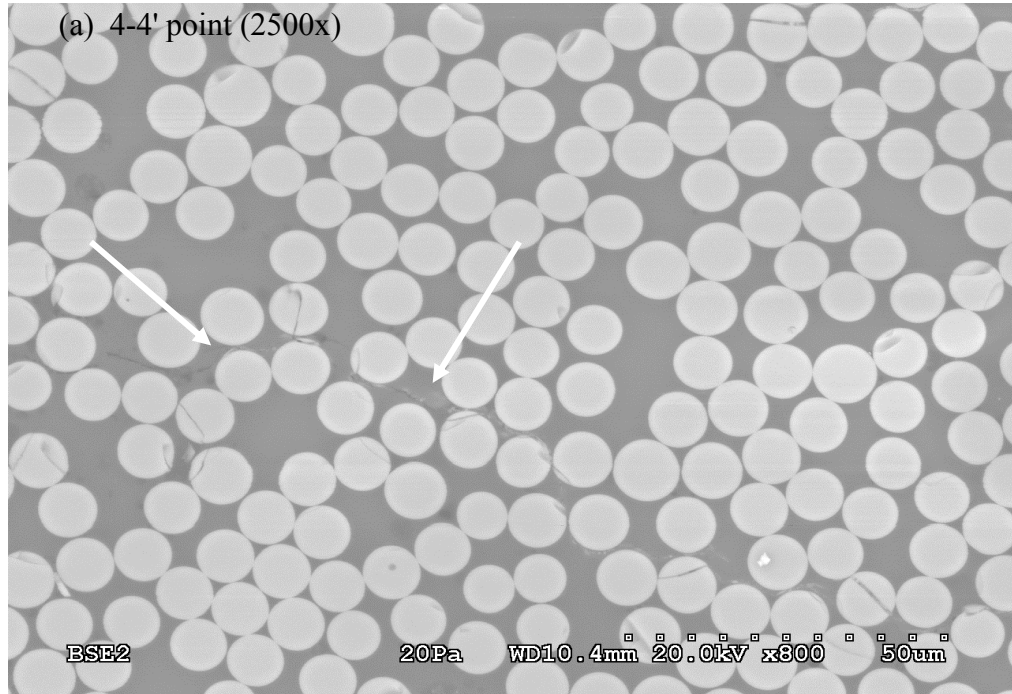


Figure 4.13 a) SEM images at different through thickness positions for sample III, (maximum 3000 N)

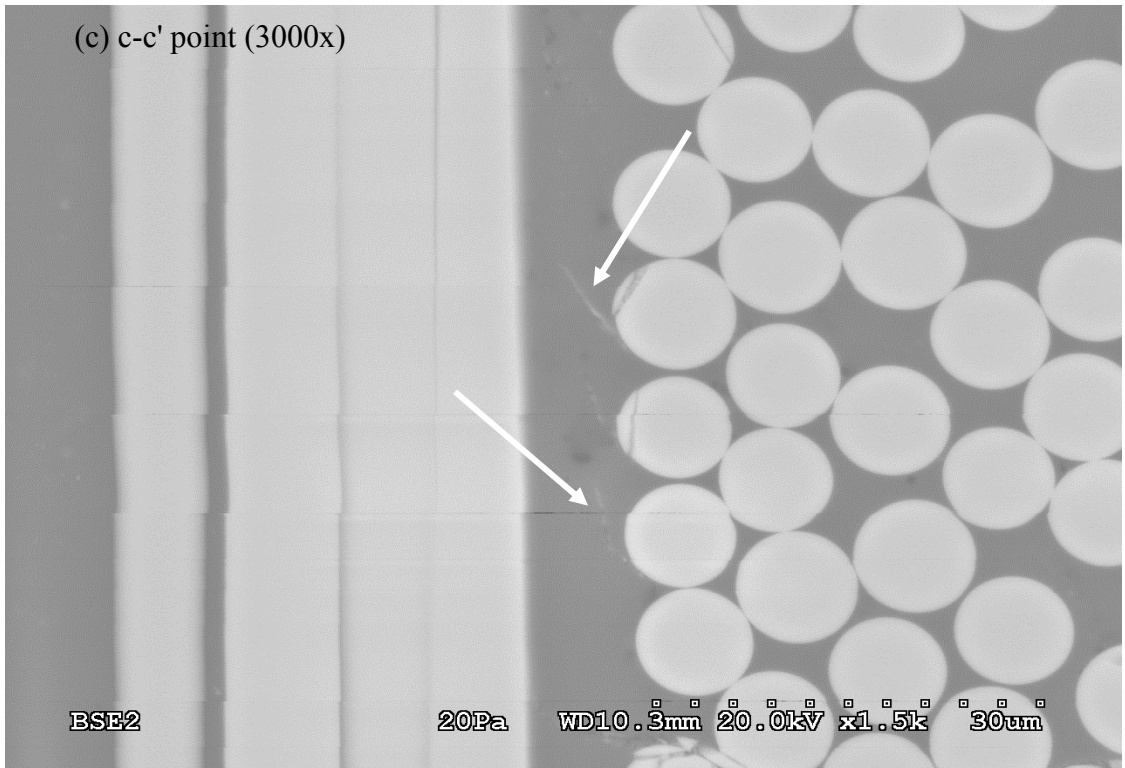
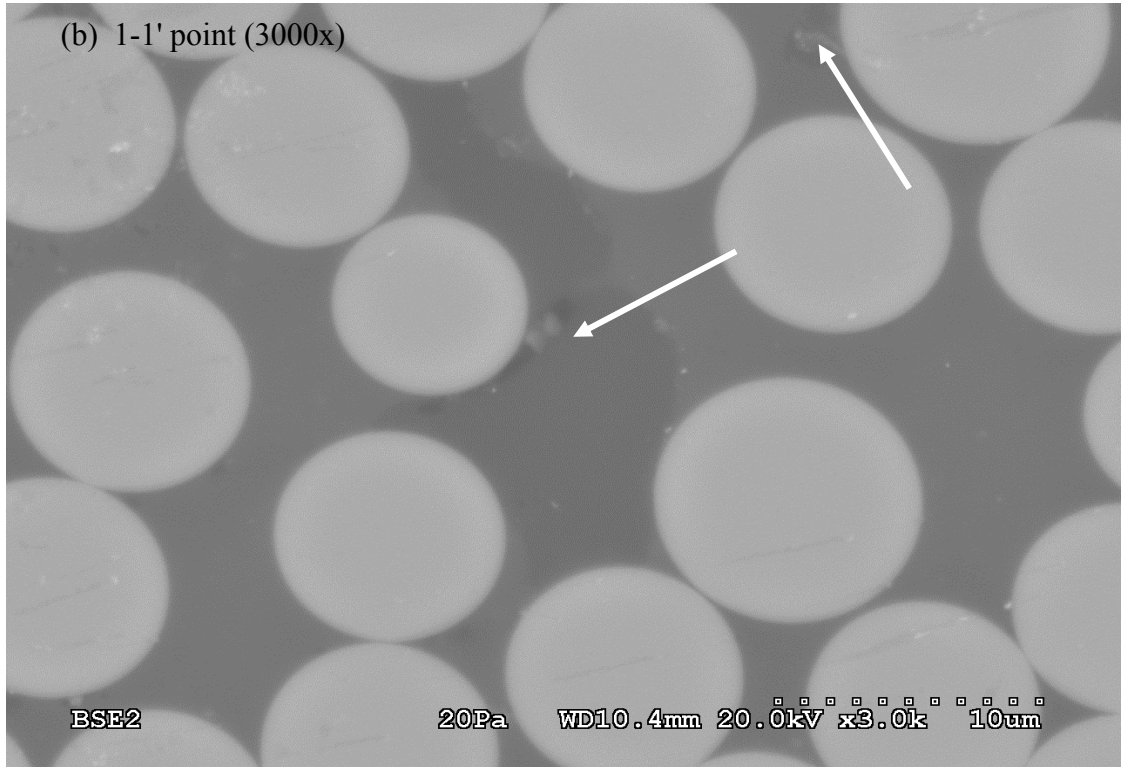


Figure 4.13 b, c) SEM images at different through-thickness positions for sample III, (maximum 3000 N)

It is thus understood from these figures that, at this level of load and cycles, the initiation of damages occur in the sample which is correlated with the changes in through-thickness electrical resistance (%). However, the in-plane resistance changes and strain changes are relatively insensitive to this initiation of micro cracks. Among the through-thickness positions, the resistance in 4-4' point increases more compared to that of other through-thickness positions, which, interestingly, corresponds to the higher accumulation of damages in 4-4' point as observed in figure 4.12 (b) and 4.13 (a). This result also highlights the capability of carbon nanotubes conductive path inside the polymer matrix, of sensing the initiation of fatigue damages, primarily via through-thickness electrical resistance response.

Finally, when the number of cycles increased to 2000 cycles, it is observed from figure 4.14 (a, b, c) below, that the in-plane change of resistances (%) (figure 4.14 a) and strains (figure 4.14 c) change slightly higher than the previous sample III. At the same time, the change in residual resistances (%) in through-thickness positions is substantially higher (figure 4.14 b) with sudden jumps near 2000 cycles. Figure 4.15 (a, b, c) shows the corresponding SEM images of sample IV at different through thickness planes where micro cracks appear at multiple locations.

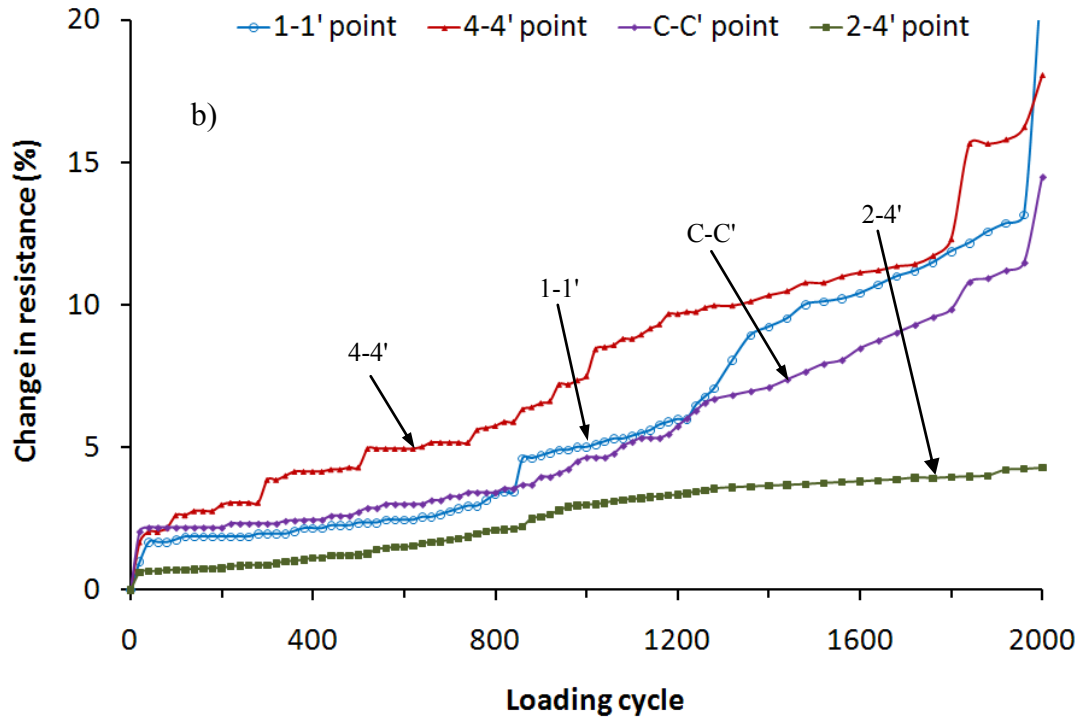
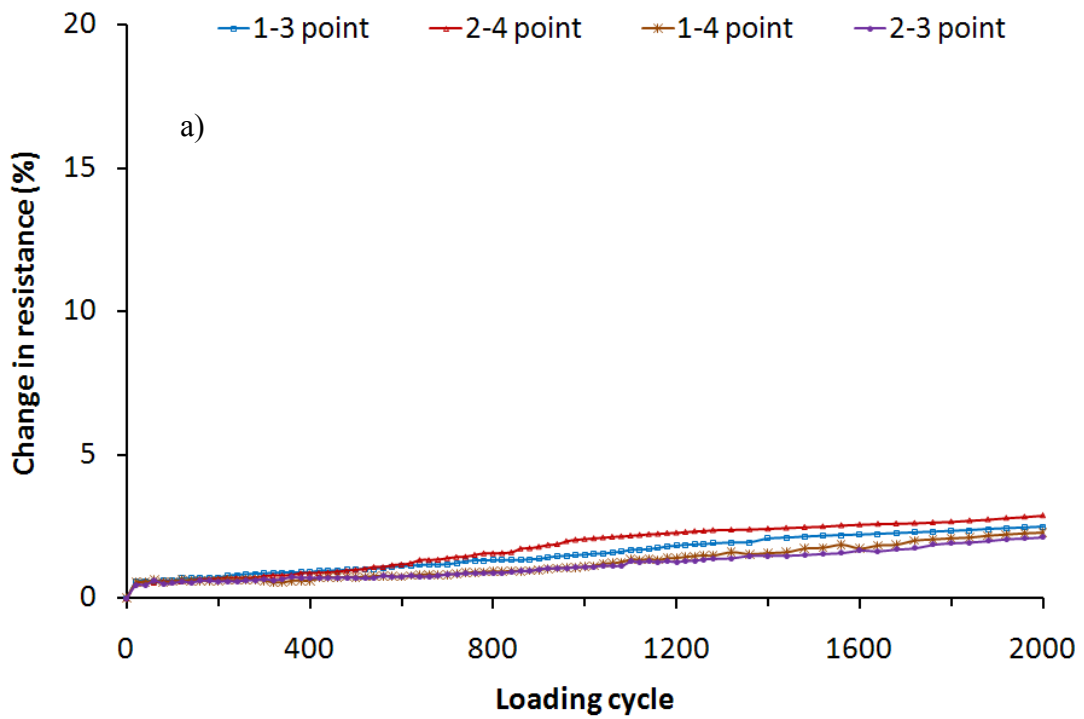


Figure 4.14 Variation of percentage change in electrical resistance in a) in-plane and b) through-thickness positions with loading cycle for sample IV, (maximum 3000 N)

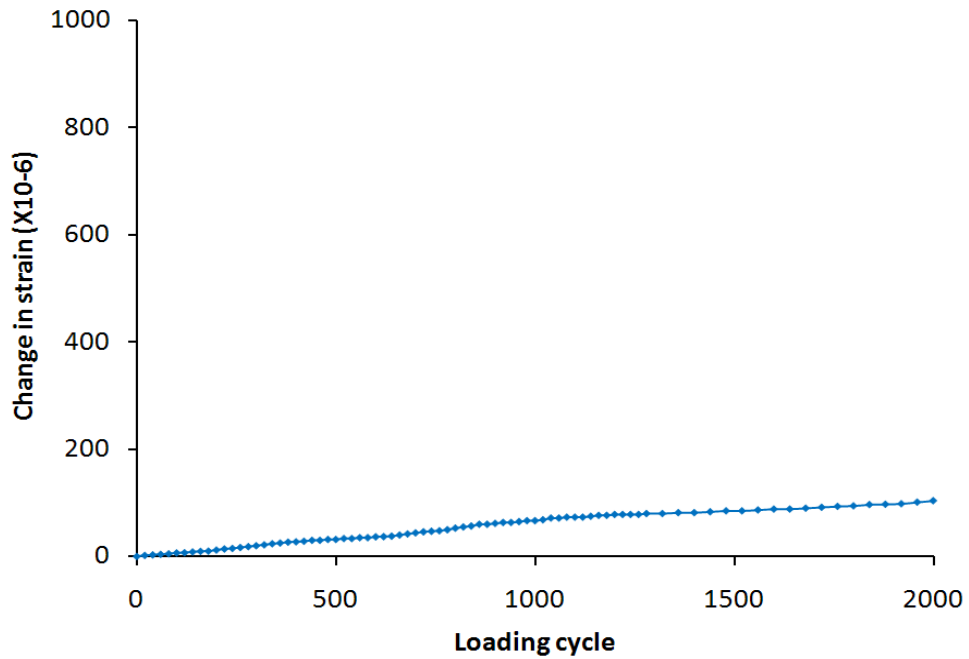


Figure 4.14 c) Variation of change in strain with loading cycles for sample IV, (maximum 3000 N)

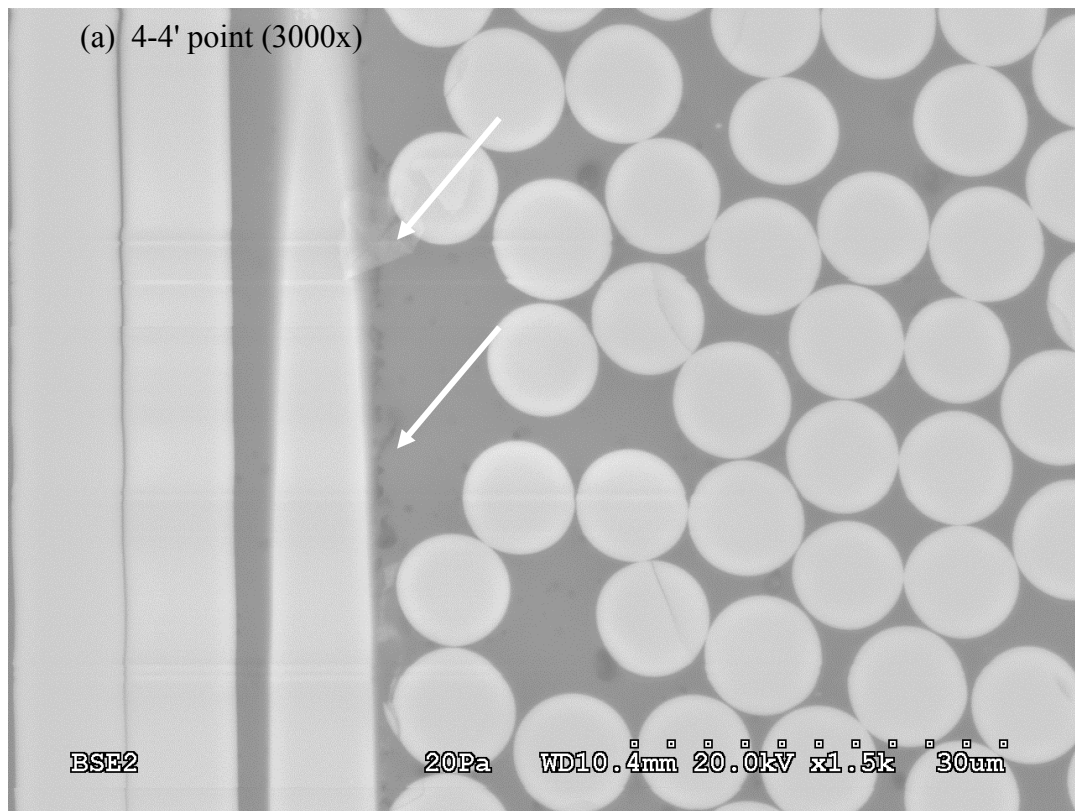


Figure 4.15 a) SEM images at different through thickness positions for sample IV, (maximum 3000 N)

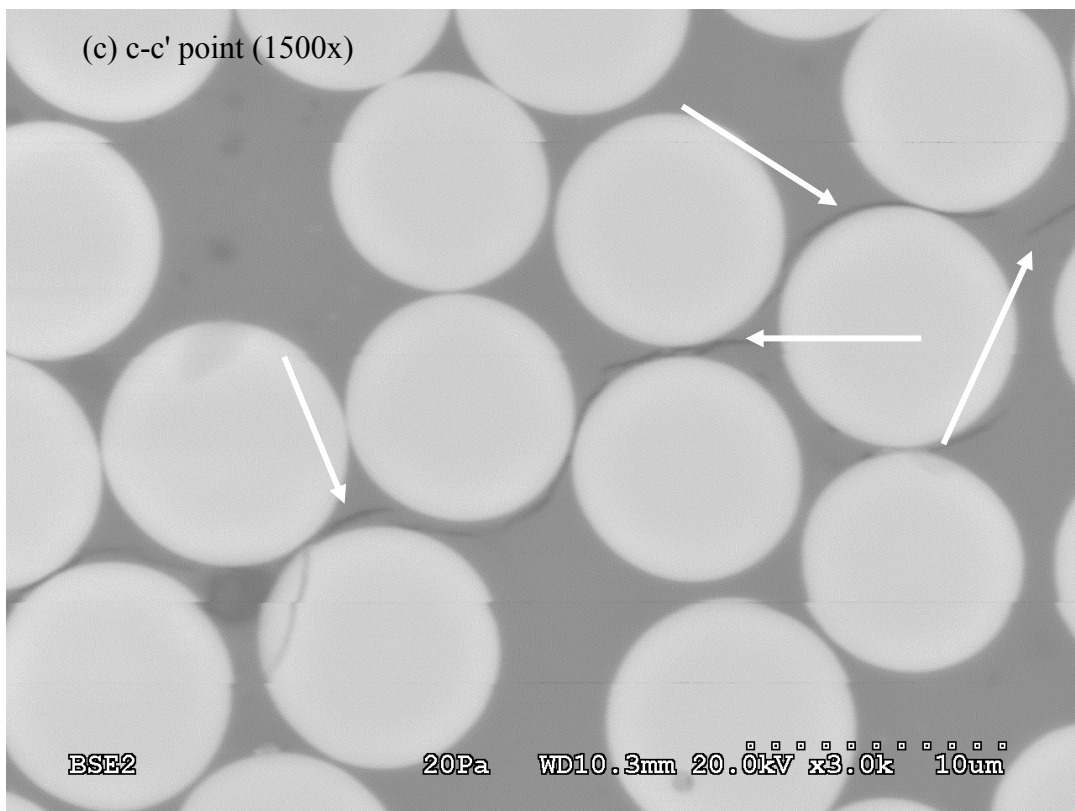
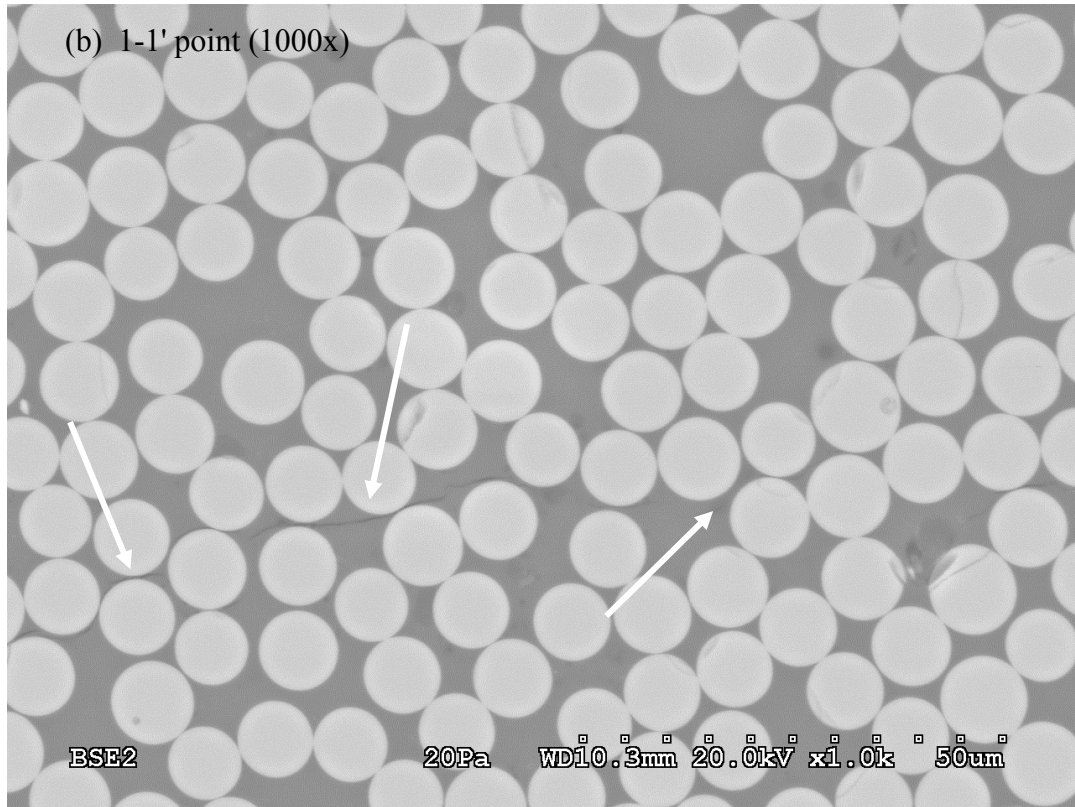


Figure 4.15 b, c) SEM images at different through thickness positions for sample IV, (maximum 3000 N)

It can thus be recognized that, at this level of load and cycles, more damages start to accumulate which clearly corresponds with the higher rate of changes in through-thickness resistance (%). The in-plane change of resistance and residual strains, however, could not correspond to the damage state distinguishably and as sensitively as that of through-thickness resistance change. With increasing loading cycles, the defects such as matrix cracks, initiation of delamination etc. occurred in the sample as shown in figures 4.15 (a, b, c). These damages, as observed visually, could be correlated quickly by an abrupt change of through-thickness electrical resistance near 2000 cycles as in figure 4.14 (b).

In summary, one sees that with 3000N load, microcracks initiates in sample III with 1500 cycles. Microcracks start to accumulate in sample IV with 2000 cycles. The rate of change of strains and changes in resistance (%) increases progressively with increasing number of cycles for different samples under the given load. However, the change in through-thickness resistance increases much earlier than in-plane resistance and strains. Thus, the through-thickness resistance response is more sensitive than the in-plane resistance and strains and corresponds well to the initiation of damages in the laminates.

# CHAPTER 5

## Conclusion, Contributions and Recommendations

### 5.1 Conclusion

Based on the above results, it can be concluded that CNTs are effective sensors for monitoring damages in glass/epoxy composite. Although, both strain and electrical resistance changes with the accumulation of damages, the change in resistance in through thickness positions is found to be more sensitive as it increases earlier in the loading cycles. In general, the electrical resistance response is found to correlate well with the extent and progression of damages. While the strain gauge can not to monitor damage with a certain level of loads after certain cycles, the electrical resistance can monitor the accumulation of damages with a very high number of cycles. Further, among the in-plane and through thickness resistance response, the through thickness response can represent the initiation of damages more sensitively and quickly. The greatest benefit of electrical resistance method thus can be realized in case of lower loads. At this load levels, the through-thickness resistance can detect the initiation of damage effectively in the GFRP composites. Thus, the conductive percolating network of CNTs can be effectively utilized to predict the degradation of structural components made of non-conductive GFRP composite.

## **5.2 Contribution**

The electrical resistance method is proved to be more reliable in detecting damage in CNT incorporated GFRP composites than strain measurements as it senses the initiation of damage earlier than strains. It is thus safer to use this method in predicting the degradation of composite parts in real applications. It thus allows more time for precautionary measures during operation of a structural component under fatigue loading. It is established in this work that the electrical resistance response, particularly, the response in through-thickness positions of the laminate can effectively be utilized for monitoring the damage in GFRP composites under cyclic loading.

## **5.3 Recommendations**

It would be very useful if the changes in electrical resistances can be monitored continuously during the test instead of taking readings manually after certain intervals.

To study the effectiveness of electrical resistance response in real applications, a structural component made of GFRP composites instead of laminate samples can be tested. Instead of GFRP composites, other advanced non-conductive fiber reinforced composite laminates can also be incorporated with MWCNTs and tested to evaluate the performance of electrical resistance method. The current method can also be extended to carbon/epoxy composites.

## References

- [1] Thostenson, E.; Ren, Z. and Chou, T.; "Advances in the science and technology of carbon nanotubes and their composites: a review"; *Composites Science and Technology*, vol. 61 (13), p: 1899-1912, (2001)
- [2] Che, J., Cagin, T. and Goddard III, W.; "Thermal conductivity of carbon nanotubes"; *Nanotechnology*, vol. 11 (2), p: 65-69, (2000)
- [3] Thostenson, E.; Li, C. and Chou, T., "Nanocomposites in context "; *Composites Science and Technology*; vol. 65 (3-4), p: 491-516, (2005)
- [4] Thostenson, E.; Gendlin, V. and Chou, T., "Carbon nanotube composites for self-sensing of deformation and damage" *International SAMPE Symposium and Exhibition (Proceedings)*, vol. 52, *SAMPE '07: M and P - From Coast to Coast and Around the World; Conference Proceedings E.* (2007)
- [5] Thostenson, E. and Chou, T., "Multifunctional composites with self-sensing capabilities: Carbon nanotube-based networks"; *Proceedings of the SPIE -The International Society for Optical Engineering*, vol.6526, p: 65261X, (2007)
- [6] Zhang, W.; Sakalkar, V. and Koratkar, N., "In Situ Health Monitoring and Repair in Composites using Carbon Nanotube Additives", *Applied Physics Letters*, vol. 91 (13), p: 1-3, (2007)
- [7] Schulte, K., " Damage monitoring in polymer matrix structures "; *Journal De Physique*, vol. 3 (7), pt 3, p 1629-1636, (1993)
- [8] Wang, X. and Chung, D. "Sensing delamination in a carbon fiber polymer-matrix composite during fatigue by electrical resistance measurement". *Polym. Compos.* vol. 18 (6), p: 692-700, (1997)
- [9] Irving, P. and Thiagarajan, C., " Fatigue damage characterization in carbon fibre composite materials using an electrical potential technique", *Smart Mater. Struct.* vol. 7 (4), p: 456-466, (1998)
- [10] Kupke, M., Schulte, K. and Schüler, R., " Non-destructive testing of FRP by d.c. and a.c. electrical methods" *Composites Science and Technology*, vol. 61(6), p: 837-847, (2001)
- [11] Seo, D.; Lee, J., "Damage detection of CFRP laminates using electrical resistance measurement and neural network", *Composite Structures*, vol. 47, p: 525-530, (1999)
- [12] Vavouliotis, A.; Tsotra, P.; Kostopoulos, V.; Karapappas, P.; Miaris, A.; Nikolaou, N., "MWCNT-modified fiber reinforced composites with nano-sensing

capabilities: A way towards the development of the new functional materials for space applications, *AIAA 57th International Astronautical Congress, IAC 2006*, vol. 8, , p: 5523-5530, (2006)

- [13] Kostopoulos, V.; Vavouliotis, A. Karapappas, P; Miaris, Tsotra, P. and Paipetis, A. "Damage monitoring of carbon fiber reinforced laminates using resistance measurements. Improving sensitivity using carbon nanotube doped epoxy matrix system" *Journal of intelligent material systems and structures*, vol. 20, p:1025-10, (2009)
- [14] Schulte, K.; "Damage development under cyclic loading loading"; *Polymer Engineering and Science*, vol. 42, p: 1815-1826, (2002)
- [15] Hahn, H. & Kim, R.; "Fatigue behavior of composite laminate" *Composite Materials*, vol. 10, p: 156-180, (1976)
- [16] Highsmith, A.; Stinchcomb, W. and Reifsnider, K., "Effect of fatigue-induced defects on the residual response of composite laminates". *ASTM Special Technical Publication*, p: 194-216, (1984)
- [17] Reifsnider, K. and Talug, A., "Analysis of fatigue damage in composite laminates" *International Journal of Fatigue*, vol. 2 (1), p: 3-11, (1980)
- [18] Stinchcomb, W. and Reifsnider, K. "Fatigue damage mechanisms in composite materials: a review" *ASTM Special Technical Publication*, n 675, p:762-787, (1979)
- [19] Reifsnider, K. "Fatigue behavior of composite materials" *International Journal of Fracture*, vol. 16 (6), p: 563-83, (1980)
- [20] O'Brien, T. and Reifsnider, K. "Fatigue damage evaluation through stiffness measurements in boron-epoxy laminates"; *Journal of Composite Materials*, vol. 15, p: 55-70, (1981)
- [21] Reifsnider, K.; Jamison, R. " Fracture of fatigue-loaded composite laminates"; *International Journal of Fatigue*, vol. 4 (4), p: 187-197, (1982)
- [22] Hahn, H. and Kim, R. " Fatigue behavior of composite laminate"; *Journal of Composite Materials*, vol. 10, p: 156-180, (1976)
- [23] Reifsnider, K., "Fatigue of Composite Materials", Elsevier, Amsterdam, 1991.
- [24] Jamison, R.; "Role of micro damage in tensile failure of graphite/epoxy laminates"; *Composites Science and Technology*, vol. 24 (2), p. 83-99, (1985)

- [25] Philippidis, T. and Vassilopoulos, A.; "Fatigue design allowable for GRP laminates based on stiffness degradation measurements"; *Composites science and technology*, vol. 60(15), p: 2819-28, (2000)
- [26] Philippidis, T. and Vassilopoulos, A. "Fatigue of composite laminates under off-axis loading "; *International Journal of Fatigue*, vol. 21(3) p: 253-62, (1999)
- [27] Crane, R.; Macander, A. and Gagorik, J. "Fiber optics for a damage assessment system for fiber reinforced plastic composites structures"; *Review of Progress in Quantitative Nondestructive Evaluation*, vol.2B, p: 1419-30, (1983)
- [28] <http://www.ndt-ed.org/>
- [29] <http://rope-access.co.za/>
- [30] Fiedler, B.; Gojny, F.; Wichmann, M.; Bauhofer, W. and Schulte, K.; " Can carbon nanotubes be used to sense damage in composites? *Annales de Chimie (Science des Materiaux)*, vol. 29 (6), p : 81-94, (2004)
- [31] Ramirez, A., "Carbon nanotubes for science and technology" *bell labs technical journal*, vol. 10(3), p : 171-185, (2005)
- [32] Bandaru, P.," Electrical properties and applications of carbon nanotube structures", *Journal of Nanoscience and Nanotechnology*, vol. 7 (4-5), p: 1239-1267, (2007)
- [33] <http://nanopedia.case.edu/>
- [34] <http://conf.ncku.edu.tw/>
- [35] <http://www.google.ca/imgres>
- [36] <http://nanotube.korea.ac.kr/>
- [37] Iijima, S. "Helical microtubules of graphitic carbon"; *Nature*, vol. 354 (6348), p: 56-8, (1991)
- [38] Iijima, S. and Ichihashi, T. " Single-shell carbon nanotubes of 1-nm diameter" *Nature*, v 363, n 6430, p 603-15, 17, (1993)
- [39] Bethune, D.; Kiang, C.; deVries, M.; Gorman, G.; Savoy, R.; Vazquez, J.; Beyers, R., "Cobalt-catalysed growth of carbon nanotubes with single-atomic-layer walls" *Nature*, vol. 363(6430), p : 605-7, 17, (1993)

- [40] Falvo, M.; Clary, G.; Taylor, R.; Chi, V.; Brooks, F.; Washburn, S. and Superfine, R. " Bending and buckling of carbon nanotubes under large strain"; *Nature*, vol. 389 (6651), p: 582-4, (1997)
- [41] Chou, T., "Microstructural design of fiber composites"; Cambridge (UK): Cambridge University Press; (1992)
- [42] Berber, S.; Kwon, Y.; Tomanek, D., " Unusually high thermal conductivity of carbon nanotubes"; *Physical Review Letters*, vol. 84 (20), p: 4613,(2000)
- [43] Heer, W.; Bacsá, W.; Chatelain, A.; Gerfin, T.; Humphrey-Baker, R.; Forro, L.; Ugarte, D.; "Aligned carbon nanotube films: production and optical and electronic properties"; *Science*, vol. 268 (5212), p: 845-7, (1995)
- [44] Kasumov, A.; Deblock, R.; Kociak, M.; Reulet, B.; Bouchiat, H.; Khodos, I.; Gorbatov, Y.; Volkov, V.; Journet, C.; Burghard, M.; " Supercurrents through single-walled carbon nanotubes"; *Science*, vol. 284 (5419), p: 1508-11, (1999)
- [45] Wang, S. ; Zhang, Q.; Yoon, S.; Ahn, J.; Yang, D.; Wang, Q.; Zhou, Q.; Li, J. "Electron field emission from carbon nanotubes and undoped nanodiamond "; *Diamond and Related Materials*, vol. 12 (1), p: 8-14, (2003)
- [46] Dresselhaus, M.; Dresselhaus, G. and Avouris, P., "Carbon Nanotubes: Synthesis, Structure, Properties, and Applications", Springer, London, (2001).
- [47] Yoneya, N.; Tsukagoshi, K. and Aoyagi, Y. " Charge transfer control by gate voltage in crossed nanotube junction" *Applied Physics Letters*, vol. 81 (12), p: 2250, (2002)
- [48] Vaia, R. and Wagner, H.; "Framework for nanocompsite"; *Materials Today*, vol. 7 (11), p: 32-37, (2004)
- [49] Curtin, W. and Sheldon, B., "CNT-reinforced ceramics and metals", *Mater Today*, vol. 7 (11), p: 44–49, (2004)
- [50] Li, C. and Chou, T.," A structural mechanics approach for the analysis of carbon nanotubes", *International Journal of Solids and Structures*, vol. 40 (10), p:2487-99, (2003)
- [51] Iijima, S. and Ichihashi, T. " Single-shell carbon nanotubes of 1-nm diameter" *Nature*, vol. 363 (6430), p: 603-15, 17, (1993)
- [52] Gojny, F.; Wichmann,M.; Fiedler, B. and Schulte,K." Influence of different carbon nanotubes on the mechanical properties of epoxy matrix composites – a comparative study", *Compos Sci Technol.*, vol. 65 (15–16), p: 2300–2313, (2005)

- [53] Grunlan, J.; Mehrabi, A.; Bannon, M. and Bahr, J., "Water-based single-walled nanotube filled polymer composite with an exceptionally low percolation threshold", *Advanced Materials*, vol.16 (2), p: 150-153, (2004)
- [54] Gojny, F. Wichmann, M.; Fiedler, B.; Kinloch, I.; Bauhofer, W.; Windle, A.; Schulte, K. , "Evaluation and identification of electrical and thermal conduction mechanisms in carbon nanotube/epoxy ", *Polymer*, vol. 47 (6), p: 2036-45,(2006)
- [55] Schulte, K.; Gojny, F.; Wichmann, M. and Fiedler, B., "Influence of different carbon nanotubes on the mechanical properties of epoxy matrix composites – a comparative study", *Compos Sci Technol.*, vol. 65 (15–16), p: 2300–2313, (2005)
- [56] Struempfer, R. and Glatz-Reichenbach, J., “Conducting Polymer Composites”, *Journal of Electroceramics*, vol.3 (4), p: 329-346, (1999)
- [57] Vavouliotis, A.; Fiamegou, E.; Karapappas, P. Psarras, G. and Kostopoulos, V. “Electrically conductive epoxies using multiwall carbon nanotubes” *Society of Plastics Engineers*, 10.1002/spepro.002915, (2010)
- [58] Thostenson, E. and Chou, T., “Carbon nanotubes networks: sensing of distributed strain and damage for life prediction and self healing, *Adv Mater* vol. 18, p: 2837–2841, (2006)
- [59] Wu, H.; Wu, X.; Ge, M.; Zhang, G.; Wang, Y. and Jiang, J., “Effect analysis of filler sizes on percolation threshold of isotropical conductive adhesives”, *Compos. Sci. Technol.*, vol. 67 (6), p: 1116–1120, (2007)
- [60] Bigg, D. and Stutz,D. “Plastic composites for electromagnetic-interference shielding applications”, *Polym. Compos.*, vol. 4, p: 40–46, (1983)
- [61] Sandler, J.; Kirk, J., Kinloch, I., Shaffer, M. and Windle, A.," Ultra-low electrical percolation threshold in carbon-nanotube–epoxy composites", *Polymer*, vol. 44 (19) p: 5893–5899,(2009)
- [62] Moisala, A.; Li, Q.; Kinloch. I. and Windle, A., "Thermal and electrical conductivity of single- and multi-walled carbon nanotube–epoxy composites", *Compos Sci Technol.*, vol. 66 , p: 1285–1288, (2006)
- [63] Thostenson, E. and Chou, T., "Processing-structure-multi-functional property relationship in carbon nanotube/epoxy composites", *Carbon*, vol. 44, p: 3022–3029, (2006)
- [64] Bryning, M.; Islam, M.; Kikkawa, J. and Yodh, A., "Very low conductivity threshold in bulk isotropic single-walled carbon nanotube–epoxy composites", *Adv. Mater.*, vol. 17 (9), p: 1186–1191, (2005)

- [65] Kymakis, E.; Alexandou, I. And Amaratunga, G., "Single-walled carbon nanotube–polymer composites: electrical, optical and structural investigation", *Synth Met.*, vol. 127(1–3), p: 59–62, (2002)
- [66] Sumfleth, J.; Prehn, K.; Wichmann, M.; Wedekind, S. and Schulte, K. " A comparative study of the electrical and mechanical properties of epoxy nanocomposites reinforced by CVD- and arc-grown multi-wall carbon nanotubes", *Composites Science and Technology*, vol. 70 (1), p: 173-80, (2010)
- [67] Li, C.; Thostenson, E. and Chou, T.," Dominant role of tunneling resistance in the electrical conductivity of carbon nanotube-based composites", *Appl Phys Lett.*, vol. 91(22), p: 223114, (2007)
- [68] Zhan G.; Kuntz J.; Wan J. and Mukherjee A., "Single-wall carbon nanotubes as attractive toughening agents in alumina-based nanocomposites". *Nat.Mater.* vol. 2(1), p: 38-42, (2003)
- [69] Miyagawa H, Drzal LT. Thermo-physical and impact properties of epoxy nanocomposites reinforced by single-wall carbon nanotubes. *Polymer*, vol. 45 (15), p: 5163–70, (2004)
- [70] Fidelus. J.; Wiesel, E.; Gojny, F.; Schulte, K.; Wagner,H., “Thermomechanical properties of randomly oriented carbon/epoxy nanocomposites”. *Compos. A.* vol. 36 (11), p: 1555–61, (2001)
- [71] Rajoria, H. and Jalili, N., “Passive vibration damping enhancement using carbon nanotube–epoxy reinforced composites”. *Compo Sci Technol*, vol. 65(14), p: 2079–93, (2005)
- [72] Koratkar, N.; Suhr, J.; Joshi, A.; Kane, R.; Schadler, L. and Ajayan, P., “Characterizing energy dissipation in single-walled carbon nanotube polycarbonate composites”. *Appl. Phys. Lett.*, vol. 87 (6). Art. no. 063102, (2005)
- [73] Gojny, F.; Wichmann, M.; Köpke, U.; Fiedler, B. and Schulte, K., “Carbon nanotube-reinforced epoxy-composites – enhanced stiffness and fracture toughness at low nanotube contents, *Compos Sci Technol* , vol. 64, , pp. 2363–2371, (2004)
- [74] Rosca, I. and Hoa, S., “Highly conductive multiwall carbon nanotube and epoxy composites produced by three-roll milling” *Carbon*, vol. 47 (8), p: 1958-1968, (2009)
- [75] Gamstedta, E.; Berglund, L. and Peijs, T., “Fatigue mechanisms in unidirectional glass-fibre-reinforced polypropylene”, *Composites Science and Technology*, vol. 59 (5), p: 759-768, (1999)

- [76] Lagece, P. and Weems, D. "A through-the-thickness strength specimen for composites" *Proc of 2nd ASTM Syrup on Test Methods and Design Allowable, Phoenix, USA, 1986* (American Society for Testing and Materials, 1986)
- [77] Schulte, K. and Baron, C., "Load and failure analysis of cfrp laminates by means of electrical resistivity measurements", *Composites Science and Technology*, vol. 36, p: 63–76, (1989)
- [78] Zhang, C.; Ni, Q., Fu, S. and Kurashiki, K., "Electromagnetic interference shielding effect of nanocomposites with carbon nanotube and shape memory polymer" *Compos. Sci. Technol.* vol. 67 (14), p: 2973-80, (2007),
- [79] Li, N.; Huang, Y.; Du, F.; He, X.; Lin, X.; Gao. H.; Ma, Y.; Li, F.; Chen, Y. and Eklund, P., "Electromagnetic Interference (EMI) shielding of single-walled carbon nanotubes epoxy composites", *Nano Letters*, vol. 6 (6), p: 1141-1145, (2006)
- [80] Dresselhaus, M. "Electronic properties of carbon nanotubes and applications", *Carbon Filaments and Nanotubes: Common Origins, Differing Applications? Proceedings of the NATO Advanced Study Institute*, p: 11-49, 2001
- [81] Gao, L; Thostenson, E. ; Zhang, Z. and Chou, T., "Sensing of damage mechanisms in fiber-reinforced composites under cyclic loading using carbon nanotubes" *Adv. Funct. Mater.*, vol. 19 (1), p: 123-130, 2009
- [82] Thostenson, E. and Chou, T. " Real-time in situ sensing of damage evolution in advanced fiber composites using carbon nanotube networks" *Nanotechnology*, vol.19 (21), p: 215713-1-6, (2008)
- [83] Gao, L; Thostenson, E. ; Zhang, Z. and Chou, T., " Coupled carbon nanotubes network and acoustic emission monitoring for sensing of damage development in composites" *Carbon*, vol. 47(5), p: 1381-8, (2009)
- [84] Gao, L.; Thostenson, E.; Zhang, Z.; Byun, J. and Chou, T., "Damage monitoring in fiber-reinforced composites under fatigue loading using carbon nanotube networks"; *Philosophical Magazine*, vol. 90 (31-32), p: 4085-4099, (2010)
- [85] Gao, L. ; Thostenson, E.; Zhang, Z.; and Chou, T. ; ." Multifunctional carbon nanotube network sensors for damage sensing and health monitoring of fiber-reinforced composites"; SAMPE '09 International SAMPE Symposium and Exhibition (54th:2009: Baltimore, Md.) vol.54, (2009)
- [86] Boger, L.; Wichmann, M.; Meyer, L. and Schulte, K. ; "Load and health monitoring in glass fibre reinforced composites with an electrically conductive nanocomposite epoxy matrix ", *Compos. Sci. Technol.*, vol. 68, (7-8), p: 1886-94, (2008)

- [87] Nofar, M., Hoa, S., Pugh, M.; "Failure detection and monitoring in polymer matrix composites subjected to static and dynamic loads using carbon nanotube networks"; *Compos. Sci. Tech.*, vol. 69 (10), p : 1599-1606, ((2009)
- [88] <http://www.cheaptubesinc.com/MWNTs.htm>
- [89] <http://www.hexion.com/>
- [90] <http://www.resins.com/>
- [91] <http://www.agy.com/>